Technische Universität München
Ingenieurfakultät Bau Geo Umwelt
Lehrstuhl für Astronomische und Physikalische Geodäsie
Univ.-Prof. Dr.techn. Mag.rer.nat. Roland Pail

Designing robust pose estimator for non-cooperative space targets for visual servoing during approach maneuvers

Hrishik Mishra

Master's Thesis

Master's Course in Earth Oriented Space Science and Technology

Supervisor(s):

1. Roberto Lampariello
   Deutsches Zentrum für Luft- und Raumfahrt
2. Phillip Schmidt
   Deutsches Zentrum für Luft- und Raumfahrt

October, 2016

Earth Oriented Space Science and Technology (ESPACE)

Master's Thesis

Technische Universität München (TUM)

TUM Department of Civil, Geo and Environmental Engineering

Deutsches Zentrum für Luft- und Raumfahrt (DLR)

Robotics and Mechatronics Center (RMC)

Designing robust pose estimator for non-cooperative space targets for visual servoing during approach maneuvers

Author:	Hrishik Mishra
Adviser:	Phillip Schmidt
Supervisor:	Roberto Lampariello
Submission Date:	31/10/2016

This master's thesis is a presentation of my original research work. Wherever contributions of others are involved, every effort is made to indicate this clearly, with due reference to the literature, and acknowledgement of collaborative research and discussions.

Munich, 31/10/2016 Hrishik Mishra

Acknowledgments

I am extremely thankful to all the people who provided their timely support, even at unearthly hours. Without it, the completion of this thesis would have been subject to some probabilistic uncertainty.

Firstly, I am deeply grateful to my adviser, Mr. Phillip Schmidt, who provided his able guidance and pointed out the right direction, even when the project was not converging towards desirable results. His technical command was often motivating since my interest areas are deeply linked to his work at DLR. Secondly, I would like to express my gratefulness to my supervisor Mr. Roberto Lampariello for his routine discussions which helped maintain a steady mission objective. Their mentorship was particularly pivotal during the times when literature survey concerning a given problem created a state of flux due to overwhelming amounts of information. That often helped me sidestep positive eigenvalues, literally and figuratively. Although Mr. Schmidt oversaw all the experiments at DLR, the other personnel like Mr. Marco Stefano, who also worked in On-Orbit Servicer (OOS)-sim area were supportive in terms of their technical inputs. It would also behoove me to express my gratitude towards the open communities on `Coppelia Robotics`, `StackExchange` and `Mathworks` who provided critical inputs during challenging times of the project.

I would like to thank Ms. Anastasia Churazova who allowed me access to her workstation which proved incredibly useful for developing some computationally intensive simulations.

I am deeply thankful to my parents for having supported my endeavors in pursuing my ambition. Especially, I am grateful to my father for sharing his Aerospace books which have been seminal in developing the technical background in order to pursue this thesis work. I am thankful to them for always finding enough to tolerate my idiosyncrasies and still supporting my struggles.

Abstract

For on-orbit autonomous grasping of an uncooperative spacecraft using visual servo control of a robotic manipulator, it is imperative that the pose estimation algorithm provide accurate estimates of relative motion parameters from the noisy vision measurements. These non-uniformly sampled measurements have variable noise characteristics and represent a past state owing to the processing time. In this thesis, an event-driven and Out of Sequence Measurement (OOSM)-capable Extended Kalman Filter (EKF) observer with adaptive behavior is derived for estimating motion, inertial and geometric characteristics of an uncooperative Target spacecraft with an objective of grasping while using the measurements of the kind mentioned above. Observability and stability analyses have been presented with conclusions about target inertia and geometry that affect the estimation process. Special focus has been laid on the vision sensor's noise and time-response characteristics to improve the estimator's robustness and optimality. Robustness is analysed in terms of convergence, immunity towards outliers and adaptive behaviour in the face changing noise characteristics. The adaptive behaviour in the EKF is achieved using a Variational Bayesian (VB) approach and an assessment is presented for a step-change in noise characteristics. A nonlinear state-space model for relative dynamics between the OOS's end-effector and the tumbling target have been derived which incorporate orbital dynamics and manipulator's servoing motion. In order to avoid rank-deficiency variances for the attitude quaternion, a Multiplicative Extended Kalman Filter (MEKF) approach with a reduced state-vector is used. The small angular rotation and the Gibbs vector were used as candidates and an evaluation of both of these representations is provided. A Software In Loop (SIL) has been developed which allows fast prototyping of estimation/control algorithms for the grasping problem using an eye-in-hand topology for position-based servo control.

Contents

List of Figures

List of Tables

List of Symbols

$\{\mathcal{A}\}$ Servicer Base Frame (Orbital) after manipulator motion. xii–xiv, 5, 6, 9, 14, 15

$\{\mathcal{A}_{ee}\}$ Servicer end-effector frame aligned with Camera frame. xii–xiv, 5, 15

$\mathbb{E}$ Expectation. xii

$\boldsymbol{I}_M$ Servicer's manipulator joint Inertia. xii, 9

$\boldsymbol{I}_S$ Servicer's base Inertia. xii, 9

$\bar{\boldsymbol{\mu}}$ quaternion orientation between $\{\mathcal{C}\}$ and $\{\mathcal{A}\}$. xii, 15, 16

$\boldsymbol{\Phi}$ State transition matrix. xii, 38–40, 44, 45

$\boldsymbol{\theta}$ Manipulator joint angle vector. xii, 16

$\check{\boldsymbol{a}}$ 3-component orientation error measurement. xii, 12, 13

$\hat{\boldsymbol{a}}$ 3-component orientation error estimate. xii

$\boldsymbol{a}$ 3-component orientation error. xii, xiii, 10–14

$\boldsymbol{CRB}$ Cramer Rao bound. xii, 49, 51

$\delta\bar{\boldsymbol{q}}$ quaternion error in world frame. xii, 10, 12

∇ Gradient of a scalar. xii, 25, 26, 30, 36, 44, 46, 49

$\dot{e}$ error rate of estimator. xii, 36

$\bar{\boldsymbol{\eta}}$ quaternion orientation of $\{\mathcal{C}\}$ relative to $\{\mathcal{B}\}$. xii, 6, 15, 16

$\bar{\gamma}$ quaternion orientation of $\{\mathcal{A}\}$ relative to $\{\mathcal{O}\}$. xii

$\bar{\Im}$ quaternion orientation of $\{\mathcal{A}\}$ relative to $\{\mathcal{A}_{ee}\}$. xii, 5, 16

κ_i Local unobservability index. xii, 27–29, 32, 33

κ_n Local Estimation condition number. xii, 27–29, 32, 33

$\boldsymbol{L_0}$ Initial Servicer angular momentum. xii, 9

λ eigenvalues in a system. xii, 28

μ_e Gravitational parameter of Earth. xii, 14, 15

$\mathcal{N}$ Normal distribution. xii

$\boldsymbol{n}$ mean motion of the spacecraft in Earth-centered inertial frame. xii, 9, 14, 15

$\mathcal{G}_o$ Observability Gramian of a system. xii, 28

$\boldsymbol{\omega}_{base}$ Angular velocity of Servicer's base relative to inertial frame. xii, 9

$\boldsymbol{\omega}_n$ Servicer's angular rate around Earth. xii, 9

$\hat{\boldsymbol{\omega}}$ quaternion equivalent of $\boldsymbol{\omega}$. xii, 12

$\boldsymbol{\omega}$ Angular velocity $\{\mathcal{B}\}$ relative to $\{\mathcal{A}\}$ expressed in $\{\mathcal{B}\}$. xii, xiv, 6, 8–10, 12–14, 16

$\dot{\boldsymbol{\phi}}_M$ Servicer's manipulator joint angular rates. xii, 9

$\dot{\boldsymbol{\phi}}_S$ Servicer's base angular rates. xii, 9

$\boldsymbol{p}$ Inertia ratios. xii, 13, 14, 16

$\bar{\boldsymbol{q}}_{ref}$ reference quaternion which obeys unit-norm constraint. xii, 10, 11, 13

$\bar{\boldsymbol{q}}$ quaternion orientation between $\{\mathcal{B}\}$ and $\{\mathcal{A}\}$. xii–xiv, 6–13, 16

$\boldsymbol{r}_c$ Position vector between $\{\mathcal{A}\}$ and $\{\mathcal{C}\}$. xii, 16

$\boldsymbol{r}_e$ Position vector of spacecraft in Earth-centered inertial frame. xii, 14

$\boldsymbol{r}_o$ Position of origin of $\{\mathcal{A}\}$ relative to $\{\mathcal{O}\}$. xii, 5

$\boldsymbol{\rho}_c$ Position of $\{\mathcal{A}\}$ relative to $\{\mathcal{A}_{ee}\}$. xii, 6

$\boldsymbol{\rho}_t$ Position of $\{\mathcal{C}\}$ relative to $\{\mathcal{B}\}$. xii, 6

$\boldsymbol{r}$ Position vector between $\{\mathcal{B}\}$ and $\{\mathcal{A}\}$. xii, xiv, 6, 14–16

$\mathbf{स}_1$ Dynamic system for motion parameters only. xii, 16

$\mathbf{स}_2$ Dynamic system for motion parameters and inertia only. xii, 16

$\mathbf{स}_3$ Dynamic system for motion parameters, inertia and geometry. xii, 16

$\{u\}^{t_f}$ Input sequence till t_f. xii, 22, 23

$\{\boldsymbol{y}\}^{1:k}$ Output measurement sequence from 1 to k. xii, 38, 39, 42

$\{y\}^{t_f}$ Measurement sequence till t_f. xii, 23

$\{\mathcal{B}\}$ Body centered frame aligned with Target's principal axes. xii–xiv, 6, 15

$\{\mathcal{C}\}$ Body fixed frame aligned with Target's vision-feature plane. xii–xiv, 6, 15, 16

$\{\mathcal{O}\}$ Servicer Base Frame (Orbital) before manipulator motion. xii–xiv, 5, 14

Abbreviations

ADR Active Debris Removal. xii, 1, 2, 87

ARAMIS Automation, Robotics and Machine Intelligence Systems. xii, 1

B- Bump. xii, 4, 63, 64, 68

CAD Computer-Aided Design. xii, 15, 92, 93

DEOS Deutsche Orbitale Servicing Mission. xii, 1

DLR Deutsches Zentrum für Luft- und Raumfahrt. ii, iv, ix, xii, 1, 4, 5, 7, 15, 32, 33, 75, 87, 90, 91, 94

EKF Extended Kalman Filter. v, vii, x–xii, 2–4, 35, 43, 44, 47, 48, 51, 54, 59–74, 78–82, 86, 87, 90, 91

EPOS European Proximity Operations Simulator. xii, 32, 33

ESPACE Earth Oriented Space Science and Technology. ii, xii

ETS Engineering Test Satellite. xii, 1

GNSS Global Navigation Satellite System. xii, 86

GPS Global Positioning System. xii, 1

HCW Hill-Clohessy-Wiltshire. xii, 14

HIL Hardware In Loop. xii, 4

LVLH Local Vertical Local Horizontal. xii, 5

MEKF Multiplicative Extended Kalman Filter. v, ix, xii, 11, 13

NASA National Aeronautics and Space Administration. xii, 1

OOS On-Orbit Servicer. iv, v, ix, xii, 1–3, 5, 7, 87

OOSM Out of Sequence Measurement. v, xi, xii, 4, 40, 81, 83, 84, 87, 90, 91

ORC Observability Rank Condition. xii, 25–27, 29–33

RMC Robotics and Mechatronics Center. ii, xii

ROTEX Robot Technology Experiment. xii, 1

RRM Robotic Refueling Mission. xii, 1

SIL Software In Loop. v, vii, xi, xii, 4, 5, 87, 90–95

TUM Technische Universität München. ii, xii

V-REP Virtual Robot Experimentation Platform. xi, xii, 5, 15, 91–94

VB Variational Bayesian. v, x, xii, 3, 4, 64, 66–69, 72, 87

Chapter 1: Problem Definition

1.1. Introduction

Teleoperated Space Robotic systems have been successful in the past and there has been an increased interest for developing an analogous autonomous capability in such an OOS. The concept was first mentioned by National Aeronautics and Space Administration (NASA) in the Automation, Robotics and Machine Intelligence Systems (ARAMIS) in 1980s and since then, several demonstration missions like Engineering Test Satellite (ETS)-VII, Orbital Express and Robotic Refueling Mission (RRM) have corroborated it. Robot Technology Experiment (ROTEX) and ETS-VII proved to be quintessential in key robotic technologies in microgravity environment. Deutsche Orbitale Servicing Mission (DEOS) developed by DLR and Astrium GmbH was pivotal in steering this application towards capture of noncooperative spacecraft as mission objectives. Although equipped with Global Positioning System (GPS), the relative navigation in this instance was planned with a vision-based system.

Because of the maturity in technologies employed in DEOS, it is one of the most promising solutions in Active Debris Removal (ADR) as well. Inevitably, the future of On-orbit Servicing and ADR using space robots are conflated [**Lieuwen2016**]. A simplified objective of an OOS is to capture a cooperative spacecraft having known mass properties and motion about its mass center. This is analogous to catching a ball on earth whose mass properties are well known, for instance, a tennis ball. In contrast, a ADR mission involves capturing an unknown object with unknown mass properties and significant tumbling motion. Drawing on the ball's analogy as before, in this case, the impact is unpredictable because of the uncertainties. A servicer should be able to determine the relative pose of the target with respect to itself, de-tumble it and aid de-orbiting. Of course, a fundamental requirement for this is to ensure accurate and precise relative navigation [**Palmerini2016**].

Even though telepresence is a proven alternative, autonomy is a desirable option because of the communication time-delay involved in remote control from ground stations on earth [**Aghili2013**]. In order to achieve a higher degree of autonomy in servicing

and ADR tasks, it is important to have accurate estimates of the torque-free motion parameters of target spacecraft.

Hence, it becomes imperative to be able to reconstruct [**Palmerini2016**] these parameters in order to aid the servoing process in the Pre-Grasping phase while using noisy information from sensors. The primary focus of this thesis is to develop the estimator and analyze the estimator behavior in the scenario of space-based visual servoing for grasping uncooperative targets.

1.2. Literature review and discussion

Visual servoing techniques have been successfully employed in terrestrial applications since 1980s, as has been surveyed by Hutchinson, Hager, and Corke in [**Hutchinson1996**]. Space manipulator visual servoing though is presently a pertinent area of research in the leading space agencies around the globe [**Lieuwen2016**]. In contrast to terrestrial visual servoing techniques, for space applications, free-flying or free-floating kinematics/dynamics of the servicer have to be considered. The motion controller for such a space manipulator had already been discussed by Umetani and Yoshida in [**Umetani1989**] by 1990. In 1993, [**Dubowsky1993**] presented the analytical virtual manipulator for planning and control of a robotic manipulator in space.

Prior to that, the Clohessy-Wiltshire [**Clohessy1960**] equations (1960) were one of the earliest linearized models for the relative translational dynamics between chaser and target. The model was approximated to the first order effects and is used commonly for rendezvous and docking applications. It is natural that these equations are also common to the relative motion dynamics between OOS and Target.

As recent as 2016, Palmerini, Sabatini, and Gasbarri in [**Palmerini2016**] have mentioned some of the challenges faced with such an On-Orbit Servicing mission, especially concerning uncooperative targets. According to them, vision-based navigation is one of the appealing choices for aiding uncooperative target-grasping. In other words, machine vision techniques are employed for closed-loop control of the the space robotic manipulator. Irrespective of sensor selection, however, it is imperative for the OOS to employ an estimation scheme which is able to use the noisy sensor data to predict the relative kinematics for servoing.

Since the relative kinematics and dynamics of such a system is nonlinear, EKF is often a suitable candidate [**Palmerini2016**]. This had been demonstrated by Aghili and Parsa in various instances of their work like [**Aghili2007**], [**Aghili2009**] and [**Aghili2012**]. Furthermore, the target maybe uncooperative not just in the context of attitude-control but also that its geometry and mass properties maybe unknown. Hence, any estimator should also perform parameter identification along with state estimation for servo-

ing. Previously, such an approach had been identified in [**Aghili2009**] and [**Aghili2007**]. However, the authors have not performed an observability analysis. From studies based on Kalman filters, [**Boutayeb1997**] and other observers, [**Birk1988**], it is clear that an observability analysis should precede the design. An observability analysis for nonlinear systems, like the relative motion between OOS and Target, was shown by Hermann and Krener in [**Hermann1977**] (1977). Subsequently, there were other techniques like the Observability Gramian, [**Krener2009**] which provided degrees of observability of a nonlinear system. These studies provide a qualitative and quantitative intuition to the performance of estimators developed by [**Aghili2009**].

The relative orientation is modeled using a multiplicative quaternion so that it can be used by a stochastic estimator, EKF. This has been documented adequately in [**Landis2003**], [**Landis2004**] and [**Lefferts1982**]. Aghili and Parsa employed the small rotation approximation as suggested in [**Lefferts1982**]. From the theory in the three references above, the Gibbs vector attitude error representation is more robust since it is able to represent an angular axis rotation error of up to 180°.

In an estimation scheme based on vision-measurements, there are some quintessential challenges which have to be surmounted. Firstly, the sampling rate of a vision-based sensor (pose-estimator) is non-uniform. Secondly, due to occlusion or indequate lighting conditions, the probability of outliers in measurements is higher than what a Gaussian distribution would allow. In [**Alcantarilla2016**], Alcantarilla and Woodford has explained noise characteristics of measurements based on vision algorithms. Additionally, as shown in [**Aghili2009**], the error characteristics are state-dependent. Hence, it is imperative for an estimator to have an adaptive response to vision-based measurements.

For implementing a noise-adaptive behavior, the different topologies can be found in [**Mehra1970**]. [**Aghili2009**] used a finite memory covariance-matching technique. Among Bayesian approaches, several methods based on VB have been used in the past like [**Särkkä2009**], [**Särkkä2013**], [**Piché2012**] and [**Roth2013**]. All these methods are like the Iterated Extended Kalman Filter which uses an iterated update like Expectation-Minimization to adapt to the residual disturbance.

For outlier robustness in an estimator, the Mahalanobis distance as a discriminating function was proposed in [**Chang2014**]. Chang chose to manipulate the noise error covariance based on optimization techniques to achieve robustness against outliers. The disadvantages of this method have been narrated by Da Ren in [**Da Ren1994**] and an alternative - State Chi-Square Test (SCST) - has been suggested. In any case, it is clear that χ^2-test is a suitable way to test for outliers.

For an EKF, convergence is a major problem for uncertain initial conditions [**Boutayeb1997**]. In the current problem of space-based estimation, the initial conditions are uncertain with no prior on the degree of uncertainty. Since the advent of the Kalman Filter in 1960s, few studies have focused on convergence from condition of no knowledge. Out of

these, the convergence studies and suitable actions to ensure convergence in EKF has been discussed with examples in [**Perea2007**] and [**Boutayeb1997**]. Along with Jazwinski's work, it becomes clear that suboptimal methods have to be adopted to ensure convergence despite unknown initial conditions.

For implementing such a complicated system on hardware, it is important to perform SIL and Hardware In Loop (HIL) tests. An instance of such a SIL is given in [**Hosseini2016**] for an octorotor. At the time of writing this thesis at DLR, a SIL testbench was simultaneously developed so that the algorithms for estimation and control can be seamlessly tested before implementation.

1.3. Brief outline of the thesis

In the chapter 1, sections 1.4 and 1.5, the model [**Aghili2009**] used in the thesis has been derived. A comparative study is made in section 1.5.2 to evaluate attitude error-representations [**Landis2003**], [**Landis2004**], [**Lefferts1982**]. At the end of this chapter, three models have been derived for further analysis.

In chapter 2, detailed observability analyses have been performed and suitable conclusions in regards to the Target spacecraft have been made. The relevant derivations and explanations for nonlinear observability studies have been provided in this chapter. After satisfying observability criterion, Chapter 3 is a continuity towards design of EKF observers. In this chapter the state estimates and errors have been presented. In [**Aghili2007**] and [**Aghili2009**], an approximation for the deriving the state-transition matrix from the system matrix has been used. From the perspective of a realtime estimation, this is an apt choice. In this work, the approximation was dropped for implementing a non-singular representation. Although, a rudimentary Padé's approximation [**Arioli1996**] was used for the fruition of the work in this thesis, the reader is referred to [**Moler2004**] for more computation-efficient solutions.

In chapter 4, convergence studies have been performed in 4.1. Appropriate steps to ensure convergence have been laid out with results. In order to ensure the convergence of the estimator, a Bump (B-)-EKF [**Perea2007**] strategy was put in place. It is demonstrated that without this strategy, the estimator is more likely to diverge as suggested by the authors. The following section outlines steps taken to improve robustness of the EKF design with an adaptive system. In this chapter, a VB approach was adopted to derive the noise covariance from the approximated *a posteriori* distribution. In the latter part, for the purposes of this thesis, Outlier-Rejection was performed using a χ^2 *p-value* on the residual after convergence. Results have been accordingly shown.

In chapter 5, implementation details have been detailed. Specially pertaining to vision-based systems, an EKF has to be designed as multi-rate, event-driven and OOSM-

enabled. The results of such an implementation have been detailed. It has also been emphasized that for dynamic systems, the vision system's inherent delay in reporting cannot be ignored.

In the appendix section, chapter A gives implementation details about simulating an asynchronous camera. The details of the SIL test being developed for the thesis has been explained. The steps taken and the results have been pointed out.

Three models were implemented in `MATLAB` for the problem demonstrated in figure 1.1 (explained in the next section) and the comparative results with different approaches have been presented. A reduced-state observer is implemented in `Simulink` which demonstrated asynchronous, mutli-rate operation for hardware implementation on the OOS-SIM at DLR. As a part of the thesis implementation, a client-server software was developed to link `Simulink-MATLAB` with `V-REP` [**Rohmer2013**] and visualize the resultant motion. Since pose-estimation itself is not in the scope of this thesis, an AprilTag [**Olson2011**] based pose-estimator is employed which is then used in the architecture defined above. A UR5 Robot was configured in the `V-REP` environment and an elementary inverse-Jacobian position-controller was implemented which shall be used for performing estimation during manipulator motion. The present volume of work naturally leads to this. The asynchronous behavior of the optical sensor was implemented using `SimEvents` toolbox [**Gray2007**] in `Simulink`. A complete Software-in-loop demonstration is made whose details will be provided in the latter sections.

1.4. Defining the Model

As a convention, vectors are indicated by boldface symbols of lowercase alphabet and so are quaternions, but with an overline ($\bar{\cdot}$). Matrices will be indicated with boldface symbols of the uppercase alphabet. Figure 1.1 is a diagrammatic representation of the scenario in which an On-Orbit Servicer is approaching the Target spacecraft on a similar orbit. The axes triads have been color-coded for ease of comprehension. The initial orbital frame of the Servicer's base $\{\mathcal{O}\}$ is a Local Vertical Local Horizontal (LVLH) frame which rotates about the orbit and points along the position vector from Earth centre towards Servicer mass center. The z-axis points along the angular momentum vector and y-axis completes the triad. After the base-perturbation due to manipulator motion, the LVLH frame shifts to $\{\mathcal{A}\}$. The relative pose of this frame with respect to $\{\mathcal{O}\}$ is indicated by position $\boldsymbol{r}_o$ and an orientation quaternion, $\bar{\boldsymbol{\gamma}}$. The camera is assumed to be mounted on the end-effector and the camera frame $\{\mathcal{A}_{ee}\}$ is also an LVLH frame with it's z-axis perpendicular to the image plane, x-axis to the right of image center and the y-axis completing the triad. We express the relative orientation of the end-effector $\{\mathcal{A}_{ee}\}$ with respect to the current base-frame $\{\mathcal{A}\}$ by a quaternion, $\bar{\Im}$, and its relative

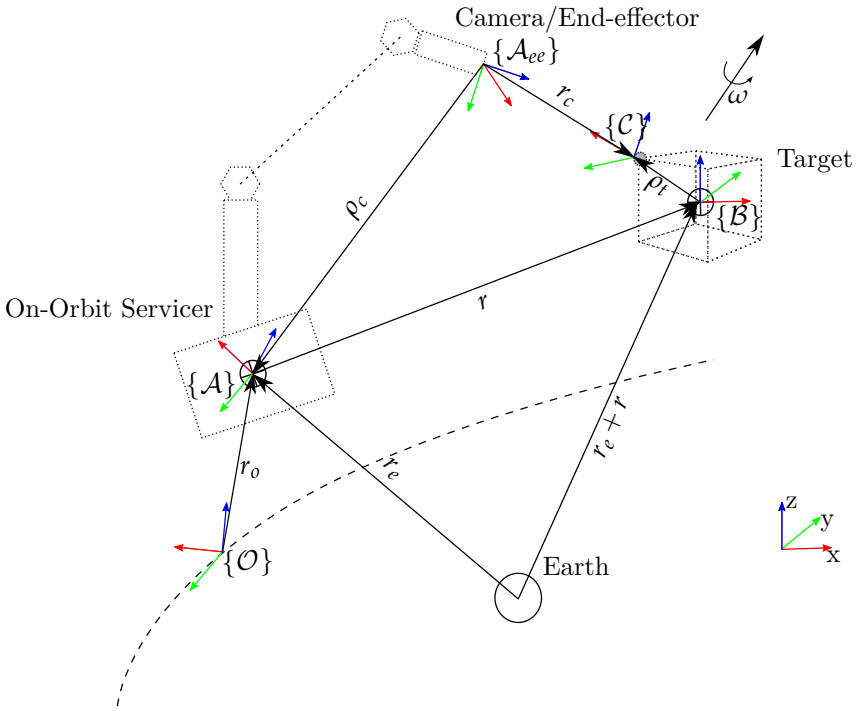

Figure 1.1.: Body diagrams of servicer and tumbling spacecraft

position as $\boldsymbol{\rho}_c$. Like [**Aghili2009**], the Target body frame $\{\mathcal{B}\}$ is the oriented parallel to the principal axes of inertia and is centered at the mass center of the Target. The feature/grasping plane (marked by grey) that is visible to the camera lies in $\{\mathcal{C}\}$ at the feature center. The relative pose of the grasping frame $\{\mathcal{C}\}$ with respect to body frame $\{\mathcal{B}\}$ is given by position $\boldsymbol{\rho}_t$ and an orientation quaternion $\bar{\boldsymbol{\eta}}$. The Target is assumed to be have to torque-free motion in space characterized by an angular velocity $\boldsymbol{\omega}$ expressed with respect to $\{\mathcal{A}\}$ in the Target body frame. Moreover, $\{\mathcal{A}\}$ is the Orbital Reference Frame and is non-inertial.

The Target spacecraft has a relative position $\boldsymbol{r}$ and an orientation quaternion $\bar{\boldsymbol{q}}$ with respect to the Servicer's base. As in [**Aghili2009**], $\{\mathcal{A}\}$ is assumed to be located at the mass center of the Servicer. One of the primary advantages of this representation that has been advocated by Aghili and Parsa in [**Aghili2009**] and [**Aghili2007**] is decoupling of translational and rotational dynamics. Additionally, the expression of rotational dynamics in body frame is convenient since the Inertia Matrix can be assumed to diagonal and constant. This also simplifies the quaternion calculations since the error dynamics for $\bar{\boldsymbol{q}}$ and $\bar{\boldsymbol{\eta}}$ are expressed in the Target's body frame. This aspect will become clear once the attitude error dynamics are derived in section 1.5.2.

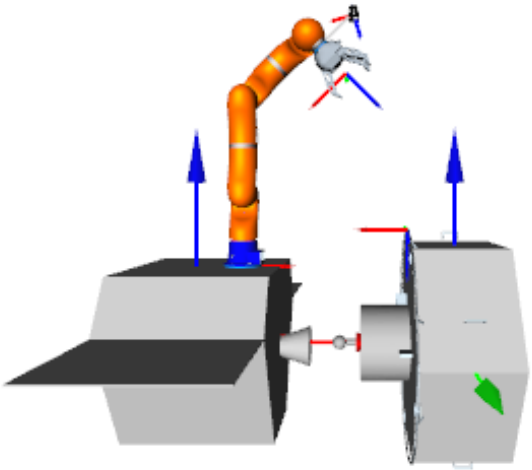

Figure 1.2.: Simulated scenario of the grasping problem at DLR's OOS-simulator

1.5. Deriving the Model

1.5.1. Attitude

The fundamental representation of attitude/orientation is a 3×3 matrix that belongs to the special orthogonal group, $SO(3)$. Due to the problem of storage and constraints, a lower-dimensional representation is employed, as enunciated in [**Landis2003**] [**Landis2004**]. In this thesis, the following derivations are made from quaternion representations of attitude/orientation.

A quaternion representation of rotation is a $\mathbb{R}^4$ vector given as [**Trawny2005**],

$$\bar{q} = \begin{pmatrix} \hat{\mathbf{k}}\, sin(\theta/2) \\ cos(\theta/2) \end{pmatrix} = \begin{bmatrix} q_1 \\ q_2 \\ q_3 \\ q_0 \end{bmatrix} = \begin{bmatrix} \boldsymbol{q}_v \\ q_0 \end{bmatrix} \tag{1.1}$$

where θ is the angle of rotation around an axis whose orthogonal basis in reference frame is given by a $\mathbb{R}^3$ vector $\hat{\mathbf{k}}$ and the subscripts $\mathbf{v}$ and 0 indicate the vector and scalar

components. This representation is the same as used in [**Aghili2007**], [**Aghili2009**] and [**Trawny2005**]. The algebra rules that have been used are described below.

A quaternion multiplication between two $\mathbb{R}^4$ vectors $\bar{\boldsymbol{p}}$ and $\bar{\boldsymbol{q}}$ is indicated by two operations, $\otimes$ and $\circledast$ which are defined as,

$$\bar{\boldsymbol{p}} \otimes \bar{\boldsymbol{q}} = \begin{bmatrix} -\lceil \boldsymbol{p}_v \rceil + p_0 \mathbb{I}_3 & \boldsymbol{p}_v \\ -\boldsymbol{p}_v^T & p_0 \end{bmatrix} \begin{bmatrix} \boldsymbol{q}_v \\ q_0 \end{bmatrix} \tag{1.2a}$$

$$\bar{\boldsymbol{p}} \circledast \bar{\boldsymbol{q}} = \begin{bmatrix} \lceil \boldsymbol{p}_v \rceil + p_0 \mathbb{I}_3 & \boldsymbol{p}_v \\ -\boldsymbol{p}_v^T & p_0 \end{bmatrix} \begin{bmatrix} \boldsymbol{q}_v \\ q_0 \end{bmatrix} \tag{1.2b}$$

where $\lceil \boldsymbol{a} \rceil$ is the skew-symmetric matrix of the form $\begin{bmatrix} 0 & -a_3 & a_2 \\ a_3 & 0 & -a_1 \\ -a_2 & a_1 & 0 \end{bmatrix}$.

Let $\boldsymbol{R}(\bar{\boldsymbol{p}})$ and $\boldsymbol{R}(\bar{\boldsymbol{q}})$ be two attitude matrices corresponding to $\bar{\boldsymbol{p}}$ and $\bar{\boldsymbol{q}}$ respectively, then the attitude matrix composition $\boldsymbol{R}(\bar{\boldsymbol{r}}) = \boldsymbol{R}(\bar{\boldsymbol{p}})\boldsymbol{R}(\bar{\boldsymbol{q}})$ is given by a quaternion $\bar{\boldsymbol{r}}$,

$$\bar{\boldsymbol{r}} = \bar{\boldsymbol{q}} \otimes \bar{\boldsymbol{p}} = \bar{\boldsymbol{p}} \circledast \bar{\boldsymbol{q}} \tag{1.2c}$$

where $\boldsymbol{R}(.)$ is the attitude matrix that transforms a body-referenced vector to world coordinates.

A rotation quaternion has a conjugate property which in terms of rotation implies an inverse rotation which is given by $\bar{\boldsymbol{q}}^*$,

$$\bar{\boldsymbol{q}}^* = \begin{bmatrix} -\boldsymbol{q}_v \\ q_0 \end{bmatrix} \tag{1.2d}$$

which has the property $\bar{\boldsymbol{q}} \otimes \bar{\boldsymbol{q}}^* = \bar{\boldsymbol{q}}^* \otimes \bar{\boldsymbol{q}} = \begin{bmatrix} 0 & 0 & 0 & 1 \end{bmatrix}^T$.

An attitude matrix $\boldsymbol{R}(\bar{\boldsymbol{q}})$ is defined as,

$$\boldsymbol{R}(\bar{\boldsymbol{q}}) = (2q_0 - 1)\mathbb{I}_3 + 2q_0 \lceil \boldsymbol{q}_v \rceil + 2\boldsymbol{q}_v \boldsymbol{q}_v^T \tag{1.2e}$$

More detailed properties and derivations are provided in [**Trawny2005**] and [**Diebel2006**].

The time-derivative of the quaternion with respect to the world-frame is related to the angular velocity (expressed in body frame) as given by,

$$\dot{\bar{\boldsymbol{q}}}(t) = \frac{1}{2} \bar{\boldsymbol{\omega}} \otimes \bar{\boldsymbol{q}}(t) \tag{1.2f}$$

where $\bar{\boldsymbol{\omega}}$ is simply $\begin{bmatrix} \boldsymbol{\omega}(t) \\ 0 \end{bmatrix}$.

Remark 1. In (1.2f), $\boldsymbol{\omega}$ is the angular velocity of the Target with respect to the Servicer in the Target's body frame. It should be noted though that in orbit, the angular motion of the Servicer due to Attitude Control in the Target's frame needs to be accounted for. Additionally, if the robotic manipulator moves, it will also create a disturbance in $\boldsymbol{\omega}$ by virtue of reaction forces.

So, $\boldsymbol{\omega}$ in (1.2f) can be expanded for this scenario as follows,

$$\boldsymbol{\omega} = \boldsymbol{\omega}_t - \boldsymbol{\omega}_n - \boldsymbol{\omega}_{base} \tag{1.2g}$$

where $\boldsymbol{\omega}_t$ is the angular velocity of the Target with respect to Servicer, $\boldsymbol{\omega}_n$ is the angular velocity of Servicer in orbit and $\boldsymbol{\omega}_{base}$ is the Servicer base motion due to robotic manipulation or attitude control.

In this thesis, an assumption of is made that there is no robotic manipulator motion. In that case, $\boldsymbol{\omega} = \boldsymbol{\omega}_t - \boldsymbol{\omega}_n$.

In [**Aghili2009**], the AOCS is assumed to make the Servicer turn at the mean motion rate in orbit. It is easy to see that, $\boldsymbol{\omega}_n$ can be found by expressing the orbital velocity vector in the Target frame. For this, the quaternion transformation can be used as follows,

$$\bar{\omega}_n = \bar{\boldsymbol{q}} \otimes \bar{\boldsymbol{n}} \otimes \bar{\boldsymbol{q}}^* \tag{1.2h}$$

where $\bar{\boldsymbol{n}} = \begin{bmatrix} \boldsymbol{n}^T & 0 \end{bmatrix}^T$ and $\boldsymbol{n} = \begin{bmatrix} 0 & 0 & n \end{bmatrix}^T$. By using (1.2h), (1.2g) and (1.2f) and dropping the explicit representation for functions of time, we derive,

$$\dot{\bar{\boldsymbol{q}}} = \frac{1}{2}\bar{\omega}_t \otimes \bar{\boldsymbol{q}} - \frac{1}{2}\bar{\boldsymbol{q}} \otimes \bar{\boldsymbol{n}} \otimes \bar{\boldsymbol{q}}^* \otimes \bar{\boldsymbol{q}} \tag{1.2i}$$

$$= \frac{1}{2}\bar{\omega}_t \otimes \bar{\boldsymbol{q}} - \frac{1}{2}\bar{\boldsymbol{q}} \otimes \bar{\boldsymbol{n}} \tag{1.2j}$$

$$= \frac{1}{2}\bar{\omega}_t \otimes \bar{\boldsymbol{q}} - \frac{1}{2}\bar{\boldsymbol{n}} \circledast \bar{\boldsymbol{q}} \tag{1.2k}$$

$$= \frac{1}{2}(\bar{\omega}_t \otimes -\bar{\boldsymbol{n}}\circledast)\bar{\boldsymbol{q}} \tag{1.2l}$$

$$\tag{1.2m}$$

In [**Umetani1989**, eq. 18], the unknown Servicer attitude angles ($\boldsymbol{\phi}_S = \begin{bmatrix} \alpha & \beta & \gamma \end{bmatrix}^T$) have been derived using Momentum Conservation principle.

$$\dot{\boldsymbol{\phi}}_S = -\boldsymbol{I}_S{}^{-}\boldsymbol{I}_M\dot{\boldsymbol{\phi}}_M + \boldsymbol{I}_S{}^{-}\boldsymbol{L_0} \tag{1.2n}$$

where, $\boldsymbol{\phi}_m = \begin{bmatrix} \theta_1 & ... & \theta_n \end{bmatrix}^T$ are the joint angles, $\boldsymbol{L_0}$ is the initial Servicer momentum and, $\boldsymbol{I}_S$ and $\boldsymbol{I}_M$ are the inertia for Servicer body and Manipulator respectively. (1.2n) can be related to Servicer's angular rates ω_{base} expressed in $\{\mathcal{A}\}$. But, one must take into

account that in [**Umetani1989**], the authors have assumed an inertial frame as reference. In [**Rouleau2006**], the authors have mentioned several servoing tasks which can cause a Servicer base perturbation. These include, tracking visual features in field-of-view, translational alignment and capture/grasp.

The solution to (1.2f) by integration gives us the quaternion at a given time which under basic assumptions for $\boldsymbol{\omega}$ can be solved in a closed-form. In [**Trawny2005**, ch.1.6.1, p.12], Trawny and Roumeliotis have derived the zeroth and first order quaternion integrators. In this thesis, it is assumed that $\boldsymbol{\omega}$ remains piecewise constant over a sampling period, ΔT. Therefore, the zeroth-order quaternion is used in the following form. In [**Landis2003**], it has been stated that the skew-symmetric $\bar{\boldsymbol{\omega}}\otimes$ preserves the unit-norm constraint of quaternions.

$$\bar{\boldsymbol{q}}(k+1) = e^{\frac{1}{2}\bar{\boldsymbol{\omega}}\otimes\Delta T}\bar{\boldsymbol{q}}(k) \tag{1.2o}$$

The equation (1.2o) can be further approximated as given in [**Trawny2005**] or in [**Aghili2009**] using a Taylor Series. In this thesis, only (1.2o) has been used for deriving the attitude expression.

In the case of a very small angular rotation $\delta\theta$, the differential quaternion can be written as,

$$\delta\bar{\boldsymbol{q}} = \begin{bmatrix}\delta\boldsymbol{q}_v\\ \delta q_0\end{bmatrix} = \lim_{\delta\theta\to 0}\begin{bmatrix}\hat{\boldsymbol{k}}\ sin(\delta\theta/2)\\ cos(\delta\theta/2)\end{bmatrix} \tag{1.2p}$$

$$\approx \begin{bmatrix}\frac{1}{2}\delta\boldsymbol{\theta}\\ 1\end{bmatrix} \tag{1.2q}$$

$$\Rightarrow \delta\bar{\boldsymbol{q}} = \delta\bar{\boldsymbol{q}}(\delta\boldsymbol{\theta}) \tag{1.2r}$$

The three Rodrigues parameters or the Gibbs Vector has been defined succinctly in [**Landis2003**] as,

$$\boldsymbol{g} = \frac{\boldsymbol{q}_v}{q_0} = \frac{\hat{\boldsymbol{k}}\ sin(\theta/2)}{cos(\theta/2)} = \hat{\boldsymbol{k}}\ tan(\theta/2) \tag{1.2s}$$

$\boldsymbol{g}$ is a projection of the $SO(3)$ quaternion onto a thee-dimensional Eucledian space. The vector is infinite for a rotation of 180°.

1.5.2. Multiplicative Quaternion

The nonlinear quaternion expression in multiplicative form given a unit reference quaternion $\bar{\boldsymbol{q}}_{ref}$ and a small error quaternion $\delta\bar{\boldsymbol{q}}$ which represents a rotation from $\bar{\boldsymbol{q}}_{ref}$ to true quaternion $\bar{\boldsymbol{q}}$ is given as,

$$\bar{\boldsymbol{q}}(t) = \delta\bar{\boldsymbol{q}}\otimes\bar{\boldsymbol{q}}_{ref} \tag{1.3a}$$

$\delta\bar{\boldsymbol{q}}$ can be parametrized as $\delta\bar{\boldsymbol{q}}(\boldsymbol{a})$ where $\boldsymbol{a}$ represents a vector in the body-frame coordinates. In an attitude observer, the unconstrained estimate of $\boldsymbol{a}$ is computed and the

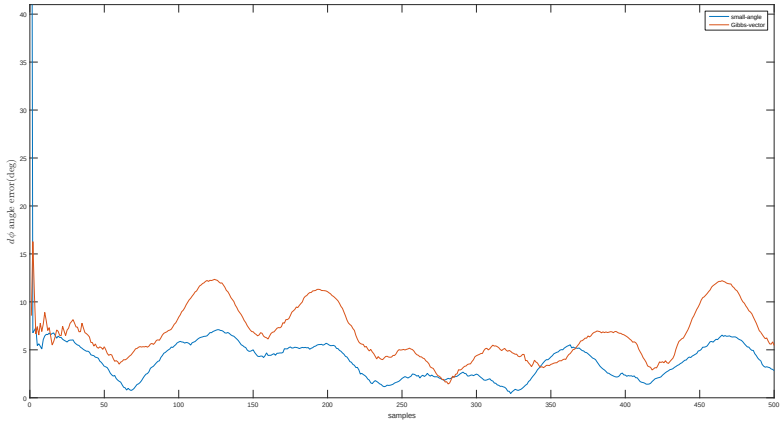

Figure 1.3.: Attitude error representations in an MEKF red -twice Gibbs vector, blue -small angle

equation (1.3a) is used to extract the estimate of attitude quaternion. This is shown as follows,

$$\hat{\bar{\boldsymbol{q}}}(t) = \delta\bar{\boldsymbol{q}}(\hat{\boldsymbol{a}}) \otimes \bar{\boldsymbol{q}}_{ref} \tag{1.3b}$$

(1.3b) provides a way of computing attitude estimates without having to explicitly normalize the quaternion since it preserves the unit-norm constraint. This representation of attitude errors is often known in literature [**Landis2003**], [**Landis2004**] as the MEKF.

Remark 2. In the MEKF attitude observer, a three dimensional Euclidean vector $\boldsymbol{a}$ is estimated using some form of linear injection. This vector corresponds to the attitude error $\delta\bar{\boldsymbol{q}}$ and the correct attitude $\bar{\boldsymbol{q}}$ is obtained simply by multiplicative correction as shown in (1.3b).

Remark 3. It is worth pointing out that the covariance matrix for a full-state quaternion is singular due to the unit-norm constraint as discussed in [**Lefferts1982**]. Representing attitude as a reduced-dimension vector is one of the effective ways to surmount this singularity.

Several authors have provided different expressions for $\boldsymbol{a}$ in [**Landis2003**] through attitude errors. In this thesis, two methods have been explored. Small-angle rotation (Leffert's method) as shown in [**Shuster1993**] and [**Lefferts1982**] is one of the trivial parametrizations and Twice Gibbs Vector is an alternative as suggested in [**Landis2003**]. These are shown in the equations below.

$$\delta\bar{\boldsymbol{q}}(\boldsymbol{a}_l) = \begin{bmatrix} \boldsymbol{a}_l \\ 1 \end{bmatrix} \tag{1.3c}$$

$$\delta\bar{\boldsymbol{q}}(\boldsymbol{a}_g) = \frac{1}{\sqrt{4 + |\boldsymbol{a}_g|^2}} \begin{bmatrix} \boldsymbol{a}_g \\ 2 \end{bmatrix} \tag{1.3d}$$

where $\boldsymbol{a}_l = \frac{1}{2}\delta\boldsymbol{\theta} = \delta\boldsymbol{q}_v$ and $\boldsymbol{a}_g = \frac{2\delta\boldsymbol{q}_v}{q_0}$. From (1.3c) and (1.3d), it is evident that the Leffert's method has a major drawback that it will fail if an unconstrained estimate is produced such that $|\boldsymbol{a_l}| > 1$. The alternative Twice Gibbs Vector appears to be a more robust representation. This has also been advocated by Landis in [**Landis2003**].

In [**Landis2003**, eq. 36] the quaternion error vector $\dot{\boldsymbol{a}_g}$ propagation has been defined. Considering only the linear terms in this, for the Twice Gibbs vector representation, we get,

$$\dot{\boldsymbol{a}}_g \approx -\hat{\boldsymbol{\omega}} \times \boldsymbol{a}_g + \delta\boldsymbol{\omega} \tag{1.3e}$$

This expression is similar to the one derived by [**Aghili2009**, see App. A]

$$\dot{\boldsymbol{a}}_l \approx -\hat{\boldsymbol{\omega}} \times \boldsymbol{a}_l + \frac{1}{2}\delta\boldsymbol{\omega} \tag{1.3f}$$

where $\hat{\boldsymbol{\omega}}$ is piecewise constant as mentioned in the 1.5.1 section. The difference between the expressions is self-explanatory and can be generalized as,

$$\dot{\boldsymbol{a}} = f_a(\boldsymbol{a}, \delta\boldsymbol{\omega}) \tag{1.3g}$$

Since the orientation quaternion is expressed as a three-dimensional vector $\boldsymbol{a}$, the measurement must be a similar expression. In case the measurement is a set of vector observations, [**Landis2003**] provides a model that can be readily used. If the measurement is a quaternion expression itself, one has two choices.

If the measurement is of the form $\bar{\boldsymbol{r}} = \bar{\boldsymbol{p}} \otimes \bar{\boldsymbol{q}}$ and the state to be estimated is $\bar{\boldsymbol{q}}$, an equivalent expression of $\boldsymbol{a}$ has to be derived from which the residual can be computed during the update stage of estimation. In [**Landis2003**], [**Landis2004**] and [**Shuster1993**], it has already been mentioned that the vector quantity $\boldsymbol{a}$ is reset after an update and is set only when a measurement arrives. Hence, in the event of an incoming measurement, (1.3b) is rewritten as $\delta\bar{\boldsymbol{q}}(\hat{\boldsymbol{a}}) = \hat{\bar{\boldsymbol{q}}} \otimes \bar{\boldsymbol{q}}^*_{ref}$. The measurement is modified as,

$$\begin{aligned} \delta\bar{\boldsymbol{q}}(\breve{\boldsymbol{a}}) &= \bar{\boldsymbol{p}}^* \otimes \bar{\boldsymbol{r}} \otimes \bar{\boldsymbol{q}}^*_{ref} \\ &= \bar{\boldsymbol{p}}^* \otimes \bar{\boldsymbol{p}} \otimes \bar{\boldsymbol{q}} \otimes \bar{\boldsymbol{q}}^*_{ref} \end{aligned} \tag{1.4}$$

By using the relations given in 1.3c and 1.3d, a prediction $\hat{\boldsymbol{a}}$ and a measurement $\breve{\boldsymbol{a}}$ is obtained which can be used in the estimator as an output injection.

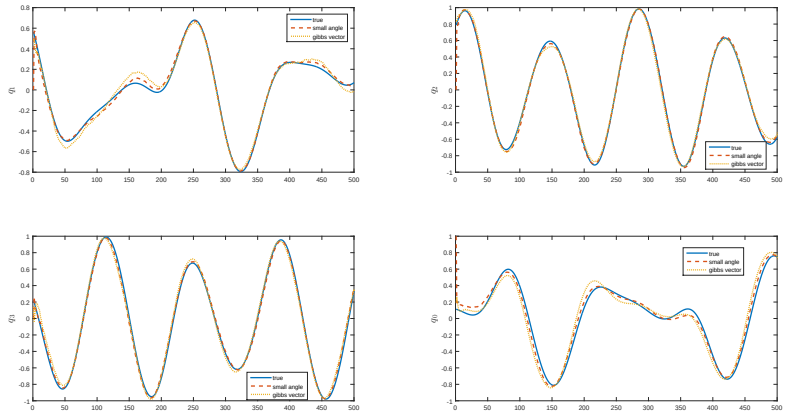

Figure 1.4.: Comparison of true and MEKF states using small angle and Twice-Gibbs vector

An alternative is to simply set $\breve{\boldsymbol{a}} = \mathbf{0}$.

Since (1.2o) conserves the unit-norm property, it is the best candidate for $\bar{\boldsymbol{q}}_{ref}$.

$$\bar{\boldsymbol{q}}_{ref}(k+1) = e^{\frac{1}{2}\bar{\omega}\otimes\Delta T}\bar{\boldsymbol{q}}_{ref}(k) \tag{1.5}$$

This method has also been employed in [**Aghili2009**] and [**Aghili2007**].

1.5.3. Attitude Dynamics

Following the authors in [**Aghili2009**] and [**Aghili2007**], the rotational dynamics are expressed in terms of inertial ratios $\boldsymbol{p}$ by modifying the Newton-Euler equations for torque-free motion. [**Aghili2009**, see App. B]

$$\dot{\boldsymbol{\omega}} = \boldsymbol{\psi}(\boldsymbol{p},\boldsymbol{\omega}) + \mathbf{J}(\boldsymbol{p})\epsilon_\tau \tag{1.6a}$$

where $\boldsymbol{\psi}(\boldsymbol{p},\boldsymbol{\omega}) = \begin{bmatrix} p_x\omega_y\omega_z \\ p_y\omega_x\omega_z \\ p_z\omega_x\omega_y \end{bmatrix}$, $\mathbf{J}(\boldsymbol{p}) = \begin{bmatrix} 1 & 0 & 0 \\ 0 & \frac{1-p_y}{1+p_x} & \\ 0 & 0 & \frac{1+p_z}{1-p_x} \end{bmatrix}$ and $\boldsymbol{p} = \begin{bmatrix} \frac{I_{yy}-I_{zz}}{I_{xx}} \\ \frac{I_{zz}-I_{xx}}{I_{yy}} \\ \frac{I_{xx}-I_{yy}}{I_{zz}} \end{bmatrix}$ and ϵ_τ is the disturbance torque.

Linearizing about a nominal point $\underline{\boldsymbol{\omega}}$ gives

$$\frac{d}{dt}\delta\boldsymbol{\omega} = \mathbf{M}(\underline{\boldsymbol{\omega}})\delta\boldsymbol{\omega} + \mathbf{J}(\boldsymbol{p})\epsilon_\tau \tag{1.6b}$$

where $\mathbf{M}(\underline{\boldsymbol{\omega}}) = \nabla_\omega\boldsymbol{\psi} = \begin{bmatrix} 0 & p_x\omega_z & p_x\omega_y \\ p_y\omega_z & 0 & p_y\omega_x \\ p_z\omega_y & p_z\omega_x & 0 \end{bmatrix}$

Similarly, linearizing about a nominal state-space point, $\underline{\boldsymbol{\omega}}$ and $\underline{\boldsymbol{p}}$ gives,

$$\frac{d}{dt}\delta\boldsymbol{\omega} = \mathbf{M}(\underline{\boldsymbol{\omega}}, \underline{\boldsymbol{p}})\delta\boldsymbol{\omega} + \mathbf{N}(\underline{\boldsymbol{\omega}})\delta\boldsymbol{p} + \mathbf{J}(\boldsymbol{p})\epsilon_\tau \tag{1.6c}$$

Remark 4. (1.6b) is used when the state-estimate for attitude dynamics/kinematics is defined as $\vec{x}_a = \begin{bmatrix}\boldsymbol{a}^T & \boldsymbol{\omega}^T\end{bmatrix}^T$ whereas, (1.6c) is used when state-estimate includes the inertial ratios $\boldsymbol{p}$ as well, $\vec{x}_a = \begin{bmatrix}\boldsymbol{a}^T & \boldsymbol{\omega}^T & \boldsymbol{p}^T\end{bmatrix}^T$. In the latter case, the inertial properties of the tumbling Target are either completely unknown or uncertain. The dynamic equation for this case is

$$\dot{\boldsymbol{p}} = \mathbf{0} \tag{1.6d}$$

1.5.4. Translational motion

The linear time-evolution of relative position between two bodies around a central body is given by the Hill-Clohessy-Wiltshire (HCW) equations [**Clohessy1960**]. Under the assumptions that the Target body is in a reasonably circular orbit (eccentricity, $e \approx 0$), the Earth being spherical and insignificant contribution from nonlinear terms, the HCW equations give closed-form solutions for relative position of a follower (Target) with respect to leader (Servicer). In figure 1.1, $\{\mathcal{A}\}$ is the defined Hill frame and r is the solution to the HCW equations whose components are are given as,

$$\begin{aligned} \ddot{x} - 2n\dot{y} - 3n^2x &= 0 \\ \ddot{y} + 2n\dot{x} &= 0 \\ \ddot{z} + n^2z &= 0 \end{aligned} \tag{1.6e}$$

where n is the mean motion of the Servicer spacecraft in its orbit of radius r_e around Earth, x is directed radially outwards from Earth, y is in-plane tangential to the orbit and z is parallel to the angular momentum vector of the Servicer.

Remark 5. It is important to point out that if the robotic manipulator configuration on the Servicer changes, r_e will be perturbed. In figure 1.1, this perturbation is indicated in change of orbit from $\{\mathcal{O}\}$ to $\{\mathcal{A}\}$. In this thesis, like in [**Aghili2009**], robotic manipulator is assumed to be fixed.

The translation motion r of the Target is given in [**Aghili2009**] as

$$\ddot{\boldsymbol{r}} = -2\boldsymbol{n}\times\dot{\boldsymbol{r}} - \boldsymbol{n}\times(\boldsymbol{n}\times\boldsymbol{r}) + \left(-\mu_e\frac{\boldsymbol{r}_e+\boldsymbol{r}}{||\boldsymbol{r}_e+\boldsymbol{r}||^3} + n^2\boldsymbol{r}_e\right) + \epsilon_f \tag{1.6f}$$

where μ_e is the gravitational parameter of Earth, ϵ_f is a force perturbation, the angular rate n is given by $\sqrt{\frac{\mu_e}{|r_e|^3}}$ and $\boldsymbol{r}_e = \begin{bmatrix} a_s & 0 & 0 \end{bmatrix}^T$ with a_s as the semi-major axis or radius of the orbit.

In [**Aghili2009**] and [**Aghili2007**] the linearization for the translational component is done about $r = \mathbf{0}$ which holds true for the time-interval of a grasping manoeuvre. So, the corresponding state $\vec{x}_r = \begin{bmatrix} r & \dot{r} \end{bmatrix}$ is linearized to,

$$\frac{d}{dt}\delta\vec{x}_r = \begin{bmatrix} \mathbb{O}_3 & \mathbb{I}_3 \\ \boldsymbol{K(n)} & -2\lceil \boldsymbol{n} \rceil \end{bmatrix} \tag{1.6g}$$

where $\boldsymbol{K(n)}$ has been defined in [**Aghili2009**] as $\begin{bmatrix} 3n^2 & 0 & 0 \\ 0 & 0 & 0 \\ 0 & 0 & -n^2 \end{bmatrix}$ and $\boldsymbol{n} = \begin{bmatrix} 0 & 0 & n \end{bmatrix}^T$.

1.5.5. Target geometry

It is quite probable to face a sceneario in which the Target's geometrical parameters are uncertain or unknown. Usually, model-based pose estimation [**Drummond2002**] techniques use a Computer-Aided Design (CAD)-model to compute pose of the Target body. If the model is unavailable, a feature-based pose estimation scheme [**Pi2015**] may be employed. In this case, however, the pose of the grasping point is an unknown. The dynamics of the grasping point pose are unchanging in time. With $\boldsymbol{\rho}_t$ as the position and $\bar{\boldsymbol{\eta}}$ as the orientation quaternion in the body-frame $\{\mathcal{B}\}$, the time-derivatives of pose states, $\vec{x}_\theta = \begin{bmatrix} \boldsymbol{\rho}_t^T & \bar{\boldsymbol{\eta}}^T \end{bmatrix}^T$ is given by,

$$\dot{\vec{x}}_\theta = \mathbf{0} \tag{1.7a}$$

1.6. Measurement Model

The measurement comprises of pose-estimates from a camera which is mounted on the end-effector as shown in figure 1.2. Since, we assume no manipulator motion, $\{\mathcal{A}\}$ and $\{\mathcal{A}_{ee}\}$ are essentially the same. The pose-estimates may be based on a CAD-model, features or fiducial markers like AprilTags. The On-Orbit Simulator at DLR uses a redundant monocular odometry system based on CAD model. In this thesis, for simulation using `V-REP`, AprilTags were employed. Since, the pose determination using visual features is not in the scope of the problem discussed here, the source is not significant.

The measurement comprises of the position vector $\boldsymbol{r_c}$ as observed from $\{\mathcal{A}_{ee}\} \equiv \{\mathcal{A}\}$ to the grasping frame $\{\mathcal{C}\}$, as shown in figure 1.1. The orientation quaternion of the grasping frame as observed from the camera frame is denoted as $\bar{\boldsymbol{\mu}}$. So, the output

function is described as,

$$y : \left\{ \begin{bmatrix} \boldsymbol{r}_c \\ \bar{\boldsymbol{\mu}} \end{bmatrix} = \begin{bmatrix} \boldsymbol{\rho}_c(\boldsymbol{\theta}) + \boldsymbol{r} + \boldsymbol{R}(\bar{\boldsymbol{q}})\boldsymbol{\rho}_t \\ \bar{\boldsymbol{\eta}} \otimes \bar{\boldsymbol{q}} \otimes \bar{\Im}(\boldsymbol{\theta}) \end{bmatrix} \right. \tag{1.8}$$

where $\boldsymbol{\theta}$ is a set of manipulator parameters and $\boldsymbol{\rho}_t$ is expressed in the Target body frame $\{\mathcal{C}\}$.

Going by above assumption, the the Measurement model can be expressed with constant $\bar{\Im}$ and $\boldsymbol{\rho}_c$ as in [**Aghili2009**].

$$y : \left\{ \begin{bmatrix} \boldsymbol{r}_c \\ \bar{\boldsymbol{\mu}} \end{bmatrix} = \begin{bmatrix} \boldsymbol{\rho}_c + \boldsymbol{r} + \boldsymbol{R}(\bar{\boldsymbol{q}})\boldsymbol{\rho}_t \\ \bar{\boldsymbol{\eta}} \otimes \bar{\boldsymbol{q}} \end{bmatrix} \right. \tag{1.9}$$

Rewriting the observation equations in terms of noisy measurements,

$$\boldsymbol{y}_k = \boldsymbol{h}_k(\breve{\boldsymbol{r}}_{c_k}, \breve{\bar{\boldsymbol{\mu}}}_k) \doteq \begin{bmatrix} \boldsymbol{r}_{c_k} - \boldsymbol{\rho}_c \\ (\bar{\boldsymbol{\eta}}_k^* \otimes \breve{\bar{\boldsymbol{\mu}}}_k \otimes \bar{\boldsymbol{q}}_k^*)_v \end{bmatrix} \tag{1.10}$$

Based on the equations derived above, three state-space definitions for a system स (/ˈs/, `Devanagari`) were investigated which are defined as

$$\text{स}_1 : \vec{\mathcal{X}} = \begin{bmatrix} \bar{\boldsymbol{q}}^T & \boldsymbol{\omega}^T & \boldsymbol{r}^T & \dot{\boldsymbol{r}}^T \end{bmatrix}^T \tag{1.11}$$

$$\text{स}_2 : \vec{\mathcal{X}} = \begin{bmatrix} \bar{\boldsymbol{q}}^T & \boldsymbol{\omega}^T & \boldsymbol{p}^T & \boldsymbol{r}^T & \dot{\boldsymbol{r}}^T \end{bmatrix}^T \tag{1.12}$$

$$\text{स}_3 : \vec{\mathcal{X}} = \begin{bmatrix} \bar{\boldsymbol{q}}^T & \boldsymbol{\omega}^T & \boldsymbol{p}^T & \boldsymbol{r}^T & \dot{\boldsymbol{r}}^T & \boldsymbol{\rho}_t^T & \bar{\boldsymbol{\eta}}^T \end{bmatrix}^T \tag{1.13}$$

स_1 is a pose model wherein, the Target's inertial ratios and geometric parameters are assumed to be known. In स_2, the inertial ratios are uncertain while स_3 represents the full-order dynamics of the system. All the above equations can be formed by simply using the relationships given in (1.2f), (1.6a), (1.6d), (1.6f) and (1.7a).

References

[**Lieuwen2016**] Timothy Lieuwen. *Asteroid and Space Debris Manipulation: Advances from the Stardust Research Network*. Reston, VA: American Institute of Aeronautics and Astronautics, 2016.

[**Palmerini2016**] G. B. Palmerini, M. Sabatini, and P. Gasbarri. "Guidelines for active removal of non-functional targets designed to assist rendezvous and capture." In: *2016 IEEE Aerospace Conference*. Mar. 2016, pp. 1–13. DOI: 10.1109/AERO.2016.7500709.

[**Aghili2013**] Farhad Aghili. "Pre- and Post-Grasping Robot Motion Planning To Capture and Stabilize a Tumbling/Drifting Free-Floater with Uncertain Dynamics." In: *IEEE International Conference on Robotics and Automation (ICRA)* 18 (May 2013), pp. 5461–5468.

[**Hutchinson1996**] S. Hutchinson, G. D. Hager, and P. I. Corke. "A tutorial on visual servo control." In: *IEEE Transactions on Robotics and Automation* 12.5 (Oct. 1996), pp. 651–670. ISSN: 1042-296X. DOI: 10.1109/70.538972.

[**Umetani1989**] Yoji Umetani and Kayuya Yoshida. "Resolved Motion Rate Control Of Space Manipulators with Generalized Jacobian Matrix." In: *IEEE Transactions on Robotics and Automation* 5.3 (1989), pp. 303–313.

[**Dubowsky1993**] S. Dubowsky and E. Papadopoulos. "The kinematics, dynamics, and control of free-flying and free-floating space robotic systems." In: *IEEE Transactions on Robotics and Automation* 9.5 (Oct. 1993), pp. 531–543. ISSN: 1042-296X. DOI: 10.1109/70.258046.

[**Clohessy1960**] W. H. Clohessy and R.S. Wiltshire. "Terminal Guidance System for Satellite Rendezvous." In: *Journal of the Aerospace Sciences* 27.9 (1960). doi: 10.2514/8.8704, pp. 653–658. DOI: http://dx.doi.org/10.2514/8.8704.

[**Aghili2009**] Farhad Aghili and Kourosh Parsa. "Motion and Parameter Estimation of Space Objects Using Laser-Vision Data." In: *JOURNAL OF GUIDANCE, CONTROL, AND DYNAMICS* 32.2 (Mar. 2009), pp. 538–550. ISSN: 10.2514/1.37129. DOI: 10.1109/70.258046.

[**Aghili2007**] Farhad Aghili and Kourosh Parsa. "Adaptive motion estimation of a tumbling satellite using laser-vision data with unknown noise characteristics." In: *2007 IEEE/RSJ International Conference on Intelligent Robots and Systems*. Oct. 2007, pp. 839–846. DOI: 10.1109/IROS.2007.4399143.

[**Aghili2012**] F. Aghili. "A Prediction and Motion-Planning Scheme for Visually Guided Robotic Capturing of Free-Floating Tumbling Objects With Uncertain Dynamics." In: *IEEE Transactions on Robotics* 28.3 (June 2012), pp. 634–649. ISSN: 1552-3098. DOI: 10.1109/TRO.2011.2179581.

[**Boutayeb1997**] M. Boutayeb, H. Rafaralahy, and M. Darouach. "Convergence analysis of the extended Kalman filter used as an observer for nonlinear deterministic discrete-time systems." In: *IEEE Transactions on Automatic Control* 42.4 (Apr. 1997), pp. 581–586. ISSN: 0018-9286. DOI: 10.1109/9.566674.

[**Birk1988**] J. Birk and M. Zeitz. "Extended Luenberger observer for non-linear multivariable systems." In: *International Journal of Control* 47.6 (1988), pp. 1823–1836. DOI: 10.1080/00207178808906138. eprint: http://dx.doi.org/10.1080/00207178808906138. URL: http://dx.doi.org/10.1080/00207178808906138.

[**Hermann1977**] Robert Hermann and Arthur Krener. "Nonlinear Controllability and Observability." In: *IEEE transactions on Automatic Control* AC-22.5 (Oct. 1977), pp. 728–740.

[**Krener2009**] Arthur Krener and Kayo Ide. "Measures of Unobservability." In: *Joint 48th IEEE Conference on Decision and Control and 28th Chinese Control Conference Shanghai* AC-22.FrA04.1 (Dec. 2009), pp. 6401–6406.

[**Landis2003**] Markley Landis. "Attitude Error Representations for Kalman Filtering." In: *Journal of Guidance, Control, and Dynamics* 26.2 (2003). doi: 10.2514/2.5048, pp. 311–317. ISSN: 0731-5090. DOI: http://dx.doi.org/10.2514/2.5048.

[**Landis2004**] Markley F. Landis. "Attitude Estimation or Quaternion Estimation?" In: *Journal of the Astronautical Sciences* 52.1/2 (2004), pp. 221–238.

[**Lefferts1982**] E.J. Lefferts, F.L. Markley, and M.D. Shuster. "Kalman filtering for spacecraft attitude estimation." In: Aerospace Sciences Meetings. doi:10.2514/6.1982-70. American Institute of Aeronautics and Astronautics, Jan. 1982. DOI: http://dx.doi.org/10.2514/6.1982-70.

[**Alcantarilla2016**] Pablo Alcantarilla and Oliver Woodford. "Noise Models in Feature-based Stereo Visual Odometry." In: *Physics Letters A* (July 2016). arXiv: 1607.00273v1 [Computer Vision and Pattern Recognition (cs.CV)].

[**Mehra1970**] R. K. Mehra. "Approaches to adaptive filtering." In: *Adaptive Processes (9th) Decision and Control, 1970. 1970 IEEE Symposium on.* Dec. 1970, pp. 141–141. DOI: 10.1109/SAP.1970.269992.

[**Särkkä2009**] S. Särkkä and A. Nummenmaa. "Recursive Noise Adaptive Kalman Filtering by Variational Bayesian Approximations." In: *IEEE Transactions on Automatic Control* 54.3 (Mar. 2009), pp. 596–600. ISSN: 0018-9286. DOI: 10.1109/TAC.2008.2008348.

[**Särkkä2013**] S. Särkkä and J. Hartikainen. "Non-linear noise adaptive Kalman filtering via variational Bayes." In: *2013 IEEE International Workshop on Machine Learning for Signal Processing (MLSP)*. Sept. 2013, pp. 1–6. DOI: 10.1109/MLSP.2013.6661935.

[**Piché2012**] R. Piché, S. Särkkä, and J. Hartikainen. "Recursive outlier-robust filtering and smoothing for nonlinear systems using the multivariate student-t distribution." In: *2012 IEEE International Workshop on Machine Learning for Signal Processing*. Sept. 2012, pp. 1–6. DOI: 10.1109/MLSP.2012.6349794.

[**Roth2013**] M. Roth, E. Özkan, and F. Gustafsson. "A Student's t filter for heavy tailed process and measurement noise." In: *2013 IEEE International Conference on Acoustics, Speech and Signal Processing*. May 2013, pp. 5770–5774. DOI: 10.1109/ICASSP.2013.6638770.

[**Chang2014**] Guobin Chang. "Robust Kalman filtering based on Mahalanobis distance as outlier judging criterion." In: *Journal of Geodesy* 88.4 (2014), pp. 391–401. ISSN: 1432-1394. DOI: 10.1007/s00190-013-0690-8. URL: http://dx.doi.org/10.1007/s00190-013-0690-8.

[**Da Ren1994**] Da Ren. "Failure detection of dynamical systems with the state chi-square test." In: *Journal of Guidance, Control, and Dynamics* 17.2 (1994). doi: 10.2514/3.21193, pp. 271–277. ISSN: 0731-5090. DOI: http://dx.doi.org/10.2514/3.21193.

[**Perea2007**] Laura Perea et al. "Nonlinearity in Sensor Fusion: Divergence Issues in EKF, Modified Truncated GSF, and UKF." In: Guidance, Navigation, and Control and Co-located Conferences. doi:10.2514/6.2007-6514. American Institute of Aeronautics and Astronautics, Aug. 2007. DOI: http://dx.doi.org/10.2514/6.2007-6514.

[**Jazwinski2007**] A.H. Jazwinski. *Stochastic Processes and Filtering Theory*. Dover Books on Electrical Engineering Series. Dover Publications, 2007. ISBN: 9780486462745. URL: https://books.google.co.in/books?id=4AqL3vE2J-sC.

[**Hosseini2016**] A. Hosseini et al. "Modeling and control of an octorotor flying robot using the software in a loop." In: *2016 4th International Conference on Control, Instrumentation, and Automation (ICCIA)*. Jan. 2016, pp. 52–57. DOI: 10.1109/ICCIAutom.2016.7483135.

[**Arioli1996**] M. Arioli, B. Codenotti, and C. Fassino. "The Padé method for computing the matrix exponential." In: *Linear Algebra and its Applications* 240 (1996), pp. 111–130. ISSN: 0024-3795. DOI: 10.1016/0024-3795(94)00190-1. URL: http://www.sciencedirect.com/science/article/pii/0024379594001901.

[**Moler2004**] Cleve Moler and Charles Van Loan. "Nineteen Dubious Ways to Compute the Exponential of a Matrix, Twenty-Five Years Later." In: *Society for Industrial and Applied Mathematics* 45.1 (2004), pp. 1–45.

[**Rohmer2013**] E. Rohmer, S. P. N. Singh, and M. Freese. "V-REP: A versatile and scalable robot simulation framework." In: *2013 IEEE/RSJ International Conference on Intelligent Robots and Systems*. Nov. 2013, pp. 1321–1326. DOI: 10.1109/IROS.2013.6696520.

[**Olson2011**] Edwin Olson. "AprilTag: A robust and flexible visual fiducial system." In: *Proceedings of the IEEE International Conference on Robotics and Automation (ICRA)*. IEEE, May 2011, pp. 3400–3407.

[**Gray2007**] M. A. Gray. "Discrete Event Simulation: A Review of SimEvents." In: *Computing in Science Engineering* 9.6 (Nov. 2007), pp. 62–66. ISSN: 1521-9615. DOI: 10.1109/MCSE.2007.112.

[**Trawny2005**] Nikolas Trawny and Stergios Roumeliotis. *Indirect Kalman Filter for 3D Attitude Estimation*. Technical Report 2005–002. Multiple Autonomous Robotic Systems Laboratory, Mar. 2005.

[**Diebel2006**] James Diebel. *Representing Attitude: Euler Angles, Unit Quaternions, and Rotation Vectors*. Oct. 2006.

[**Rouleau2006**] G. Rouleau et al. "Autonomous capture of a tumbling satellite." In: *Proceedings 2006 IEEE International Conference on Robotics and Automation, 2006. ICRA 2006.* May 2006, pp. 3855–3860. DOI: 10.1109/ROBOT.2006.1642292.

[**Shuster1993**] Malcolm Shuster. "Quaternion in Kalman Filtering." In: *AAS/AIAA Astrodynamics Conference* 85.AAS 93-553 (Aug. 1993), pp. 25–37.

[**Drummond2002**] T. Drummond and R. Cipolla. "Real-time visual tracking of complex structures." In: *IEEE Transactions on Pattern Analysis and Machine Intelligence* 24.7 (July 2002), pp. 932–946. ISSN: 0162-8828. DOI: 10.1109/TPAMI.2002.1017620.

[**Pi2015**] Edgar Riba Pi. "Implementation of a 3D pose estimation algorithm." Masters Thesis. Insitut de Robotica i Informatica Industrial, 2015.

Chapter 2: Observability

2.1. Dynamic Systems

From the theory of dynamic systems that have been investigated in [**Hermann1977**], we know that a time-varying deterministic system स (/'s/, `Devanagari`) can be modeled as a state-space representation as follows,

$$\text{स} : \begin{cases} \dot{x}(t) = f(t, x(t), u(t)) \\ y(t) = h(x(t), u(t)) \end{cases} \tag{2.1a}$$

We assume that in the system स, states $x(t) \in \mathbb{X}$, observation $y(t) \in \mathbb{Y}$ and control inputs $u(t) \in \mathbb{U}$, with $\mathbb{X}$, $\mathbb{U}$ and $\mathbb{Y}$ being sufficiently continuously differentiable manifolds of dimensions n, n_u and p respectively, where $f : \mathbb{X} \times \mathbb{U} \to \mathbb{X}$, $h : \mathbb{X} \to \mathbb{Y}$, the state-space $\mathbb{X} = \mathbb{R}^n$, input space $\mathbb{U} = \mathbb{R}^{n_u}$, and the observation space, $\mathbb{Y} = \mathbb{R}^p$. The system स evolves from time, $t = t_0$ with an initial state $x(t = t_0) = x_{t_0}$ and the sequences of inputs and outputs in time $t \in (t_0, t_f]$ are denoted as $\{u\}^{t_f}$ and $\{y\}^{t_f}$ respectively.
The system in (2.1a) is a generic nonlinear representation. If the system is completely linear but time varying, as is the case for linearized systems, we get the form,

$$\text{स} : \begin{cases} \dot{x}(t) = A_t x(t) + B_t u(t) \\ y(t) = H_t x(t) + D_t u(t) \end{cases} \tag{2.1b}$$

where system matrix $A_t \in \mathbb{R}^{n \times n}$, input matrix $B_t \in \mathbb{R}^{n \times n_u}$, output matrix $H_t \in \mathbb{R}^{p \times n}$ and feedthrough matrix $D_t \in \mathbb{R}^{p \times n_u}$.

If the model in (2.1b) is time-invariant, it can be represented as a Linear Time Invariant (LTI) system in a further simplified form,

$$\text{स} : \begin{cases} \dot{x}(t) = Ax(t) + Bu(t) \\ y(t) = Hx(t) + Du(t) \end{cases} \tag{2.1c}$$

where the matrices, A, B, C, and D carry the same definitions as in (2.1b).

2.2. Observability Problem

In [**Liu2002**], Liu, in his thesis, has provided some theoretical definitions which we are going to mention here for developing the the theory.

Definition 2.1. The initial state x_{t_0} is *observable* if after some some finite time τ and any $t_f > \tau$, the output sequence $\{y\}^{t_f}$ and input sequence $\{u\}^{t_f}$ uniquely determines x_{t_0}.

The Observability problem, as explained in [**Anguelova2004**], is an investigation of the existing relationships of the state variables with the derivatives of the inputs and outputs of the system which ensures their uniqueness in a local neighbourhood. In [**Anguelova2004**], Anguelova further explains that in the absence of such a relationship, there can be multiple solutions that produce the same output for every input and hence the states cannot be reliably observed from experimental measurements.

Definition 2.2. Any arbitrary state (like current-state) x_{t_f} is said to be *reconstructible* if after some some finite time τ and any $t_f > \tau$, the output sequence $\{y\}^{t_f}$ and input sequence $\{u\}^{t_f}$ uniquely determines x_{t_f}.

It is important to note that if there are no input disturbances to स, *observability* is a sufficient condition for *reconstructability*. Furthermore, the observability problem must be satisfied in some abstract form for ensuring correct state estimates from experimental measurements.

Remark 6. Under the assumption that the models employed in this thesis do not have any inputs, we need to determine the Observability to establish reconstructability.

While definitions 2.1 and 2.2 in [**Liu2002**] have described the observability problem from the perspective of linear systems, we are interested in the same problem in nonlinear systems. The theoretical basis for such an approach can be found in [**Hermann1977**] which shall be explained in brief.Hermann and Krener have described two possible deficiencies of the state space $\mathbb{X}$. In the first kind, $\mathbb{X}$ maybe too trivial which results in the observer tracking incorrect trajectories in the state space. To understand this, we should look at the state space $\mathbb{X}$ in (2.1) as a union of the state spaces spanned by the dynamic states and constant parameters. To simplify the problem, let us assume that the system has no measurable external input, $u(t) = \mathbf{0}$, and is not explicitly time-dependent.

$$\text{स} : \begin{cases} \dot{x}(t) = f(x_s, \theta) \\ y(t) = h(x_s, \theta) \end{cases} \tag{2.2}$$

The model defined in (2.2) is additionally parametrized by a constant unknown vector θ and dynamic states x_s in comparison to (2.1) and $x = [x_s^T \, \theta^T]^T$. In the state space

deficiency of the first kind, we refer to a reduced order Observer system, where some or all of θ are assumed to be known. In case, there is an error in this prior knowledge, the state vector $\hat{x}$ will converge to incorrect values in $\mathbb{X}$. On the other hand, if the state space $\mathbb{X}$ is too complex, it becomes increasingly difficult to distinguish between similar states for the same output observations. At this point, it is important to put forth some definitions based on [**Hermann1977**], in the absence of inputs.

Definition 2.3. In the dynamic system स, given by (2.1), two initial states x_0, $x_1 \in \mathbb{X}$ are *indistinguishable* if

$$y(x_0, t) = y(x_1, t) \quad \forall\ t \in [t_0, t_f]$$

where $\mathbb{I}$ is an equivalence relation on $\mathbb{X}$, and is denoted as $x_0 \mathbb{I} x_1$.

Definition 2.4. The dynamic system स is said to be observable at x_0 if $\mathbb{I}(x_0) = \{x_0\}$ and, it is observable if $\mathbb{I}(x) = \{x\}\ \forall x \in \mathbb{X}$.

Observability is a global concept and hence the trajectories spanned in $\mathbb{X}$ could be tediously long and traversed over a long time to ensure that it is satisfied by *indistinguishability* in 2.4. Hence it is prudent to provide more locally specific definitions which serve the same purpose.

Definition 2.5. In the dynamic system स, two initial states x_0, $x_1 \in U$ and $U \subset \mathbb{X}$ are *U-indistinguishable* if the state trajectories, $x_0(t), x_1(t) \in U$ and

$$y(x_0, t) = y(x_1, t) \quad \forall\ t \in [t_0, t_f]$$

where $\mathbb{I}_U$ is a relation (not equivalence) on U, and is denoted as $x_0 \mathbb{I}_U x_1$.

Definition 2.6. The dynamic system स is said to be be *locally* observable at initial state x_0 if for every open neighbourhood U of x_0, $\mathbb{I}_U(x_0) = \{x_0\}$; and it is *locally* observable if it is so $\forall x \in \mathbb{X}$.

In practice, it is sufficient to distinguish x_0 from its immediate neighbours and hence a weaker definition can be given.

Definition 2.7. The dynamic system स is said to be be *weakly* observable at initial state x_0 if there exists a neighbourhood U of x_0 such that $\mathbb{I}(x_0) \cap U = \{x_0\}$; and it is *weakly* observable if it is so $\forall x \in \mathbb{X}$.

The definition in 2.7, like 2.3 also suffers from possibly tedious trajectories and large time-intervals before the *indistinguishability* relation is satisfied.

Definition 2.8. The dynamic system स is said to be be *locally weakly* observable at initial state x_0 if there exists an open neighbourhood U of x_0 such that for every neighbourhood V of x_0 contained in U, $\mathbb{I}_V(x_0) = \{x_0\}$; and it is *locally weakly* observable if it is so $\forall x \in \mathbb{X}$.

In [**Hermann1977**], the authors have provided a taxonomical relationship between different forms of observability as follows:

स : *Locally Observable* ⇒ स: *Observable*

⇓ ⇓

स : *Locally Weakly Observable* ⇒ स: *Weakly Observable*

The main importance of the definition 2.8 is that it lends to a simple algebraic test - The *Observability Rank Condition (ORC)* - which can be used to indicate a notion of observability.

For simple Linear Time Invariant (LTI) systems, the aforementioned definitions of observability are all equivalent.

An alternative approach to the Observability problem has been given in [**Kou1973**] where the authors have provided tests based on ratios and positive semi-definiteness of Jacobian of Output mappings (Observability Matrix); however, the methods are difficult for complicated systems to derive. In [**Zhirabok2012**], Zhirabok and Shumsky have introduced a new approach to nonlinear observability study by fragmenting the system into a linear and nonlinear part. The observability study is then extended to the nonlinear parts only if the linear parts are unobservable. The current work does not explore this approach but this is a germane topic for future study. In [**Anguelova2004**], it was mentioned that if the system is not observable, the state estimates do not converge to correct trajectories. It is important to cite Detectability as a weaker concept which ensures convergence by virtue of stability of unobservable modes of a Linear System. An analogous concept for nonlinear systems of Output-to-State stability has been discussed in [**Sontag1997**] which is based on identifying the Lyapunov function. In this thesis, this method was not investigated since the models were too complex and moreover, all studies were made under observable conditions.

2.3. The Observability Rank Condition

This section describes the observability evaluation by investigating the local distinguishability property using the *Observability Rank Condition (ORC)* as introduced before.

We define the Lie differentiation of C^∞ function ϕ on $\mathbb{X}$ by a vector field v on $\mathbb{X}$ as,

$$L_v(\phi)(x) := < \nabla_x(\phi), v >$$

here, $<>$ defines the inner product and $d\phi$ is the gradient operator on scalar function ϕ.

We redefine (2.1) to drop the explicit time-dependence and assume control inputs,

$u = \mathbf{0}$.

$$\text{स} : \begin{cases} \dot{x}(t) = f(x(t)) \\ y(t) = h(x(t)) \end{cases} \tag{2.3}$$

In the previous section, it was mentioned that the observability problem is aimed at finding relationships between states and derivatives of outputs and inputs of the system स. The first time-derivative, Y^1 of the output y in (2.3) can be found as follows

$$\begin{aligned} Y^1 = \frac{dh}{dt} = \frac{\partial h}{\partial x}.\frac{dx}{dt} = \frac{\partial h}{\partial x}.\dot{x} \\ =< \nabla_x(h), f > = L_f(h) \end{aligned}$$

by replacing *Lie Derivative* defined above for the function ϕ as f and v as h. Similarly, taking *mth* time derivative of the output function,

$$\begin{aligned} Y^m = \frac{d^m h}{dt^m} = \frac{d^{m-1} L_f(h)}{dt^{m-1}} = \frac{d^{m-2}}{dt^{m-2}}\left(\frac{dL_f(h)}{dt}\right) \\ = \frac{d^{m-2}}{dt^{m-2}}(L_f.L_f(h)) = {L_f}^m h \end{aligned}$$

Hence, we see that the time-derivatives of the observation function are nothing but the Lie differentials of the same order.

In [**Hermann1977**] and in [**Anguelova2004**], the ORC has been defined as,

$$\mathcal{O}^\infty = \begin{bmatrix} \nabla_x(h) \\ \nabla_x L_f(h) \\ ... \\ \nabla_x L_f^{n-1}(h) \\ ... \end{bmatrix} \tag{2.4a}$$

where, the Observability matrix in (2.4a) is the local infinite dimensional matrix for the nonlinear system. If $rank(\mathcal{O}^\infty)$ is equal to n, the system is locally weakly observable. Since no bound is provided for the number of Lie Derivatives to be computed, it is impractical for sophisticated systems. In [**Anguelova2004**], Chapter-4, it has been proven that for control affine systems, only $n-1$ derivatives have to be computed for a state vector of dimension n. Furthermore, in case the state $x = [x_1^T, x_2^T, ...x_n^T]^T$, where x_i is a vector representing a measurable quantity in all its dimensions, it is sufficient to find n Lie derivatives and determine $\mathcal{O}^n$.

$$\mathcal{O}^n = \begin{bmatrix} \nabla_x(h) \\ \nabla_x L_f(h) \\ ... \\ \nabla_x L_f^{n-1}(h) \end{bmatrix} \tag{2.4b}$$

The system is said to be locally weakly observable when $rank(\mathcal{O}^n)$ is n.

Remark 7. Since, we are concerned with no-input systems, we can assume our system to be input-affine and hence applying $n-1$ derivatives is sufficient to determine Observability using (2.4b). In order to construct the matrix, a symbolic tools like `sympi` and `MATLAB Symbolic Toolbox` can be employed.

2.4. Unobservability

In the previous section, it was established that observed nonlinear dynamics are observable only if the mapping from an initial condition, x_{t_0} to the output trajectory are unique. To establish this mapping, ORC provides a simple algebraic test. However,the computation of (2.4b) for sophisticated state-space models is tedious and time-consuming, even on a symbolic tool. In [**Krener2009**], Krener and Ide have derived two metrics, namely, *local unobservability index*, κ_i and *local condition number*, κ_n which measure the degree of observability of the system. Hence, apart from obtaining the binary test of observability using ORC, we obtain a measure of the ease with which states can be observed/estimated. Questions pertaining to observability quality were raised for the first time by Griffith and Kumar in [**Griffith1971**].

In the following section, the metrics, κ_i and κ_n will be explained as measures of observability. Since, the derivation of these metrics is based on the linearized model, this section begins by deriving the linearized model using truncated Taylor Series which takes the form (2.1b).

2.4.1. Linearization of nonlinear system

In section 2.1, it was mentioned that a time-varying system of the form (2.1b) is obtained by approximating a nonlinear system, (2.1a), as a linearization about a point in state-space. Working under the no-input assumption, the system is reduced to the following form, if it is linearized about the initial state x_{t_0},

$$\text{स} : \begin{cases} \dot{\delta x}(t) = A_t \delta x(t) \\ \delta y(t) = H_t \delta x(t) \end{cases} \tag{2.5}$$

where,

$$A_t = \left.\frac{\partial f(x(t))}{\partial x}\right|_{x=x_{t_0}}$$
$$H_t = \left.\frac{\partial h(x(t))}{\partial x}\right|_{x=x_{t_0}}$$
$$\delta x(t) = x(t) - x_{t_0}$$
$$\delta y(t) = y(t) - h(x_{t_0})$$

Remark 8. The mapping from x_{t_0} to $\{y\}^t$ is approximated by the mapping from δx_{t_0} to $\{\delta y\}^t$ which is the tangent space of the original state-space.

According to [**Krener2009**], the *local singular values* at x_{t_0} of the system defined by (2.1a) are the same as its tangent linear mapping defined in (2.5). For distinguishability, all the singular values should be high.

2.4.2. Measures of Unobservability

In this subsection, a brief description of the singular value metrics [**Krener2009**] as measures of unobservability have been described.

Definition 2.9. *Local Unobservability index*, κ_i: The reciprocal of the smallest local singular value.

$$\kappa_i = \frac{1}{\sqrt{\lambda_{min}}}$$

If this value is very high, the measurement noise of the estimation scheme will have a large impact on Estimation error.

Definition 2.10. *Local Estimation Condition Number*, κ_n: The ratio of the largest and the smallest local singular value.

$$\kappa_n = \sqrt{\frac{\lambda_{max}}{\lambda_{min}}}$$

A large value for this metric indicates sensitivity to the initial condition. In other words, a small change in the initial state can radically change the direction of estimation in the state-space.

The metrics described above can be derived from the *Observability Gramian*, $\mathcal{G}_o$ at x_{t_0} of the time-varying system described in (2.5). In [**Krener2009**], a simpler method has been employed to compute $\mathcal{G}_o$. In the models employed in this thesis, however, the

conventional form of the Gramian is computed in order to obtain κ_i and κ_n. For the system defined by (2.5), the Gramian at x_{t_0} for $t \in [t_0, t_f]$ is,

$$\mathcal{G}_o = \int_{t_0}^{t_f} \Phi(t,\tau)^T H(\tau)^T H(\tau) \Phi(t,\tau) d\tau \tag{2.6}$$

where $\Phi(t, t_0)$ is the state-transition matrix associated with the homogeneous equation (2.5). In [**Krener2009**, eq. 4], the formula for the empirical observability gramian has been provided. The empirical observability approaches the true gramian if the displacement along the state-space basis is small. In this thesis, an analysis of the aforementioned measures of unobservabilty is performed for the systems.

In [**Krener2009**], it has been mentioned that scaling of parameters should be performed but it is not necessary for the models discussed in this thesis. Furthermore, κ_i should be a non-increasing function of time and κ_n should be atleast bounded for stability of the estimator.

2.5. Observability analysis

2.5.1. System स$_1$

In chapter 1, स$_1$ was derived to have the state-space as,

$$\begin{bmatrix} \dot{\bar{q}} \\ \dot{\omega} \\ \dot{r} \\ \ddot{r} \end{bmatrix} = \begin{bmatrix} \frac{1}{2}\bar{\omega} \otimes \bar{q}(t) \\ \psi(\omega) \\ \dot{r} \\ -2n \times \dot{r} - n \times (n \times r) + \left(- \mu_e \frac{r_e + r}{||r_e + r||^3} + n^2 r_e \right) \end{bmatrix} \tag{2.7}$$

For short time observability analysis, we can assume zero-acceleration for the model and ignore the effect of the HCW equations. Hence,

$$\text{स}_1 : \begin{cases} \dot{\mathcal{X}} = \begin{bmatrix} \dot{\bar{q}} \\ \dot{\omega} \\ \dot{r} \\ \ddot{r} \end{bmatrix} = \begin{bmatrix} \frac{1}{2}\bar{\omega} \otimes \bar{q}(t) \\ \psi(\omega) \\ \dot{r} \\ \mathbf{0} \end{bmatrix} \\ y = \begin{bmatrix} r_c(\bar{q}, r) \\ \bar{\mu}(\bar{q}) \end{bmatrix}, \qquad \bar{q}^T \bar{q} - 1 = 0 \end{cases} \tag{2.8}$$

It is important to note that $\bar{q}^T \bar{q} - 1 = 0$ is added to the above output equation [**Sabatini2011**] to ensure the quaternion constraint.

Taking the ORC of the system, we get,

$$\mathcal{O}^2 = \left[\begin{array}{cccc} \boldsymbol{\Theta}(\bar{\boldsymbol{q}}) & \mathbb{O}_{3,3} & \mathbb{I}_{3,3} & \mathbb{O}_{3,3} \\ \bar{\boldsymbol{\eta}}\otimes & \mathbb{O}_{4,3} & \mathbb{O}_{4,3} & \mathbb{O}_{4,3} \\ 2\bar{\boldsymbol{q}}^T & \mathbb{O}_{1,3} & \mathbb{O}_{1,3} & \mathbb{O}_{1,3} \\ \hdashline \boldsymbol{\Theta}_q(\boldsymbol{q},\boldsymbol{\omega}_t) & \mathbb{O}_{3,3} & \mathbb{O}_{3,3} & \mathbb{I}_{3,3} \\ \frac{1}{2}\bar{\boldsymbol{\eta}}\otimes\bar{\boldsymbol{\omega}}\otimes & \frac{1}{2}\bar{\boldsymbol{\eta}}\otimes\bar{\boldsymbol{q}}\circledast & \mathbb{O}_{4,3} & \mathbb{O}_{4,3} \\ \mathbb{O}_{1,4} & \mathbb{O}_{1,3} & \mathbb{O}_{1,3} & \mathbb{O}_{1,3} \end{array}\right] \tag{2.9}$$

where, $\boldsymbol{\Theta}(\boldsymbol{q},\boldsymbol{p}) = \nabla_q(\boldsymbol{R}(\bar{\boldsymbol{q}})\boldsymbol{p}) = \begin{bmatrix} -2q_0\lceil\boldsymbol{p}\rceil + 2(\lceil\boldsymbol{p}\rceil\lceil\boldsymbol{q}_v\rceil - 2\lceil\boldsymbol{q}_v\rceil\lceil\boldsymbol{p}\rceil) & 2\lceil\boldsymbol{q}_v\rceil\boldsymbol{p} \end{bmatrix}$ and $\boldsymbol{\Theta}_q(\bar{\boldsymbol{q}},\boldsymbol{p}) = \nabla_q(\boldsymbol{\Theta}(\boldsymbol{q},\boldsymbol{p})\frac{1}{2}\bar{\boldsymbol{\omega}}\otimes\bar{\boldsymbol{q}})$ The dashed lines indicate the Jacobian dependent on the next Lie Derivative. In this case, only the first derivative was sufficient.

Remark 9. Since, the $\otimes$ and $\circledast$ operators produce full rank matrices under all conditions for a quaternion, the ORC for the system above comes out as 13 and hence is always observable. This system is able to distinguish states even if the Target is stationary.

2.5.2. System स$_2$

Following the same course as the previous section, we derive the ORC for system स$_2$ defined in (1.12).

$$\text{स}_2 : \begin{cases} \dot{\mathcal{X}} &= \begin{bmatrix} \dot{\bar{\boldsymbol{q}}} \\ \dot{\boldsymbol{\omega}} \\ \dot{\boldsymbol{p}} \\ \dot{\boldsymbol{r}} \\ \ddot{\boldsymbol{r}} \end{bmatrix} = \begin{bmatrix} \frac{1}{2}\bar{\boldsymbol{\omega}}\otimes\bar{\boldsymbol{q}}(t) \\ \boldsymbol{\psi}(\boldsymbol{\omega}) \\ \boldsymbol{0} \\ \dot{\boldsymbol{r}} \\ \boldsymbol{0} \end{bmatrix} \\ \boldsymbol{y} &= \begin{bmatrix} \boldsymbol{r}_c(\bar{\boldsymbol{q}},\boldsymbol{r}) \\ \bar{\boldsymbol{\mu}}(\bar{\boldsymbol{q}}) \end{bmatrix}, \qquad \bar{\boldsymbol{q}}^T\bar{\boldsymbol{q}} - 1 = 0 \end{cases} \tag{2.10}$$

$$\mathcal{O}^3 = \left[\begin{array}{ccccc} \boldsymbol{\Theta}(\bar{\boldsymbol{q}}) & \mathbb{O}_{3,3} & \mathbb{O}_{3,3} & \mathbb{I}_{3,3} & \mathbb{O}_{3,3} \\ \bar{\boldsymbol{\eta}}\otimes & \mathbb{O}_{4,3} & \mathbb{O}_{4,3} & \mathbb{O}_{4,3} & \mathbb{O}_{4,3} \\ 2\bar{\boldsymbol{q}}^T & \mathbb{O}_{1,3} & \mathbb{O}_{1,3} & \mathbb{O}_{1,3} & \mathbb{O}_{1,3} \\ \hdashline \boldsymbol{\Theta}_q(\boldsymbol{q}) & \mathbb{O}_{3,3} & \mathbb{O}_{3,3} & \mathbb{O}_{3,3} & \mathbb{I}_{3,3} \\ \frac{1}{2}\bar{\boldsymbol{\eta}}\otimes\bar{\boldsymbol{\omega}}\otimes & \frac{1}{2}\bar{\boldsymbol{\eta}}\otimes\bar{\boldsymbol{q}}\circledast & \mathbb{O}_{4,3} & \mathbb{O}_{4,3} & \mathbb{O}_{4,3} \\ \mathbb{O}_{1,4} & \mathbb{O}_{1,3} & \mathbb{O}_{1,3} & \mathbb{O}_{1,3} & \mathbb{O}_{1,3} \\ \hdashline \boldsymbol{\Gamma}_q(\bar{\boldsymbol{q}},\boldsymbol{p},\boldsymbol{\omega}) & \boldsymbol{\Gamma}_\omega(\bar{\boldsymbol{q}},\boldsymbol{p},\boldsymbol{\omega}) & \boldsymbol{\Gamma}_p(\bar{\boldsymbol{q}},\boldsymbol{\omega}) & \mathbb{O}_{3,3} & \mathbb{O}_{3,3} \\ \boldsymbol{\zeta}_q(\boldsymbol{\omega},\boldsymbol{p}) & \boldsymbol{\zeta}_\omega(\bar{\boldsymbol{q}},\boldsymbol{p}) & \boldsymbol{\zeta}_p(\bar{\boldsymbol{q}},\boldsymbol{\omega}) & \mathbb{O}_{4,3} & \mathbb{O}_{4,3} \\ \mathbb{O}_{1,3} & \mathbb{O}_{1,3} & \mathbb{O}_{1,3} & \mathbb{O}_{1,3} & \mathbb{O}_{1,3} \end{array}\right] \tag{2.11}$$

Remark 10. The ORC is found to be 16 which is full rank when all three components of $\boldsymbol{\omega}$ are non-zero. For a pure spin-system, the rank is found to be 13. Even for $\boldsymbol{\omega}$

with two non-zero components, the rank is 14. Hence, it is evident that the system स_2 is observable only if the Target is exhibiting purely tumbling motion. It is evident from the ORC that the matrices in the lowest section become rank deficient when $\boldsymbol{\omega}$ has either one or more components as 0.

2.5.3. System स_3

For the full-state dynamics, the calculation of the system is defined as follows.

$$\text{स}_3 : \begin{cases} \dot{\mathcal{X}} &= \begin{bmatrix} \dot{\bar{\boldsymbol{q}}} \\ \dot{\boldsymbol{\omega}} \\ \dot{\boldsymbol{p}} \\ \dot{\boldsymbol{r}} \\ \ddot{\boldsymbol{r}} \\ \dot{\boldsymbol{\rho}}_t \\ \dot{\bar{\boldsymbol{\eta}}} \end{bmatrix} = \begin{bmatrix} \frac{1}{2}\bar{\boldsymbol{\omega}} \otimes \bar{\boldsymbol{q}}(t) \\ \boldsymbol{\psi}(\boldsymbol{\omega}) \\ \mathbf{0} \\ \dot{\boldsymbol{r}} \\ \mathbf{0} \\ \mathbf{0} \\ \mathbf{0} \end{bmatrix} \\ \boldsymbol{y} &= \begin{bmatrix} \boldsymbol{r}_c(\bar{\boldsymbol{q}}, \boldsymbol{r}, \boldsymbol{\rho}_t) \\ \bar{\boldsymbol{\mu}}(\bar{\boldsymbol{q}}, \bar{\boldsymbol{\eta}}) \end{bmatrix}, \quad \begin{matrix} \bar{\boldsymbol{q}}^T \bar{\boldsymbol{q}} - 1 = 0 \\ \bar{\boldsymbol{\eta}}^T \bar{\boldsymbol{\eta}} - 1 = 0 \end{matrix} \end{cases} \tag{2.12}$$

The ORC calculation for this system is a little more convoluted than the previous ones. But, we can draw many of the sub-matrices from them.

$\mathcal{O}^4 =$

$$\left[\begin{array}{ccccccc} \boldsymbol{\Theta}(\bar{\boldsymbol{q}}, \boldsymbol{\rho}_t) & \mathbb{O}_{3,3} & \mathbb{O}_{3,3} & \mathbb{I}_{3,3} & \mathbb{O}_{3,3} & \boldsymbol{R}(\bar{\boldsymbol{q}}) & \mathbb{O}_{3,4} \\ \bar{\boldsymbol{\eta}} \otimes & \mathbb{O}_{4,3} & \mathbb{O}_{4,3} & \mathbb{O}_{4,3} & \mathbb{O}_{4,3} & \mathbb{O}_{4,3} & \bar{\boldsymbol{\eta}} \circledast \\ 2\bar{\boldsymbol{q}}^T & \mathbb{O}_{1,3} & \mathbb{O}_{1,3} & \mathbb{O}_{1,3} & \mathbb{O}_{1,3} & \mathbb{O}_{1,3} & \mathbb{O}_{1,3} \\ \mathbb{O}_{1,4} & \mathbb{O}_{1,3} & \mathbb{O}_{1,3} & \mathbb{O}_{1,3} & \mathbb{O}_{1,3} & \mathbb{O}_{1,3} & 2\bar{\boldsymbol{\eta}}^T \\ \hline \boldsymbol{\Theta}_q(\bar{\boldsymbol{q}}, \boldsymbol{\rho}_t, \boldsymbol{\omega}) & \boldsymbol{\Theta}_\omega(\bar{\boldsymbol{q}}, \boldsymbol{\rho}_t) & \mathbb{O}_{3,3} & \mathbb{O}_{3,3} & \mathbb{I}_{3,3} & \boldsymbol{\Theta}_{\rho_t}(\bar{\boldsymbol{q}}, \boldsymbol{\omega}) & \mathbb{O}_{3,4} \\ \frac{1}{2}\bar{\boldsymbol{\eta}} \otimes \bar{\boldsymbol{\omega}} \otimes & \frac{1}{2}\bar{\boldsymbol{\eta}} \otimes \bar{\boldsymbol{q}} \circledast & \mathbb{O}_{4,3} & \mathbb{O}_{4,3} & \mathbb{O}_{4,3} & \mathbb{O}_{4,3} & \frac{1}{2}\bar{\boldsymbol{\omega}} \otimes \bar{\boldsymbol{q}} \circledast \\ \mathbb{O}_{1,4} & \mathbb{O}_{1,3} & \mathbb{O}_{1,3} & \mathbb{O}_{1,3} & \mathbb{O}_{1,3} & \mathbb{O}_{1,3} & \mathbb{O}_{1,4} \\ \mathbb{O}_{1,4} & \mathbb{O}_{1,3} & \mathbb{O}_{1,3} & \mathbb{O}_{1,3} & \mathbb{O}_{1,3} & \mathbb{O}_{1,3} & \mathbb{O}_{1,4} \\ \hline \boldsymbol{\Gamma}_q(\bar{\boldsymbol{q}}, \boldsymbol{p}, \boldsymbol{\omega}, \boldsymbol{\rho}_t) & \boldsymbol{\Gamma}_\omega(\bar{\boldsymbol{q}}, \boldsymbol{p}, \boldsymbol{\omega}, \boldsymbol{\rho}_t) & \boldsymbol{\Gamma}_p(\bar{\boldsymbol{q}}, \boldsymbol{\omega}, \boldsymbol{\rho}_t) & \mathbb{O}_{3,3} & \mathbb{O}_{3,3} & \boldsymbol{\Gamma}_p(\bar{\boldsymbol{q}}, \boldsymbol{\omega}, \boldsymbol{p}) & \mathbb{O}_{3,4} \\ \boldsymbol{\zeta}_q(\boldsymbol{\omega}, \boldsymbol{p}, \bar{\boldsymbol{\eta}}) & \boldsymbol{\zeta}_\omega(\bar{\boldsymbol{q}}, \boldsymbol{p}, \bar{\boldsymbol{\eta}}, \boldsymbol{\omega}) & \boldsymbol{\zeta}_p(\bar{\boldsymbol{q}}, \boldsymbol{\omega}) & \mathbb{O}_{4,3} & \mathbb{O}_{4,3} & \mathbb{O}_{4,3} & \boldsymbol{\zeta}_\eta(\bar{\boldsymbol{q}}, \boldsymbol{\omega}, \boldsymbol{p}) \\ \mathbb{O}_{1,4} & \mathbb{O}_{1,3} & \mathbb{O}_{1,3} & \mathbb{O}_{1,3} & \mathbb{O}_{1,3} & \mathbb{O}_{1,3} & \mathbb{O}_{1,4} \\ \mathbb{O}_{1,4} & \mathbb{O}_{1,3} & \mathbb{O}_{1,3} & \mathbb{O}_{1,3} & \mathbb{O}_{1,3} & \mathbb{O}_{1,3} & \mathbb{O}_{1,4} \\ \hline \boldsymbol{\Lambda}_q(\bar{\boldsymbol{q}}, \boldsymbol{p}, \boldsymbol{\omega}, \boldsymbol{\rho}_t) & \boldsymbol{\Lambda}_\omega(\bar{\boldsymbol{q}}, \boldsymbol{p}, \boldsymbol{\omega}, \boldsymbol{\rho}_t) & \boldsymbol{\Lambda}_p(\bar{\boldsymbol{q}}, \boldsymbol{\omega}, \boldsymbol{\rho}_t) & \mathbb{O}_{3,3} & \mathbb{O}_{3,3} & \boldsymbol{\Lambda}_p(\bar{\boldsymbol{q}}, \boldsymbol{\omega}, \boldsymbol{p}, \boldsymbol{\rho}_t) & \mathbb{O}_{3,4} \\ \boldsymbol{\Phi}_q(\boldsymbol{\omega}, \boldsymbol{p}, \bar{\boldsymbol{\eta}}, \boldsymbol{\rho}_t) & \boldsymbol{\Phi}_\omega(\bar{\boldsymbol{q}}, \bar{\boldsymbol{\eta}}) & \boldsymbol{\Phi}_p(\bar{\boldsymbol{q}}, \boldsymbol{\omega}, \boldsymbol{p}) & \mathbb{O}_{4,3} & \mathbb{O}_{4,3} & \mathbb{O}_{4,3} & \boldsymbol{\Phi}_\eta(\bar{\boldsymbol{q}}, \boldsymbol{\omega}, \boldsymbol{p}) \\ \mathbb{O}_{1,4} & \mathbb{O}_{1,3} & \mathbb{O}_{1,3} & \mathbb{O}_{1,3} & \mathbb{O}_{1,3} & \mathbb{O}_{1,3} & \mathbb{O}_{1,4} \\ \mathbb{O}_{1,4} & \mathbb{O}_{1,3} & \mathbb{O}_{1,3} & \mathbb{O}_{1,3} & \mathbb{O}_{1,3} & \mathbb{O}_{1,3} & \mathbb{O}_{1,4} \end{array}\right] \tag{2.13}$$

Remark 11. The ORC as defined in (2.13) is found to be of rank 23 when evaluated using a symbolic toolbox. Evidently, the ORC is deficient and has a rank of 14 when there is no angular velocity for the Target. For pure spin, the rank increases to 18. Even for two axis of non-zero values in $\boldsymbol{\omega}$, the rank is 22 and achieves full rank only when there is purely tumbling motion. Another point worth mentioning is the dependency on the inertial properties. If two or more principal inertia magnitudes are the equal, the local observability condition cannot be met even for fully tumbling motion. For instance, the Target satellite in the European Proximity Operations Simulator (EPOS) facility at DLR has $\begin{bmatrix}121 & 108 & 108\end{bmatrix}$ $Kg.m^2$ as its principal inertias. For proper estimation of the parameters, using the model $\mathfrak{स}_3$, it does not satisfy ORC. From an observability perspective, this indicates that for a nearly symmetrical body, the local observability is not strong enough for estimation.

2.5.4. Degrees of Observability

To enunciate the points made in the above section, two state-space initial conditions was chosen for two different Target satellites - QuickSat, the Canadian microsatellie and Target satellite from EPOS, DLR. Apart from the inertia values, the rest of the initial conditions were fixed for both turns.

	$\mathfrak{स}_1$		$\mathfrak{स}_2$		$\mathfrak{स}_3$	
Principal Inertias	κ_i	κ_n	κ_i	κ_n	κ_i	κ_n
$\begin{bmatrix}4 & 8 & 5\end{bmatrix}$ QuickSat:	0.227	277892.965	0.9031	1227418.315	0.983	1598962.639
$\begin{bmatrix}121 & 108 & 108\end{bmatrix}$ EPOS-DLR	0.248	304408.960	0.258	350950.523	0.689	1121365.622

Table 2.1.: Degrees of Observervability (80 seconds)

The `emgr` Empirical Gramian Framework developed by Himpe in [**Himpe2016**] was used for computing the Observability indexes. The function was invoked with the following parameters: handles for the nonlinear models given by $\mathfrak{स}_i$, an observation time of 80 seconds, an initial condition perturbation of 0.001 and the initial state sequence as linear.

The same test was run for 30 seconds and the results have been tabulated in 2.2. By comparing it with the results in 2.1, it is clear that the total integration time plays a major role in determining the gramian properties as described in section 2.4. Additionally, the order of observability is $\mathfrak{स}_1 > \mathfrak{स}_2 > \mathfrak{स}_3$. Also, if one looks at the κ_i values carefully, the change in going from either $\mathfrak{स}_1$ or $\mathfrak{स}_2$ to $\mathfrak{स}_3$ increases the magnitude considerably. Furthermore, this increase is much higher for the partially symmetric satellite at EPOS-

	स_1		स_2		स_3	
Principal Inertias	κ_i	κ_n	κ_i	κ_n	κ_i	κ_n
$\begin{bmatrix}4 & 8 & 5\end{bmatrix}$ QuickSat:	0.393	3299341.693	1.660	1404030.636	1.811	1832907.735
$\begin{bmatrix}121 & 108 & 108\end{bmatrix}$ EPOS-DLR	0.410	311120.016	0.420	354099.687	1.118	1127869.609

Table 2.2.: Degrees of Observervability (30 seconds)

DLR than for the QuickSat. This corroborates the ORC criterion derived above in the previous section for nearly symmetric bodies. In fact, the results of the above steps repeated for a completely symmetric body resulted in the following values for κ_i: 0.401344, 0.412574 and 3537.228345 for a period of 30 seconds. Hence, it has been analytically and experimentally proven than the model स_3 is sensitive to Target symmetries. Such an observability analysis is extremely important since poor observability can cause instability in estimators. In the Extended Kalman Filter (EKF), the problem of apparent divergence is well known. In later sections, this finding will be used to demonstrate that a system स_3 with symmetry will diverge.

References

[**Hermann1977**] Robert Hermann and Arthur Krener. "Nonlinear Controllability and Observability." In: *IEEE transactions on Automatic Control* AC-22.5 (Oct. 1977), pp. 728–740.

[**Liu2002**] Andrew Liu. "Stochastic Observability, reconstructability, controllability and reachability." PhD thesis. UC San Diego, 2002.

[**Anguelova2004**] Milena Anguelova. "Nonlinear Observability and Identifiability." Postgraduate thesis. Chalmers University of Technology and Göteborg University, 2004.

[**Kou1973**] Shauying Kou, David Elliott, and Tzyh Tarn. "Observability of Nonlinear Systems." In: *Information And Control* 22 (1973), pp. 89–99.

[**Zhirabok2012**] Alexey Zhirabok and Alexey Shumsky. "An Approach To The Analysis Of Observability And Controllability In Nonlinear Systems Via Linearmethods." In: *International Journal of Applications Mathematics Computer Science* 22.3 (2012), pp. 507–522.

[**Sontag1997**] Eduardo Sontag and Yuan Wang. "Output-to-state stability and detectability of nonlinear systems." In: *Systems and Control Letters* 29 (1997), pp. 279–290.

[**Krener2009**] Arthur Krener and Kayo Ide. "Measures of Unobservability." In: *Joint 48th IEEE Conference on Decision and Control and 28th Chinese Control Conference Shanghai* AC-22.FrA04.1 (Dec. 2009), pp. 6401–6406.

[**Griffith1971**] E. W. Griffith and K. S. P. Kumar. "On the Observability of Nonlinear Systems: 1." In: *Journal of Mathematical Analysis And Applications* 35 (1971), pp. 135–147.

[**Sabatini2011**] Angelo Maria Sabatini. "Kalman-Filter-Based Orientation Determination Using Inertial/Magnetic Sensors: Observability Analysis and Performance Evaluation." In: *Sensors* 11.10 (2011), pp. 9182–9206. ISSN: 1424-8220. DOI: 10.3390/s111009182. URL: http://www.mdpi.com/1424-8220/11/10/9182.

[**Himpe2016**] C. Himpe. *emgr - Empirical Gramian Framework (Version 5.0)*. http://gramian.de. 2016. DOI: 10.5281/zenodo.162135.

Chapter 3: Observer/Estimator

3.1. Observers/Estimators

In typical control systems, it is realistically not possible to measure all the states of the corresponding dynamic model given by (2.1). So, an observer, as defined in [**Hautus1980**] and [**Primbs1996**], is usually employed whose nonlinear dynamics are computed as the system सें,

$$\text{सें} : \begin{cases} \dot{\hat{x}}(t) = f(t, \hat{x}(t), u(t)) + K(\hat{y}(t) - y(t)) \\ \hat{y}(t) = h(\hat{x}(t), u(t)) \end{cases} \tag{3.1a}$$

For a linear (time-varying or invariant) system,

$$\text{सें} : \begin{cases} \dot{\hat{x}}(t) = A_t\hat{x} + B_t u(t) + K(\hat{y}(t) - y(t)) \\ \hat{y}(t) = H_t\hat{x}(t) + D_t u(t) \end{cases} \tag{3.1b}$$

where, $K \in \mathbb{R}^{n\times p}$ and the rest have been defined for (2.1).

As is evident from (2.2), the system सें assumes the same input controls and output observations as that of the original system given in (2.1) but is different in that, it assumes that the true dynamic states x are uniquely identified by the observed states $\hat{x}$. For this, a fundamental requisite is that $\hat{x}$ must asymptotically approach x either for all possible initial states $x(0) = x_0$ or for a fixed initial state like $x(0) = \mathbf{0}$. According to Primbs in [**Primbs1996**], (3.1) is of the form where linear output injection is used. There has been extensive study for designing Observers for Linear Systems and has proven extremely effective for Observer-based Controllers. For non-linear Systems like (2.1a), EKF has proven to be immensely successful. It is based on linear output injection or the method of Extended Linearization. Figure 3.1 protracts a block diagram of this design philosophy. Other approaches like Lyapunov-based or Lie-Algebra-based observer designs can also be employed. The merits of each of these methods has been discussed in [**Primbs1996**]. In the current thesis work, the primary area of focus is Linear Output Injection which can be used through *Extended Linearization* in the *Kalman Filter* or in the *Luenberger Observer* [**Birk1988**].

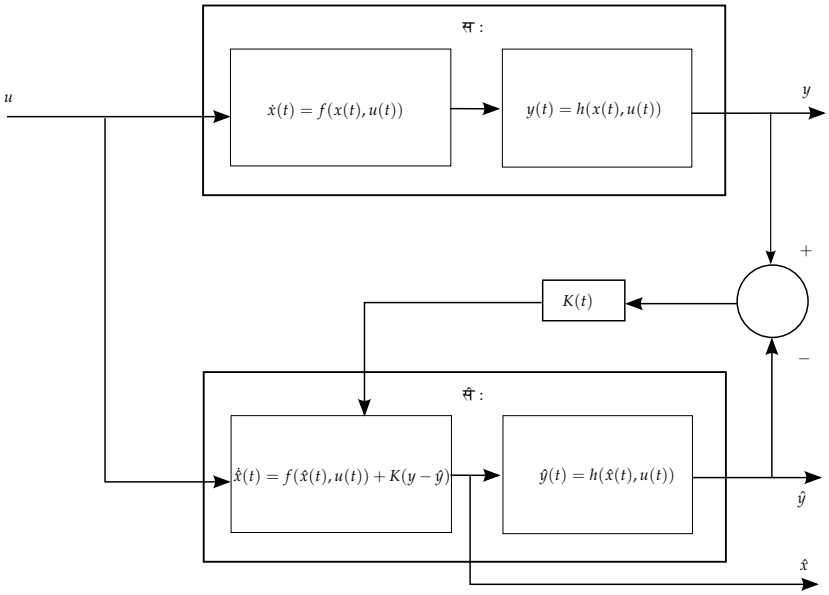

Figure 3.1.: Observer (Linear Output Injection) block diagram

3.1.1. Error Dynamics

Denoting the error in the state estimate as $\hat{x} - x$, the error dynamics can be computed by subtracting the state equations in (2.1) and (3.1). For simplicity, the error dynamics is first analyzed for the Linear System, by subtracting (2.1b) from (3.1b).

$$\dot{e} = (A_t + KH_t)e \tag{3.2a}$$

The idea of observer design is to place the eigen values of $(A_t + KH_t)$ in the left-half of the complex plane resulting in decaying dynamics. The underlying assumption is that the (A_t, H_t) pair are observable. Of course, the convergence rates of the states depends on the magnitudes of the eigen values. Adopting a similar approach, taking the difference of (2.1a) from (3.1a) after dropping time-dependence gives the nonlinear error dynamics as,

$$\begin{aligned} \dot{e} &= f(\hat{x}, u) - f(x, u) + K(h(\hat{x}, u) - h((x, u)) \\ &= f(x + e, u) - f(x, u) + K(h(x + e, u) - h(x)) \\ &\approx (\nabla_x f(x) + K\nabla_x h(x))e \end{aligned} \tag{3.2b}$$

It has been mentioned in [**Primbs1996**] that (3.2b) is dependent on the true state which is unknown and time-dependent. In the ubiquitous Kalman Filter for nonlinear systems, (3.2b) is solved by linearizing around the current estimate. This means,

$$\dot{e} \approx (\nabla_x f(\hat{x}) + K\nabla_x h(\hat{x}))e \tag{3.2c}$$

It is therefore evident that (3.2c) is largely dependent on the observer gain K and the linearization points. This is one of the seminal reasons for the divergence problems in the Kalman filters and will be discussed in detail later.

A similar approach with linear output injection can be applied to Luenberger Observers wherein the observer gain K can be set by simple pole placement techniques.

Typically, nonlinear observers are designed by employing a coordinate transformation which allows linear output injection or using nonlinear output injection. The current study does not investigate these kinds of observers but paves way for further investigation. These techniques are documented in [**Primbs1996**], [**Krener1983**] and [**Zeitz1987**].

3.2. Kalman Filter

Kalman filter [**Kalman1960**] is the workhorse observer design in engineering applications like aerospace, robotics, navigation et al. In his seminal paper Kalman has defined the optimal estimation problem as: *Given a vector-valued random process* $\{\boldsymbol{x}(t)\}$ *and observed random variables,* $\{\boldsymbol{y}\}^{t_0:t}$ *where* $\boldsymbol{y}(t) = \boldsymbol{M}\boldsymbol{x}(t)$*, find an estimate* $\hat{\boldsymbol{x}}(t)$ *which minimizes the expected loss function(L),* $\mathbb{E}[L(||\boldsymbol{x}(t_i) - \hat{\boldsymbol{x}}(t_i)||)]$.

Theorem 3.1. *According to the [**Kalman1960**, th. 2], if the random processes,* $\{\boldsymbol{x}_1(t)\}$*,* $\{\boldsymbol{x}_2(t)\}$ *and* $\{\boldsymbol{y}(t)\}$ *are gaussian and the loss function is considered* $L(\epsilon^2)$*, the optimal estimate is given by the Conditional Expectation or the Orthogonal Projection.*

$$\boldsymbol{x}_1^*(t) = \mathbb{E}[\boldsymbol{x}_1(t)|\,\{\boldsymbol{y}\}^{t_0:t}] \tag{3.3}$$

where $\boldsymbol{x}_1$ is the state being estimated, $\boldsymbol{x}_2$ is the noise affecting observations, $\{\boldsymbol{y}\}^{t_0:t}$ is the observation sequence and $\epsilon = \boldsymbol{x} - \boldsymbol{x}^*$.

A few important points from this work which are relevant to this thesis are worth pointing out.

1. Since in practice it is difficult to ascertain to what degree of approximation a random process of physical origin is gaussian, it is hard to decide whether Theorem 2 has very broad or very limited significance.

2. Linear functions (and therefore conditional expectations) on a gaussian random process are gaussian random variables. [**Kalman1960**, th. 5(a)]

Considering dynamic model (2.1) as defined in 2, the derivation for the Optimal estimator proceeds as follows. Firstly, the discretized model as in [**Kalman1960**] is considered and let us assume that instantaneous perturbations for the system are vector $\boldsymbol{w}$, and for the measurement as $\boldsymbol{v}$.

$$\text{स} : \begin{cases} \boldsymbol{x}_{k+1} &= \boldsymbol{A}_k\boldsymbol{x}_k + \boldsymbol{G}_k\boldsymbol{w}_k \\ \boldsymbol{y}_k &= \boldsymbol{H}_k\boldsymbol{x}_k + \boldsymbol{v}_k \end{cases} \tag{3.4}$$

where apart from the system parameters defined previously, $\boldsymbol{w}_k \in \mathbb{R}^n$, $\boldsymbol{v}_k \in \mathbb{R}^p$ and $\mathbb{E}[\boldsymbol{w}_k] = \mathbb{E}[\boldsymbol{v}_k] = \mathbf{0}$ and the joint covariance is given as $\mathbb{E}\left[\begin{pmatrix} \boldsymbol{w}_k \\ \boldsymbol{v}_k \end{pmatrix} \begin{pmatrix} \boldsymbol{w}_k^T & \boldsymbol{v}_k^T \end{pmatrix} \right] = \begin{bmatrix} \boldsymbol{Q}_k & \mathbf{0} \\ \mathbf{0} & \boldsymbol{R}_k \end{bmatrix}$.

The initial state is given as normal/gaussian distribution, $\boldsymbol{x}_0 = \mathcal{N}[\hat{\boldsymbol{x}}_{\mathbf{0}}, \boldsymbol{\Sigma}_0]$.

Remark 12. The initial state's probability distribution cannot always be known. In literature, many authors have resorted to using high values of $\boldsymbol{\Sigma}_0$ to overcome this lack of system knowledge to ensure stability. Other optimal methods may be used but they are not in the scope of this thesis.

The philosophy of optimal estimation is to propagate the probability distribution $p(\boldsymbol{x}_k | \{\boldsymbol{y}\}^{t_0:t})$ while satisfying an optimality condition and the Kalman Filter achieves this by minimizing the mean-squared-error and propagating the first two moments of the distribution.

3.2.1. Kalman filter dynamics

1. *Prediction*: Applying conditional expectation on (3.4) based on Theorem 3.1, and knowledge about previous state's posterior probability distribution in $\mathcal{N}[\hat{\boldsymbol{x}}(k|k), \boldsymbol{\Sigma}(k|k)]$ we get the optimal state at any time k_p where, $k_p > k$.

$$\begin{aligned} \hat{\boldsymbol{x}}(k_p|k) &= \mathbb{E}[\boldsymbol{x}_{k_p} | \{\boldsymbol{y}\}^{1:kt}] = \mathbb{E}[\boldsymbol{\Phi}(k,k_p)\boldsymbol{x}_k + \sum_{i=k}^{k_p-1} \boldsymbol{\Phi}(i,k_p-1)\boldsymbol{G}_i\boldsymbol{w}_i | \{\boldsymbol{y}\}^{1:kt}] \\ &= \boldsymbol{\Phi}(k,k_p)\mathbb{E}[\boldsymbol{x}_k | \{\boldsymbol{y}\}^{1:kt}] + \sum_{i=k}^{k_p-1} \boldsymbol{\Phi}(i,k_p-1)\boldsymbol{G}_i\mathbb{E}[\boldsymbol{w}_i | \{\boldsymbol{y}\}^{1:kt}] \\ &= \boldsymbol{\Phi}(k,k_p)\hat{\boldsymbol{x}}_k \end{aligned} \tag{3.5}$$

   where $\boldsymbol{\Phi}(k,k+n_p) = \boldsymbol{A}_{k+n_p-1}...\boldsymbol{A}_k$ is the state transition matrix from k to k_p. At this point, the errors for the estimator can be defined as

   - Prediction error: $\tilde{\boldsymbol{x}}(k_p|k) = \boldsymbol{x}_{k_p} - \hat{\boldsymbol{x}}(k_p|k)$
   - Filtering error: $\tilde{\boldsymbol{x}}(k_p|k_t) = \boldsymbol{x}_{k_p} - \hat{\boldsymbol{x}}(k_p|k_t)$, where k_t is the time at which the measurement was made but was available at k_p for fusion.

   Taking the variance of the Prediction,

$$\boldsymbol{\Sigma}(k_p|k) = \mathbb{E}[\tilde{\boldsymbol{x}}(k_p|k)\tilde{\boldsymbol{x}}(k_p|k)^T | \{\boldsymbol{y}\}^{1:kt}] \tag{3.6}$$

$$= \mathbb{E}\Bigg[\left(\boldsymbol{\Phi}(k,k_p)\tilde{\boldsymbol{x}}(k|k) + \sum_{i=k}^{k_p-1}\boldsymbol{\Phi}(i,k_p-1)\boldsymbol{G}_i\boldsymbol{w}_i\right) \left(\boldsymbol{\Phi}(k,k_p)\tilde{\boldsymbol{x}}(k|k) + \sum_{i=k}^{k_p-1}\boldsymbol{\Phi}(i,k_p-1)\boldsymbol{G}_i\boldsymbol{w}_i\right)^T\Bigg]$$

In the equation above, $\mathbb{E}[\hat{\boldsymbol{x}}_k\boldsymbol{w}_i^T] = \boldsymbol{0}$, $\mathbb{E}[\boldsymbol{w}_i\boldsymbol{w}_j^T] = \boldsymbol{0}$ and $\mathbb{E}[\boldsymbol{x}_k\boldsymbol{w}_k^T] = \boldsymbol{0}$. Hence,

$$\begin{aligned}\boldsymbol{\Sigma}(k_p|k) &= \boldsymbol{\Phi}(k,k_p)\mathbb{E}[(\tilde{\boldsymbol{x}}(k|k))(\tilde{\boldsymbol{x}}(k|k))^T]\boldsymbol{\Phi}(k,k_p)^T \\ &\quad + \boldsymbol{G}_{k_p}\mathbb{E}[(\boldsymbol{w}_{k_p})(\boldsymbol{w}_{k_p})^T]\boldsymbol{G}_{k_p}^T \\ &\quad + \sum_{i=k}^{k_p-1}\boldsymbol{\Phi}(i,k_p)\boldsymbol{G}_i\mathbb{E}[\boldsymbol{w}_i\boldsymbol{w}_i^T]\boldsymbol{G}_i^T\boldsymbol{\Phi}(i,k_p)^T \\ &= \boldsymbol{\Phi}(k,k_p)\boldsymbol{\Sigma}(k|k)\boldsymbol{\Phi}(k,k_p)^T + \boldsymbol{G}_{k_p}\boldsymbol{Q}_{k_p}\boldsymbol{G}_{k_p}^T \\ &\quad + \sum_{i=k}^{k_p-1}\boldsymbol{\Phi}(i,k_p-1)\boldsymbol{G}_i\boldsymbol{Q}_i\boldsymbol{G}_i^T\boldsymbol{\Phi}(i,k_p-1)^T\end{aligned} \tag{3.7}$$

2. *Output prediction*: The conditional expectation of the observation/output equation at any time $k_t > k$ is given as,

$$\begin{aligned}\mathbb{E}[\boldsymbol{y}_{k_t}|\{\boldsymbol{y}\}^{1:kt}] &= \mathbb{E}[\boldsymbol{H}_{k_t}\boldsymbol{x}_{k_t} + \boldsymbol{v}_{k_t}|\{\boldsymbol{y}\}^{1:kt}] \\ &= \boldsymbol{H}_{k_t}\mathbb{E}\left[\boldsymbol{\Phi}(k,k_t)\boldsymbol{x}_k + \sum_{i=k}^{k_t-1}\boldsymbol{\Phi}(i,k_t-1)\boldsymbol{G}_i\boldsymbol{w}_i\right] + \mathbb{E}[\boldsymbol{v}_{k_t}|\{\boldsymbol{y}\}^{1:kt}] \\ &= \boldsymbol{H}_{k_t}\boldsymbol{\Phi}(k,k_t)\hat{\boldsymbol{x}}(k|k) = \boldsymbol{H}_{k_t}\hat{\boldsymbol{x}}(k_t|k)\end{aligned} \tag{3.8}$$

At time k_t, let the prediction error for measurement be given by $\tilde{\boldsymbol{y}}(k_t|k)$ as

$$\begin{aligned}\tilde{\boldsymbol{y}}(k_t|k) =& \boldsymbol{y}_{k_t} - \hat{\boldsymbol{y}}(k_t|k) \\ &= \boldsymbol{H}_{k_t}\left[\boldsymbol{\Phi}(k,k_t)\boldsymbol{x}_k + \sum_{i=k}^{k_t-1}\boldsymbol{\Phi}(i,k_t-1)\boldsymbol{G}_i\boldsymbol{w}_i - \boldsymbol{\Phi}(k,k_t)\hat{\boldsymbol{x}}(k|k)\right] + \boldsymbol{v}_{k_t} \\ &= \boldsymbol{H}_{k_t}\boldsymbol{\Phi}(k,k_t)\tilde{\boldsymbol{x}}(k|k) + \boldsymbol{H}_{k_t}\left[\sum_{i=k}^{k_t-1}\boldsymbol{\Phi}(i,k_t-1)\boldsymbol{G}_i\boldsymbol{w}_i\right] + \boldsymbol{v}_{k_t}\end{aligned} \tag{3.9}$$

Taking covariance of this equation,

$$\begin{aligned}\mathbb{E}[\tilde{\boldsymbol{y}}(k_t|k)\tilde{\boldsymbol{y}}(k_t|k)^T|\,\{\boldsymbol{y}\}^{1:k_t}] &= \boldsymbol{H}_{k_t}\boldsymbol{\Phi}(k,k_t)\mathbb{E}[\tilde{\boldsymbol{x}}(k|k)\tilde{\boldsymbol{x}}(k|k)^T]\boldsymbol{\Phi}(k,k_t)^T\boldsymbol{H}_{k_t}^T \\ &+ \boldsymbol{H}_{k_t}\boldsymbol{G}_{k_t}\mathbb{E}[\boldsymbol{w}_{k_t}\boldsymbol{w}_{k_t}^T]\boldsymbol{G}_{k_t}^T\boldsymbol{H}_{k_t}^T \\ &+ \sum_{i=k}^{k_t-1}\boldsymbol{\Phi}(i,k_t)\boldsymbol{G}_i\mathbb{E}[\boldsymbol{w}_i\boldsymbol{w}_i^T]\boldsymbol{G}_i^T\boldsymbol{\Phi}(i,k_t)^T + \mathbb{E}[\boldsymbol{v}_{k_t}\boldsymbol{v}_{k_t}^T] \\ &= \boldsymbol{H}_{k_t}\boldsymbol{\Phi}(k,k_t)\boldsymbol{\Sigma}(k|k)\boldsymbol{\Phi}(k,k_t)^T\boldsymbol{H}_{k_t}^T + \boldsymbol{H}_{k_t}\boldsymbol{G}_{k_t}\boldsymbol{Q}_{k_t}\boldsymbol{G}_{k_t}^T\boldsymbol{H}_{k_t}^T \\ &+ \sum_{i=k}^{k_t-1}\boldsymbol{\Phi}(i,k_t)\boldsymbol{G}_i\boldsymbol{Q}_i\boldsymbol{G}_i^T\boldsymbol{\Phi}(i,k_t)^T + \boldsymbol{R}_{k_t} \\ &= \boldsymbol{H}_{k_t}\boldsymbol{\Sigma}(k_t|k)\boldsymbol{H}_{k_t}^T + \boldsymbol{R}_{k_t}\end{aligned} \tag{3.10}$$

Remark 13. The main reason for deriving the Prediction dynamics in this way is to provide the optimal state estimation (prediction) in a multi-rate implementation, where the sensing rate is much slower than that of controller. These equations provide the probability distribution of the state at any given time $k_p, k_t > k$.

In the same vein, we can derive the joint covariance of state $\boldsymbol{x}_k$ and measurement $\boldsymbol{y}_{k_d}$, where $k_d < k$, as

$$\mathbb{E}[\boldsymbol{x}_k\boldsymbol{y}_{k_d}^T|\,\{\boldsymbol{y}\}^{1:k_d}] = \mathbb{E}[\boldsymbol{x}_k\boldsymbol{x}_{k_d}]\boldsymbol{H}_{k_d}^T = \boldsymbol{U}_{k_d,k}\boldsymbol{H}_{k_d}^T \tag{3.11}$$

3. *Filtering*: Filtering is the process of deriving the posterior probability distribution of the state which is of the form $p(\boldsymbol{x}_k|\,\{\boldsymbol{y}\}^{1:k_d})$. This formalism is slightly different from the conventional [**Ribeiro2004**] approach to deriving filter equations because the intention in this thesis was to implement a multi-rate estimator with a OOSM.

   In [**Zhang2005**], Zhang, Li, and Zhu have described an OOSM as a measurement produced at time k_d prior to current time k, at which another current measurement is available. The problem then is to perform optimal state estimation with delayed state measurements.

   In the context of this thesis or any estimator-based on vision system, this is a pertinent problem. A pose-determination system is an image-processing algorithm which takes an unspecified amount of time. So, if the camera records images at k_d and the pose is available at k, the optimal estimator ought to perform a state estimation with respect to the state at k_d and not k.

   Theorem 3.2. *If $\boldsymbol{x}$ and $\boldsymbol{y}$ are two gaussian random variables, whose probability densities are given by $p(\boldsymbol{x}) = \mathcal{N}[\boldsymbol{x}|\boldsymbol{\mu}_x, \boldsymbol{\Sigma}_x]$, $p(\boldsymbol{y}) = \mathcal{N}[\boldsymbol{y}|\boldsymbol{\mu}_y, \boldsymbol{\Sigma}_y]$, and their joint*

distribution is given as $\begin{pmatrix} \boldsymbol{x} \\ \boldsymbol{y} \end{pmatrix} = \mathcal{N}\left(\begin{bmatrix} \boldsymbol{\mu}_x \\ \boldsymbol{\mu}_y \end{bmatrix}, \begin{bmatrix} \boldsymbol{\Sigma}_x & \boldsymbol{\Sigma}_{xy} \\ \boldsymbol{\Sigma}_{yx} & \boldsymbol{\Sigma}_y \end{bmatrix}\right)$ *then the marginal distribution* $p(\boldsymbol{x}|\boldsymbol{y}) \equiv \mathcal{N}\left(\boldsymbol{\mu}_x + \boldsymbol{\Sigma}_{xy}\boldsymbol{\Sigma}_y^{-}(\boldsymbol{y} - \boldsymbol{\mu}_y),\ \ \boldsymbol{\Sigma}_x - \boldsymbol{\Sigma}_{xy}\boldsymbol{\Sigma}_y^{-}\boldsymbol{\Sigma}_{xy}^T\right)$

Based on Theorem 3.2, the posterior distribution of state $\boldsymbol{x}_{k+1}$ can be computed based on a measurement $\boldsymbol{y}_{k+1}$. Formulating the problem in terms of the joint distribution in Theorem 3.2 by using (3.11) for the predicted state as the last optimal state, we get

$$\begin{pmatrix} \boldsymbol{x}_{k+1} \\ \boldsymbol{y}_{k+1} \end{pmatrix} = \mathcal{N}\left(\begin{bmatrix} \hat{\boldsymbol{x}}(k+1|k) \\ \boldsymbol{H}_{k+1}\hat{\boldsymbol{x}}(k+1|k) \end{bmatrix}, \begin{bmatrix} \boldsymbol{\Sigma}(k|k) & \boldsymbol{\Sigma}(k+1,k)\boldsymbol{H}_{k+1}^T \\ \boldsymbol{H}_{k+1}\boldsymbol{\Sigma}(k+1,k)^T & \boldsymbol{H}_{k+1}\boldsymbol{\Sigma}(k+1|k)\boldsymbol{H}_{k+1}^T + \boldsymbol{R}_{k+1} \end{bmatrix}\right) \tag{3.12}$$

By simply applying the marginal distribution equations, and simplifying the posterior covariance, we get the commonly known Kalman filter update,

$$\begin{aligned} \hat{\boldsymbol{x}}(k+1|k+1) &= \hat{\boldsymbol{x}}(k+1|k) + \boldsymbol{K}_{k+1}(\boldsymbol{y}_{k+1} - \boldsymbol{H}_{k+1}\hat{\boldsymbol{x}}(k+1|k)) \\ \boldsymbol{K}_{k+1} &= \boldsymbol{\Sigma}(k+1|k)\boldsymbol{H}_{k+1}^T(\boldsymbol{H}_{k+1}\boldsymbol{\Sigma}(k+1|k)\boldsymbol{H}_{k+1}^T + \boldsymbol{R}_{k+1})^{-} \\ \boldsymbol{\Sigma}(k+1|k+1) &= (\mathbb{I}_{n,n} - \boldsymbol{K}_{k+1}\boldsymbol{H}_{k+1})\boldsymbol{\Sigma}(k+1|k) \end{aligned} \tag{3.13}$$

where $\boldsymbol{K}_{k+1}$ is the Kalman gain computed at $k+1$.
Similarly, based on Theorem 3.2, the posterior distribution of state $\boldsymbol{x}_k$ can be computed based on a measurement $\boldsymbol{y}_{k_d}$. Formulating the problem in terms of the joint distribution in Theorem 3.2,

$$\begin{pmatrix} \boldsymbol{x}_k \\ \boldsymbol{y}_{k_d} \end{pmatrix} = \mathcal{N}\left(\begin{bmatrix} \hat{\boldsymbol{x}}(k|k) \\ \boldsymbol{H}_{k_d}\hat{\boldsymbol{x}}(k_d|k) \end{bmatrix}, \begin{bmatrix} \boldsymbol{\Sigma}(k|k) & \boldsymbol{U}_{k_d,k}\boldsymbol{H}_{k_d}^T \\ \boldsymbol{H}_{k_d}\boldsymbol{U}_{k_d,k}^T & \boldsymbol{H}_{k_d}\boldsymbol{\Sigma}(k_d|k)\boldsymbol{H}_{k_d}^T + \boldsymbol{R}_{k_d} \end{bmatrix}\right) \tag{3.14}$$

where $\boldsymbol{U}_{k_d,k} = \mathbb{E}[\boldsymbol{x}_k\boldsymbol{x}_{k_d}^T]$ is the covariance term between the states at different time instants. So, the marginal distribution's mean according to Theorem 3.2 is given by

$$\begin{aligned} \hat{\boldsymbol{x}}(k|k,k_d) =& \hat{\boldsymbol{x}}(k|k) + \boldsymbol{U}_{k_d,k}\boldsymbol{H}_{k_d}^T \\ & (\boldsymbol{H}_{k_d}\boldsymbol{\Sigma}(k_d|k)\boldsymbol{H}_{k_d}^T + \boldsymbol{R}_{k_d})^{-}(\boldsymbol{y}_{k_d} - \boldsymbol{H}_{k_d}\hat{\boldsymbol{x}}(k_d|k)) \end{aligned} \tag{3.15}$$

The state error covariance is,

$$\boldsymbol{\Sigma}(k|k,k_d) = \boldsymbol{\Sigma}(k|k) - \boldsymbol{K}_{k_d}\boldsymbol{S}_{k_d}\boldsymbol{K}_{k_d}^T \tag{3.16}$$

where the Kalman gain $\boldsymbol{K}_{k_d} = \boldsymbol{U}_{k_d,k}\boldsymbol{H}_{k_d}^T(\boldsymbol{H}_{k_d}\boldsymbol{\Sigma}(k_d|k)\boldsymbol{H}_{k_d}^T + \boldsymbol{R}_{k_d})^{-}$ and
$\boldsymbol{S}_{k_d} = \boldsymbol{H}_{k_d}\boldsymbol{\Sigma}(k_d|k)\boldsymbol{H}_{k_d}^T + \boldsymbol{R}_{k_d}$.

Remark 14. In (3.15) and (5.8), $\boldsymbol{\Sigma}(k_d|k)$, $\hat{\boldsymbol{x}}(k_d|k)$ are optimal estimates at time k_d while satisfying the optimality condition at k. The relevant equations will be discussed later.

Remark 15. The Kalman filter satisfies the optimality condition implicitly that $\frac{\partial}{\partial \boldsymbol{K}_k} trace(\boldsymbol{\Sigma}(k|k)) = 0$ which minimizes the squared error.

Remark 16. The residual random variable $\boldsymbol{e}_k = \boldsymbol{y}_k - \boldsymbol{H}_k\boldsymbol{x}_k$ is a zero-mean process, $\mathbb{E}[\boldsymbol{e}_k] = \boldsymbol{0}$ with a variance as derived above. It raises an important question about the situations in which this assumption may not be satisfied.

- When $\hat{\boldsymbol{x}}(0|-1) \neq \mathbb{E}[\boldsymbol{x}_0]$, the observer is in convergence, and prediction errors will be large.
- When $\mathbb{E}[\boldsymbol{w}_k\boldsymbol{w}_k^T] \neq \boldsymbol{Q}_k$, the process is perturbed by an unknown noise or by assumption deficiencies like nonlinearity.
- When $\mathbb{E}[\boldsymbol{v}_k\boldsymbol{v}_k^T] \neq \boldsymbol{R}_k$, the measurement is perturbed by an unknown noise or outliers.

3.3. Bayesian Optimal Filter

Since the Kalman filter is based on propagation of probability distributions, a discussion on a general approach to Bayesian Filtering is warranted. Under the assumption that the probability distribution of the previous estimate $p(\boldsymbol{x}_{k-1}|\{\boldsymbol{y}\}^{1:k-1})$ is known, the conditional joint distribution of the current state $\boldsymbol{x}_k$ and the previous $\boldsymbol{x}_{k-1}$ is given by the Markovian property.

$$p(\boldsymbol{x}_k, \boldsymbol{x}_{k-1}|\{\boldsymbol{y}\}^{1:k-1}) = p(\boldsymbol{x}_k|\boldsymbol{x}_{k-1})p(\boldsymbol{x}_{k-1}|\{\boldsymbol{y}\}^{1:k-1}) \tag{3.17}$$

- *Prediction*: Marginalizing over $\boldsymbol{x}_{k-1}$ gives the Chapman-Kolmogorov (CL) equation which generates the prior distribution.

$$p(\boldsymbol{x}_k|\{\boldsymbol{y}\}^{1:k-1}) = \int p(\boldsymbol{x}_k|\boldsymbol{x}_{k-1})p(\boldsymbol{x}_{k-1}|\{\boldsymbol{y}\}^{1:k-1})d\boldsymbol{x}_{k-1} \tag{3.18}$$

- *Update*: The measurement likelihood from the state-space model is given by $p(\boldsymbol{y}_k|\boldsymbol{x}_k)$. Simply applying Bayes' theorem, the posterior probability distribution is obtained as,

$$p(\boldsymbol{x}_k|\{\boldsymbol{y}\}^{1:kt}) = p(\boldsymbol{y}_k|\boldsymbol{x}_k)p(\boldsymbol{x}_k|\{\boldsymbol{y}\}^{1:k-1}) \tag{3.19}$$

Remark 17. The Kalman filter performs Bayesian filtering under the assumption of gaussian models with *mean* and *variance* as relevant statistics [**Ribeiro2004**].

3.4. Extended Kalman Filter

The EKF is a nonlinear estimator with linearized dynamics. This is applicable to state estimation of a nonlinear model (2.1a), as mentioned in Chapter 2. Considering the perturbations as in the previous section, the model in discretized form is written as,

$$\text{स} : \begin{cases} \boldsymbol{x}_{k+1} &= \boldsymbol{f}_k(\boldsymbol{x}_k) + \boldsymbol{G}_k \boldsymbol{w}_k \\ \boldsymbol{y}_k &= \boldsymbol{h}_k(\boldsymbol{x}_k) + \boldsymbol{v}_k \end{cases} \tag{3.20}$$

In light of the derivations made in the previous sections, the stochastic propagation for a Bayesian filter for the nonlinear system (3.20) under gaussian assumption needs the following statistics, [**Wu2006**]

$$\begin{aligned} \hat{\boldsymbol{x}}(k+1|k) &= \mathbb{E}[\boldsymbol{f}_k(\boldsymbol{x}_k)] \\ \boldsymbol{\Sigma}(k+1|k) &= \mathbb{E}[\tilde{\boldsymbol{x}}(k+1|k)\tilde{\boldsymbol{x}}(k+1|k)^T] + \boldsymbol{Q}_k \\ \hat{\boldsymbol{y}}(k+1) &= \mathbb{E}[\boldsymbol{h}_{k+1}(\boldsymbol{x}_{k+1})] \\ \boldsymbol{\Sigma}_y(k+1|k) &= \mathbb{E}[\tilde{\boldsymbol{y}}(k+1|k)\tilde{\boldsymbol{y}}(k+1|k)^T] + \boldsymbol{R}_k \\ \boldsymbol{\Sigma}_{xy} &= \mathbb{E}[\tilde{\boldsymbol{x}}(k+1|k)\tilde{\boldsymbol{y}}(k+1|k)^T] \end{aligned} \tag{3.21}$$

In [**Wu2006**, p.2914], the authors have made a detailed study on the approximation method for Gaussian filter variants. In accordance to the theory presented, applying (3.18),

$$\begin{aligned} \hat{\boldsymbol{x}}(k+1|k) &= \int \boldsymbol{f}_k(\boldsymbol{x}_k)\mathcal{N}[\hat{\boldsymbol{x}}(k|k), \boldsymbol{\Sigma}(k|k)]d\boldsymbol{x}_k \\ \boldsymbol{\Sigma}(k+1|k) &= \int \Big(\boldsymbol{f}_k(\boldsymbol{x}_k) - \hat{\boldsymbol{x}}(k+1|k)\Big)\Big(\boldsymbol{f}_k(\boldsymbol{x}_k) - \hat{\boldsymbol{x}}(k+1|k)\Big)^T \mathcal{N}[\hat{\boldsymbol{x}}(k|k), \boldsymbol{\Sigma}(k|k)]d\boldsymbol{x}_k \end{aligned} \tag{3.22}$$

These equations cannot be solved analytically for nonlinear models. Hence, an approximation is made in different schemes like the Unscented Kalman Filter, EKF and so forth. For the EKF, the assumption is made as follows.

Assumption 1. The resultant probability distribution is unimodal and the integrand for state mean resolves to $\boldsymbol{f}_k(\hat{\boldsymbol{x}}(k|k))$.

Assumption 2. The resultant covariance is approximated by Jacobians as described in [**Wu2006**] obtained after Taylor approximation.

A detailed derivation of the EKF by gaussian approximation is provided in [**Ribeiro2004**] which proceed from the aforementioned equations. The final equations relevant for this thesis are,

- *Predict*:

$$\begin{aligned}\hat{\boldsymbol{x}}(k+1|k) &= \boldsymbol{f_k}(\hat{\boldsymbol{x}}(k|k)) \\ \boldsymbol{\Sigma}(k+1|k) &= \boldsymbol{F}_k\boldsymbol{\Sigma}(k|k)\boldsymbol{F}_k^T + \boldsymbol{Q}_k\end{aligned} \tag{3.23}$$

- *Update*:

$$\begin{aligned}\hat{\boldsymbol{x}}(k+1|k+1) &= \hat{\boldsymbol{x}}(k+1|k) + \boldsymbol{K}_{k+1}(\boldsymbol{y}_k - \boldsymbol{H}_{k+1}\hat{\boldsymbol{x}}(k+1|k)) \\ \boldsymbol{\Sigma}(k+1|k+1) &= (\mathbb{I}_{n,n} - \boldsymbol{K}_{k+1}\boldsymbol{H}_{k+1})\boldsymbol{\Sigma}(k+1|k) \\ \boldsymbol{K}_{k+1} &= \boldsymbol{\Sigma}(k+1|k)\boldsymbol{H}_{k+1}^T\left(\boldsymbol{H}_{k+1}\boldsymbol{\Sigma}(k+1|k)\boldsymbol{H}_{k+1}^T + \boldsymbol{R}_{k+1}\right)^{-} \\ \text{where, } \boldsymbol{F}_k = \nabla_x \boldsymbol{f}_k(\boldsymbol{x}_k)\Big|_{\boldsymbol{x}_k=\hat{\boldsymbol{x}}(k|k)} &, \boldsymbol{H}_{k+1} = \nabla_x \boldsymbol{h}_{k+1}(\boldsymbol{x}_{k+1})\Big|_{\boldsymbol{x}_{k+1}=\hat{\boldsymbol{x}}(k+1|k)} \\ \boldsymbol{x}_0 &\equiv \mathcal{N}[\hat{\boldsymbol{x}}(0|0), \Sigma(0|0)]\end{aligned} \tag{3.24}$$

3.5. Design of EKF

3.5.1. Process

In chapter 1, model equations were derived which are mostly of nonlinear form. Hence, EKF presents a suitable candidature as shown in [**Aghili2009**]. In contrast to the three models that were derived, the dynamic model for the EKF employs the 3-parameter form of a quaternion as shown in the section about MEKF 1.5.2. Hence, the corresponding state space models for EKF are given by,

$$\text{स}_1 : \boldsymbol{x} = \begin{bmatrix}\boldsymbol{a}^T & \boldsymbol{\omega}^T & \boldsymbol{r}^T & \dot{\boldsymbol{r}}^T\end{bmatrix}^T \in \mathbb{R}^{12} \tag{3.25}$$

$$\text{स}_2 : \boldsymbol{x} = \begin{bmatrix}\boldsymbol{a}^T & \boldsymbol{\omega}^T & \boldsymbol{p}^T & \boldsymbol{r}^T & \dot{\boldsymbol{r}}^T\end{bmatrix}^T \in \mathbb{R}^{15} \tag{3.26}$$

$$\text{स}_3 : \boldsymbol{x} = \begin{bmatrix}\boldsymbol{a}^T & \boldsymbol{\omega}^T & \boldsymbol{p}^T & \boldsymbol{r}^T & \dot{\boldsymbol{r}}^T & \boldsymbol{\rho}_t^T & \boldsymbol{b}^T\end{bmatrix}^T \in \mathbb{R}^{21} \tag{3.27}$$

where $\boldsymbol{a} = (\bar{\boldsymbol{q}} \otimes \bar{\boldsymbol{q}}_{ref}^*)_v$ and $\boldsymbol{b} = (\bar{\boldsymbol{\eta}}_{ref}^* \otimes \bar{\boldsymbol{\eta}}_{ref})_v$ express the attitude errors using a 3-vector parametrization. While the former is an expression for the errors in body frame, the latter is the expressed in inertial frame. Although, it is not explicitly mentioned by [**Aghili2009**], one of the major advantage of the problem formulation in [**Aghili2009**] is that both the attitude errors can be operated on the Target's body frame.

The dynamic equations and linearized forms of all the vectors have been derived in 1. Rewriting the equations as a discrete-linear form, we get $\boldsymbol{x}_{k+1} = \boldsymbol{\Phi}(k, k+1)\boldsymbol{x}_k + \boldsymbol{\epsilon}_k$

where $\mathbf{\Phi} = diag(\mathbf{\Phi}_r, \mathbf{\Phi}_t, \mathbb{I}_6)$. Such an expression is possible because of decoupling of translational and rotational dynamics.

As mentioned in chapter 1, the matrix exponential required for $\mathbf{\Phi}(k, k+1)$ was computed using Padé's approximation and not in the method specified in [**Aghili2009**]. Also, the exponential was needed only for the rotational component, $\mathbf{\Phi}_r$, since the translational component can be simplified to a discrete-linear system.

For a small circular orbit, ignoring higher order terms,

$$\mathbf{\Phi}_r(k, k+1) = e^{\boldsymbol{F}_r \Delta T} \tag{3.28}$$

where $\boldsymbol{F}_r$ contains linearized equations for rotational states defined in chapter 1.

$$\mathbf{\Phi}_t(k, k+1) = \begin{bmatrix} \mathbb{I}_{3,3} & \mathbf{\Phi}_{t12} \\ \mathbb{O}_{3,3} & \mathbf{\Phi}_{t22} \end{bmatrix} \tag{3.29}$$

The sub-matrices have been described in [**Aghili2009**] as, $\mathbf{\Phi}_{t12} = \begin{bmatrix} t & nt^2 & 0 \\ 0 & t & 0 \\ 0 & 0 & t \end{bmatrix}$ and $\mathbf{\Phi}_{t22} = \mathbb{I}_{3,3} - 2\lceil \boldsymbol{n} \rceil t$.

Assumption 3. In $0 < t < \Delta T$, $nt \ll 1$, which means that the orbit is small.

The process noise is modeled to account for torque and force disturbances due to gravity gradient, Earth's oblateness, air-drag and other perturbing accelerations. In this thesis, the same set of equations from [**Aghili2009**] for Process noise has been used. From (1.6a) and (1.6f), we get the relevant perturbation elements whose variances are given as follows.

$$\begin{aligned} \mathbf{\Gamma}_{\boldsymbol{\tau}} &= \mathbb{E}[\epsilon_\tau \epsilon_\tau^T] = \sigma_\tau^2 \mathbb{I}_3 \\ \mathbf{\Gamma}_f &= \mathbb{E}[\epsilon_f \epsilon_f^T] = \sigma_f^2 \mathbb{I}_3 \end{aligned} \tag{3.30}$$

Since, the equations for rotational and translational dynamics are decoupled, $\boldsymbol{Q}_k = diag(\boldsymbol{Q}_{r_k}, \boldsymbol{Q}_{t_k}, \boldsymbol{Q}_{\theta_k})$. The detailed equations can be referred from [**Aghili2009**, p. 541].

3.5.2. Observation/Measurement

In chapter 1, an observation model was presented in terms of the noisy measurements from the vision sensor. Expressing this in terms of state model defined in (3.27), the model can be represented as,

$$\boldsymbol{y}_k = \boldsymbol{h}_k(\boldsymbol{x}_k) + \boldsymbol{v}_k = \begin{bmatrix} \boldsymbol{h}_1(\boldsymbol{x}_k) + \boldsymbol{v}_1 \\ \boldsymbol{h}_2(\boldsymbol{x}_k) + \boldsymbol{v}_2 \end{bmatrix} = \begin{bmatrix} \boldsymbol{r}_k + \boldsymbol{R}(\bar{\boldsymbol{q}}_k)\boldsymbol{\rho}_{t_k} \\ (\boldsymbol{a} \otimes \boldsymbol{b}) \end{bmatrix} \tag{3.31}$$

In order to derive the Jacobian, we find the gradient of the functions $\boldsymbol{h}_1$ and $\boldsymbol{h}_2$ with respect to the states.

$$\nabla_r \boldsymbol{h}_1(\boldsymbol{x}_k) = \mathbb{I}_{3,3} \tag{3.32}$$

Assumption 4. The following observation equation holds for small attitude errors, $||\delta\bar{\boldsymbol{q}}_v|| \ll 1$ and $\delta q_0 \approx 1$.

During convergence of the filter, this assumption is not guaranteed. That apart, the attitude matrix $\boldsymbol{R}(.)$ can be simplified as,

$$\boldsymbol{R}(\bar{\boldsymbol{q}}_k) = \mathbf{R}(\delta\bar{\boldsymbol{q}}_k \otimes \bar{\boldsymbol{q}}_{ref}) = \boldsymbol{R}(\bar{\boldsymbol{q}}_{ref})\mathbf{R}(\delta\bar{\boldsymbol{q}}_k) \approx \boldsymbol{R}(\bar{\boldsymbol{q}}_{ref})(\mathbb{I}_{3,3} + 2\lceil\delta\boldsymbol{q}_v\rceil) \tag{3.33}$$

where $\lceil\boldsymbol{.}\rceil$ is the skew-symmetric form of a vector. Hence,

$$\begin{aligned} \boldsymbol{h}_1(\boldsymbol{x}_k) &= \boldsymbol{r}_k + \boldsymbol{R}(\bar{\boldsymbol{q}}_{ref})(\mathbb{I}_{3,3} + 2\lceil\delta\boldsymbol{q}_v\rceil)\boldsymbol{\rho}_{t_k} \\ \Rightarrow \nabla_{\delta q_v}\boldsymbol{h}_1 &= \nabla_{\delta q_v} 2\boldsymbol{R}(\bar{\boldsymbol{q}}_{ref})\lceil\delta\boldsymbol{q}_v\rceil\boldsymbol{\rho}_{t_k} = -2\nabla_{\delta q_v}\boldsymbol{R}(\bar{\boldsymbol{q}}_{ref})\lceil\boldsymbol{\rho}_{t_k}\rceil\delta\boldsymbol{q}_v \\ &= -2\boldsymbol{R}(\bar{\boldsymbol{q}}_{ref})\lceil\boldsymbol{\rho}_{t_k}\rceil \end{aligned} \tag{3.34}$$

$$\nabla_{\rho_t}\boldsymbol{h}_1(\boldsymbol{x}_k) = \boldsymbol{R}(\bar{\boldsymbol{q}}_{ref}) \tag{3.35}$$

$$\boldsymbol{h}_2(\boldsymbol{x}_k) = (\delta\bar{\boldsymbol{\eta}}_k \otimes \delta\bar{\boldsymbol{q}}_k)_v = (\delta\bar{\boldsymbol{q}}_k \circledast \delta\bar{\boldsymbol{\eta}}_k)_v \tag{3.36}$$

By simply using the multiplication operators and performing derivatives for small angle rotations assumption, one obtains,

$$\begin{aligned} \nabla_{\delta q_v}\boldsymbol{h}_2 &= -\lceil\delta\boldsymbol{\eta}_v\rceil + \delta\eta_0\mathbb{I}_{3,3} \\ \nabla_{\delta\eta_v}\boldsymbol{h}_2 &= \lceil\delta\boldsymbol{q}_v\rceil + \delta q_0\mathbb{I}_{3,3} \end{aligned} \tag{3.37}$$

Based on (3.32), (3.34), (3.36) and (3.37), the linearized model for the observation can be created for the three system models defined in 1. For स_3, the full state measurement model is given as,

$$\boldsymbol{H}_k = \begin{bmatrix} -2\boldsymbol{R}(\bar{\boldsymbol{q}}_{ref})\lceil\boldsymbol{\rho}_{t_k}\rceil & \mathbb{O}_{3,6} & \mathbb{I}_{3,3} & \mathbb{O}_{3,3} & \boldsymbol{R}(\bar{\boldsymbol{q}}_{ref}) & \mathbb{O}_{3,3} \\ -\lceil\delta\boldsymbol{\eta}_v\rceil + \delta\eta_0\mathbb{I}_{3,3} & \mathbb{O}_{3,6} & \mathbb{O}_{3,3} & \mathbb{O}_{3,3} & \mathbb{O}_{3,3} & \lceil\delta\boldsymbol{q}_v\rceil + \delta q_0\mathbb{I}_{3,3} \end{bmatrix} \tag{3.38}$$

The attitude error scalars δq_0 and $\delta\eta_0$ can be found by using the unit-norm quaternion constraint. In accordance to the convention mentioned above, $a = \delta\boldsymbol{q}_v$, where any of parametrization in 1 can be used.

For the systems स_1 and स_2, the only difference is $\delta\bar{\boldsymbol{\eta}} = \begin{bmatrix}0 & 0 & 0 & 1\end{bmatrix}^T$ at all times.

In [**Aghili2009**], the measurement error covariance is said to be state-dependent because of the unit-norm constraint on quaternion with additive noise. The covariance is defined as,

$$\boldsymbol{R}_k = \mathbb{E}[\boldsymbol{v}_k \boldsymbol{v}_k^T] = diag(\boldsymbol{\Sigma}_r, \boldsymbol{T}_{\mu_k} \boldsymbol{\Sigma}_{\mu_k} \boldsymbol{T}_{\mu_k}^T) \tag{3.39}$$

where, $\boldsymbol{\Sigma}_{\mu_k}$, $\boldsymbol{\Sigma}_r$ are the noise covariances for the position and orientation respectively of the vision system and $\boldsymbol{T}_{\mu_k} = \begin{bmatrix}\mathbb{I}_{3,3} & \mathbb{O}_{3,1}\end{bmatrix} \bar{\boldsymbol{\eta}}_k^* \otimes \bar{\boldsymbol{q}}_k^* \circledast$

Remark 18. It is important to note that the EKF process is a reduced vector $\boldsymbol{x}_k$ and has to be computed on measurement arrival. $\boldsymbol{\mathcal{X}}_k$ is computed using the the quaternion attitude expressions in 1.5.2. The equations are explicitly given in [**Aghili2009**, eq. 48] to generate the full-state estimate.

3.6. Simulation

For all the simulations performed in order to validate the EKF models defined in the previous section,hereon, the following precursor data is used.

Principal Inertias $[Kg.m^2]$	$\begin{bmatrix}4 & 8 & 5\end{bmatrix}^T$
Grasping point Position, $\boldsymbol{\rho}_t$ $[m]$	$\begin{bmatrix}0.2 & 0.1 & 0.05\end{bmatrix}^T$
Grasping point Quaternion, $\bar{\boldsymbol{\eta}}$	$\begin{bmatrix}0.12 & 0.05 & -0.15 & 0.98\end{bmatrix}^T$
Camera position, $\boldsymbol{\rho}_c$ $[m]$	$\begin{bmatrix}0 & 0 & 0.9\end{bmatrix}^T$
Camera orientation, $\bar{\ni}$	$\begin{bmatrix}0 & 0 & 0 & 1\end{bmatrix}^T$
Sampling time, ΔT $[sec]$	0.1
Mean motion, n $[\frac{rad}{sec}]$	0.0012
Camera position covariance, $\boldsymbol{\Sigma}_r$ $[m^2]$	$3e^{-3}\mathbb{I}_{3,3}$
Camera quaternion covariance, $\boldsymbol{\Sigma}_\mu$	$3e^{-3}\mathbb{I}_{4,4}$
Perturbation torque, ϵ_τ $[N.m]$	$\mathbf{0}$
Perturbation force, ϵ_f $[N]$	$\mathbf{0}$

Table 3.1.: System data

3.6.1. Estimation for स$_1$

The initial system state for स$_1$ is chosen as
$\boldsymbol{x}_0 = \begin{bmatrix} 0.5625 & 0.7875 & 0.2250 & 0.1125 & 0.5 & -0.1 & -0.7 & 2.5 & 1 & -1 & 0.01 & -0.01 & 0.02 \end{bmatrix}^T$

Total time, t $[sec]$	60
Initial state estimate, $\hat{\boldsymbol{x}}(0\|0)$	$\mathbf{0}_{12,1}$
Initial state covariance estimate, $\boldsymbol{\Sigma}(0\|0)$	$\mathbb{I}_{12,12}$

Table 3.2.: स$_1$ EKF settings

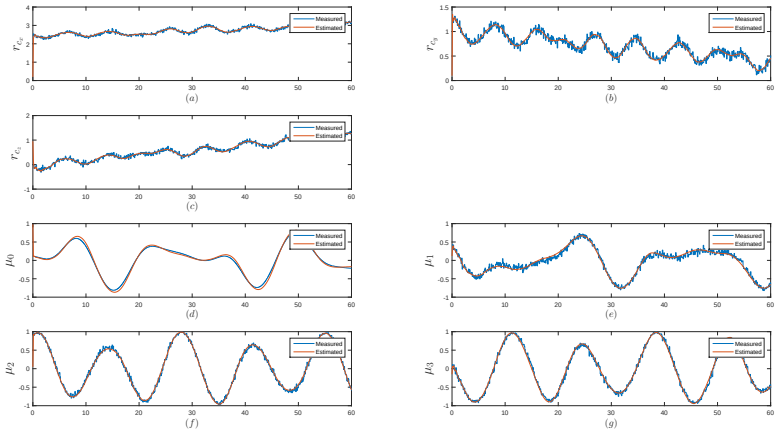

Figure 3.2.: स$_1$: Estimated pose measurements

- Figure 3.2 shows the noisy measurements and the estimated measurements from the state.
- It can be seen in 3.3 that the velocities, both linear and angular, are noisy. This is natural since the estimator does not directly sense velocity.
- Figure 3.4 is the relative pose between the centers of mass of the Servicer and the tumbling Target.
- Figure 3.5 demonstrates errors in the estimator. Using the Mahalanobis distance, the current operating health of the filter can be gauged. A high $\boldsymbol{d}(k+1|k)$ will indicate an uncertain process input while a high $\boldsymbol{d}(k|k)$ is indicative of either outliers or changing noise characteristics of observations. The Mahalanobis distance

d for a normal distribution $\boldsymbol{\mathcal{X}} \equiv \mathcal{N}[\boldsymbol{\mu}, \boldsymbol{\Sigma}]$ is given as follows,

$$d^2 = (\boldsymbol{\mathcal{X}} - \boldsymbol{\mu})^T \boldsymbol{\Sigma}^- (\boldsymbol{\mathcal{X}} - \boldsymbol{\mu}) \tag{3.40}$$

In (c), there are three traces which are defined as follows,

$$\begin{aligned}
\boldsymbol{\Sigma}(k+1|k) &= \boldsymbol{F}_k \boldsymbol{\Sigma}(k|k) \boldsymbol{F}_k^T + \boldsymbol{Q}_k \\
\boldsymbol{CRB}(k+1|k) &= \boldsymbol{\mathcal{F}}_k \boldsymbol{\Sigma}(k|k) \boldsymbol{\mathcal{F}}_k^T + \boldsymbol{Q}_k \\
\boldsymbol{\Sigma}(k+1|k+1) &= (\mathbb{I}_{n,n} - \boldsymbol{K}_{k+1} \boldsymbol{H}_{k+1}) \boldsymbol{\Sigma}(k+1|k) \\
\boldsymbol{CRB}(k+1|k+1) &= (\mathbb{I}_{n,n} - \boldsymbol{K}_{k+1} \boldsymbol{\mathcal{H}}_{k+1}) \boldsymbol{CRB}(k+1|k) \\
\text{where, } \boldsymbol{F}_k = \nabla_x \boldsymbol{f}_k(\boldsymbol{x}_k)\Big|_{\boldsymbol{x}_k = \hat{\boldsymbol{x}}(k|k)} &, \boldsymbol{H}_{k+1} = \nabla_x \boldsymbol{h}_{k+1}(\boldsymbol{x}_{k+1})\Big|_{\boldsymbol{x}_{k+1} = \hat{\boldsymbol{x}}(k+1|k)} \\
\boldsymbol{\mathcal{F}}_k = \nabla_x \boldsymbol{f}_k(\boldsymbol{x}_k)\Big|_{\boldsymbol{x} = \boldsymbol{x}_k} &, \boldsymbol{\mathcal{H}}_{k+1} = \nabla_x \boldsymbol{h}_{k+1}(\boldsymbol{x}_{k+1})\Big|_{\boldsymbol{x} = \boldsymbol{x}_{k+1}}
\end{aligned} \tag{3.41}$$

where CRB is the Cramer-Rao Bound and is differentiated from the State error covariance in that, the linearization takes place at the true state-space. In [**Havlík2015**], Havlík and Straka have used a third matrix, Square Error Matrix, $\boldsymbol{\Pi}(k|k) = \mathbb{E}[\tilde{\boldsymbol{x}}(k|k)\tilde{\boldsymbol{x}}(k|k)^T]$. These matrices are a good indicator of estimator convergence and also the sensitivity to approximation.

- In the figure 3.5, d) is simply the squared-error of the state, $\tilde{\boldsymbol{x}}(k|k)^T \tilde{\boldsymbol{x}}(k|k)$ or the Eucledian distance.
- In [**Aghili2009**], the position and orientation error formulae have been given for the observations. In e) and f), these formulae have been put to use to judge the accuracy of the estimator.

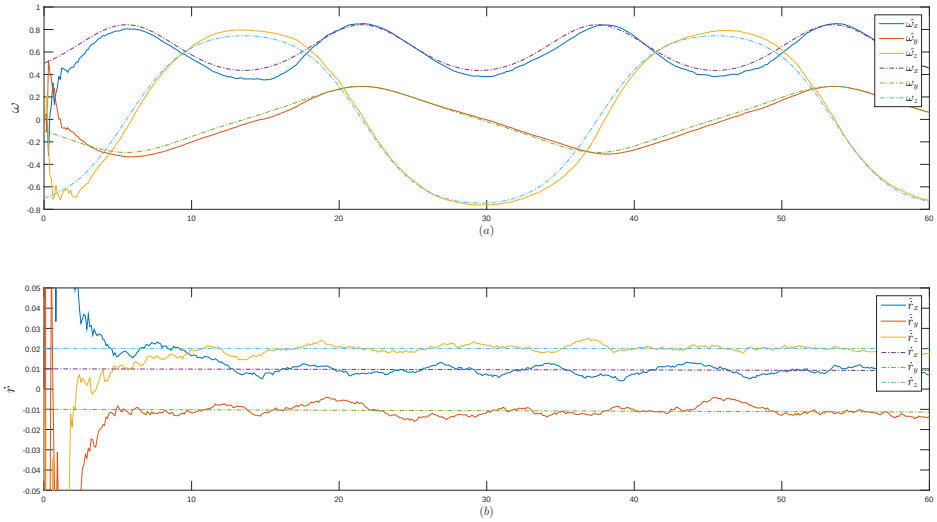

Figure 3.3.: स$_1$: a)angular velocity, and b)position rate

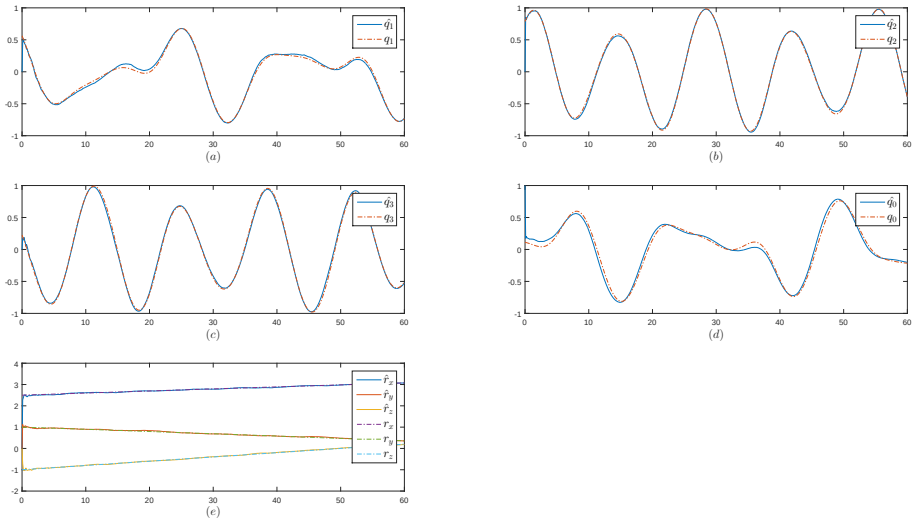

Figure 3.4.: स$_1$: Orientation and Position

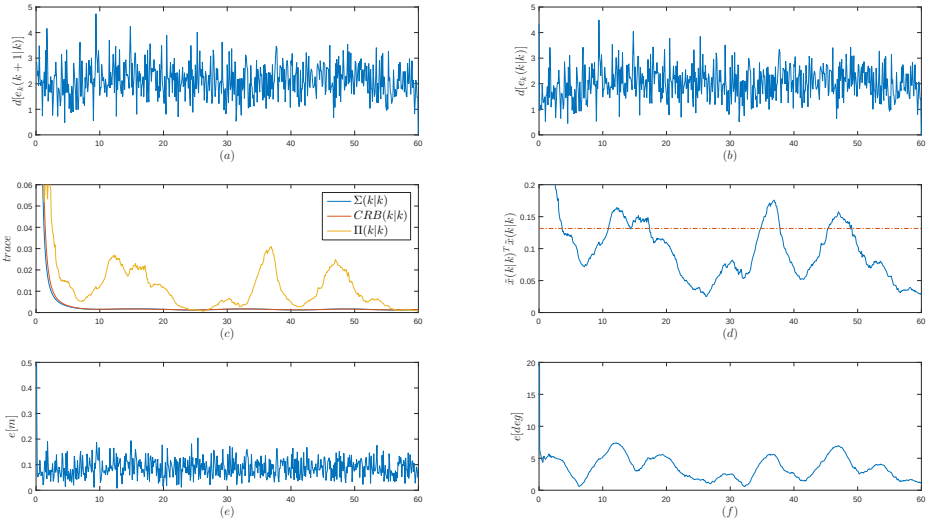

Figure 3.5.: स$_1$: Errors in Estimation a)Prediction Mahalanobis distance b)Filtering Mahalanobis distance c)Traces of State covariance, Cramer Rao Bound and the Squared Error matrix d)Squared Error e)Position Error and f)Orientation error

3.6.2. Estimation for स$_2$

Similarly the model without prior knowledge about inertias of the Tumbling satellite is estimated with the initial system state for स$_2$ chosen as
$\boldsymbol{x}_0 = \begin{bmatrix} 0.5625 & 0.7875 & 0.2250 & 0.1125 & 0.5 & -0.1 & -0.7 & 0.75 & 0.125 & -0.8 & 2.5 & 1 & -1 & 0.01 & -0.01 & 0.02 \end{bmatrix}^T$

Total time, t $[sec]$	150
Initial state estimate, $\hat{\boldsymbol{x}}(0\|0)$	$\mathbf{0}_{16,1}$
Initial state covariance estimate, $\boldsymbol{\Sigma}(0\|0)$	$\mathbb{I}_{15,15}$

Table 3.3.: स$_2$ EKF settings

- In figure 3.7, it is evident that the velocities and the inertia estimates are noisy but it is important to note that the estimator was able to start from a state of no-prior information and converge.
- In figure 3.9 b), an important observation can be made that $\boldsymbol{\Sigma}(k|k)$ is not as ideal as the $\boldsymbol{CRB}(k|k)$ as was in the previous system.
- Additionally, it is clear that the squared-error matrix $\boldsymbol{\Pi}(k|k)$ and orientation errors in f) are more variable. This is dependent on the tuning parameter for process $\boldsymbol{p}$.

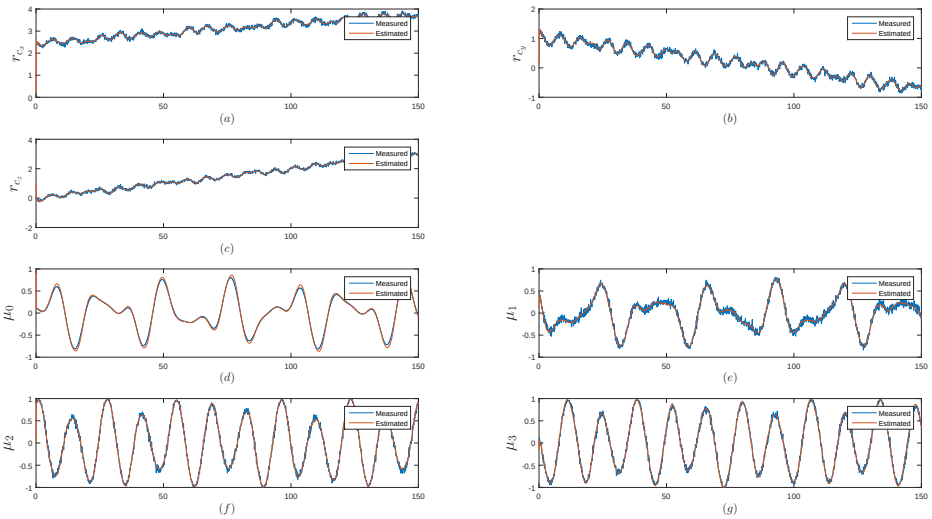

Figure 3.6.: $\mathbb{SE}_2$: Estimated pose measurements

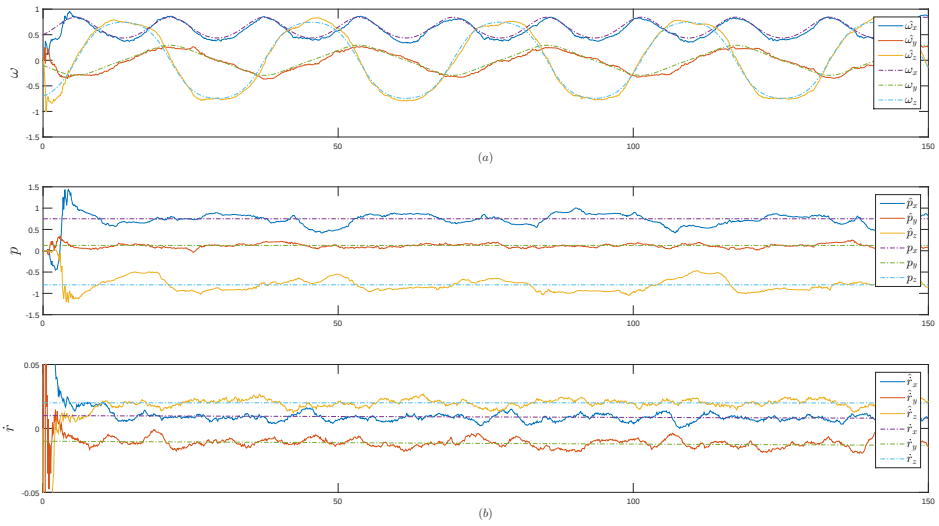

Figure 3.7.: $\mathbb{SE}_2$: a)angular velocity, inertial ratios and b)position rate

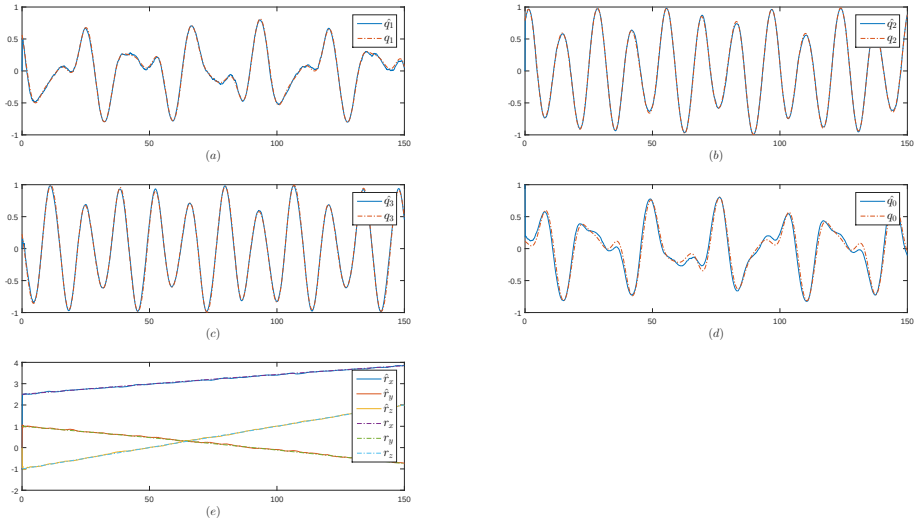

Figure 3.8.: $\mathfrak{sr}_2$: Orientation and Position

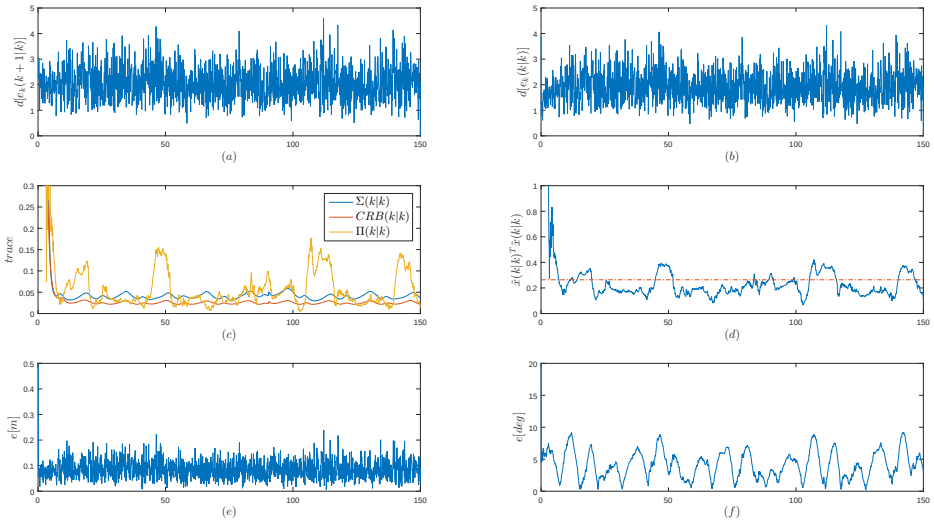

Figure 3.9.: $\mathfrak{sr}_2$: Errors in Estimation a)Prediction Mahalanobis distance b)Filtering Mahalanobis distance c)Traces of State covariance, Cramer Rao Bound and the Squared Error matrix d)Squared Error e)Position Error and f)Orientation error

3.6.3. Estimation for स$_3$

It has been previously stated that in the full-state estimator, along with unknown inertias, grasping point pose has to be estimated from a sequence of camera measurements. स$_3$ chosen as

$$\boldsymbol{x}_0 = \begin{bmatrix} 0.5625 & 0.7875 & 0.2250 & 0.1125 & 0.5 & -0.1 & -0.7 & 0.75 & 0.125 & -0.8 & 2.5 & 1 & -1 & 0.01 & -0.01 & 0.02 & 0.2 & 0.1 & 0.05 & 0.12 & 0.05 & -0.15 & 0.98 \end{bmatrix}^T$$

Total time, t $[sec]$	200
Initial state estimate, $\hat{\boldsymbol{x}}(0\|0)$	$\mathbf{0}_{21,1}$
Initial state covariance estimate, $\boldsymbol{\Sigma}(0\|0)$	$\mathbb{I}_{21,21}, \left\{ \begin{matrix} \boldsymbol{\Sigma}(0\|0)[7:9, 7:9] \\ \boldsymbol{\Sigma}(0\|0)[16:18, 16:18] \\ \boldsymbol{\Sigma}(0\|0)[19:21, 19:21] \end{matrix} \right\} = 0.05\mathbb{I}_{3,3}$

Table 3.4.: स$_3$ EKF settings

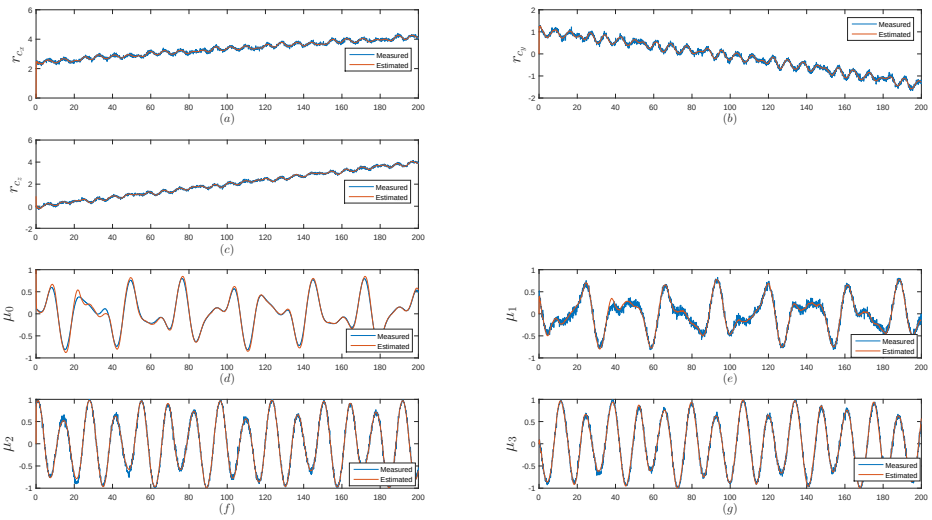

Figure 3.10.: स$_3$: Estimated pose measurements

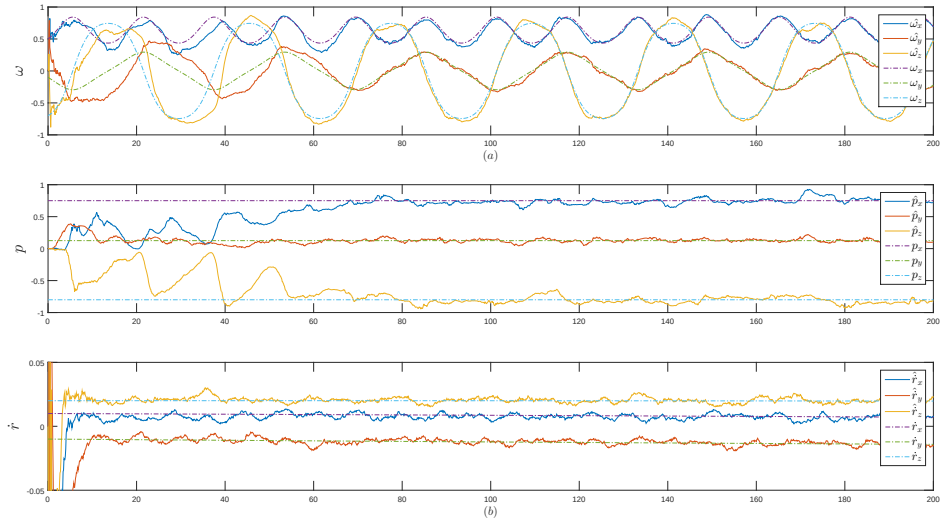

Figure 3.11.: ब्ल$_3$: a)angular velocity, inertial ratios, and b)position rate

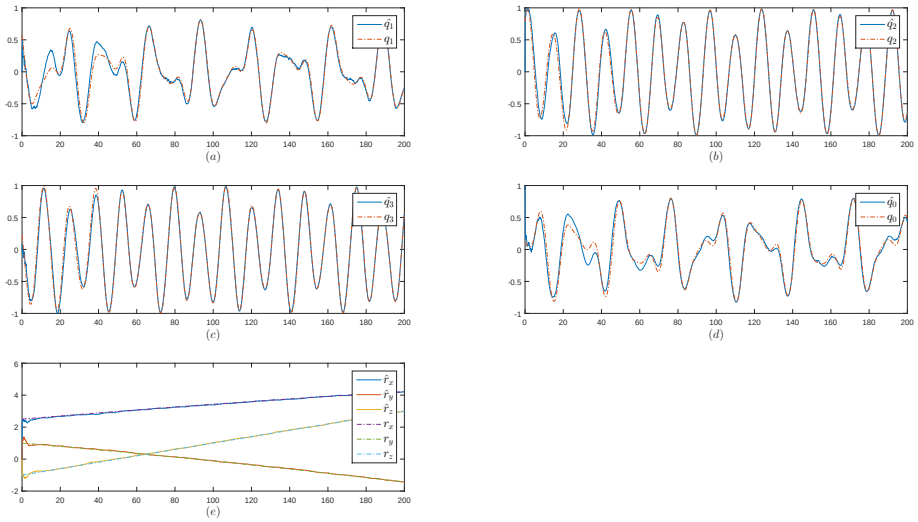

Figure 3.12.: ब्ल$_3$:Orientation and Position

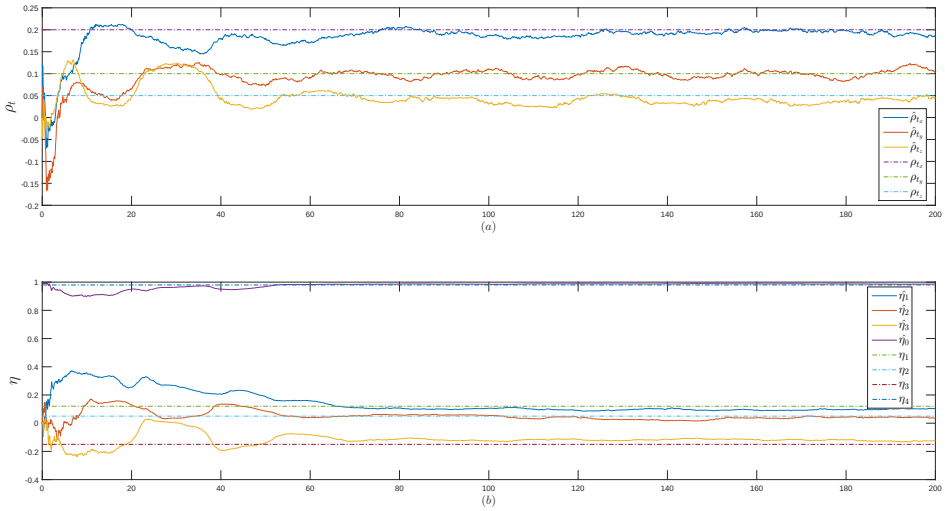

Figure 3.13.: Grasping point a)Position b)Orientation

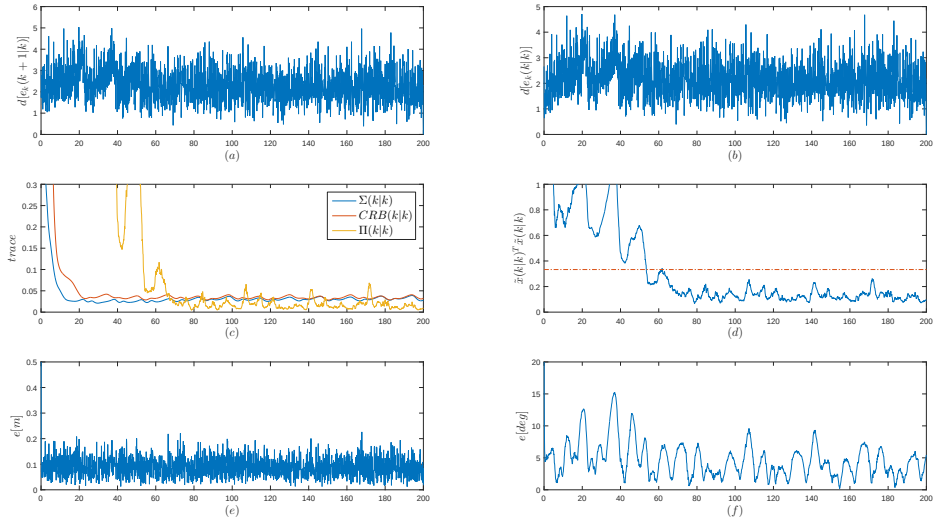

Figure 3.14.: $\mathbf{\Psi}_3$: Errors in Estimation a)Prediction Mahalanobis distance b)Filtering Mahalanobis distance c)Traces of State covariance, Cramer Rao Bound and the Squared Error matrix d)Squared Error e)Position Error and f)Orientation error

- The full-state estimator takes longer to settle or converge to the correct state values. This is evident from $\mathbf{\Pi}(k|k)$ and $\tilde{\boldsymbol{x}}^T\tilde{\boldsymbol{x}}$ curves. It is interesting to note though that the Mahalanobis distances *a*) and *b*) are still consistent. This implies that the state estimates and their Covariances are propagating equivalently. Failure to do this causes divergence in the Kalman filter.
- The estimates for grasping point pose: $\{\boldsymbol{\rho}_t, \bar{\boldsymbol{\eta}}\}$ is very noisy and is largely dependent on the values of $\boldsymbol{p}$.
- It is worth pointing out that the full-state estimator is more likely to be successful when there are uncertainties about inertia ratios and Target geometry. The sensitivity analysis has not been performed in this thesis.

References

[**Hautus1980**] M. Hautus and Eduardo Sontag. "An approach to Detectability and Observers." In: *Lectures in Applied Mathematics* 18 (1980), pp. 99–135.

[**Primbs1996**] Jim Primbs. *Survey of Nonlinear Observer Design Techniques*. CDS 122. June 1996.

[**Birk1988**] J. Birk and M. Zeitz. "Extended Luenberger observer for non-linear multivariable systems." In: *International Journal of Control* 47.6 (1988), pp. 1823–1836. DOI: 10.1080/00207178808906138. eprint: http://dx.doi.org/10.1080/00207178808906138. URL: http://dx.doi.org/10.1080/00207178808906138.

[**Krener1983**] Arthur Krener. "Linearization by output injection and nonlinear observers." In: *Systems and Control Letters* 3 (June 1983), pp. 47–52.

[**Zeitz1987**] M. Zeitz. "The extended Luenberger observer for nonlinear systems." In: *Systems and Control Letters* 9.FrA04.1 (Dec. 1987), pp. 149–156.

[**Kalman1960**] Rudolph Kalman. "A New Approach to Linear Filtering and Prediction Problems." In: *Transactions of the ASME–Journal of Basic Engineering* 82.Series D (1960), pp. 35–45.

[**Ribeiro2004**] Maria Ribeiro. *Kalman and Extended Kalman Filters: Concept, Derivation and Properties*. Feb. 2004.

[**Zhang2005**] Keshu Zhang, X. R. Li, and Yunmin Zhu. "Optimal update with out-of-sequence measurements." In: *IEEE Transactions on Signal Processing* 53.6 (June 2005), pp. 1992–2004. ISSN: 1053-587X. DOI: 10.1109/TSP.2005.847830.

[**Wu2006**] Y. Wu et al. "A Numerical-Integration Perspective on Gaussian Filters." In: *IEEE Transactions on Signal Processing* 54.8 (Aug. 2006), pp. 2910–2921. ISSN: 1053-587X. DOI: 10.1109/TSP.2006.875389.

[**Aghili2009**] Farhad Aghili and Kourosh Parsa. "Motion and Parameter Estimation of Space Objects Using Laser-Vision Data." In: *JOURNAL OF GUIDANCE, CONTROL, AND DYNAMICS* 32.2 (Mar. 2009), pp. 538–550. ISSN: 10.2514/1.37129. DOI: 10.1109/70.258046.

[**Havlík2015**] Jindich Havlík and Ondej Straka. "Performance evaluation of iterated extended Kalman filter with variable step-length." In: *Journal of Physics: Conference Series* 659.1 (2015), p. 012022. URL: http://stacks.iop.org/1742-6596/659/i=1/a=012022.

Chapter 4: EKF Robustness

4.1. Divergence of the EKF

Although it was shown in the previous chapter that the EKF converges to its true states in a Minimum squared Error (MSE) sense, there are some other aspects that are worth shedding light on to.

Firstly, the filter for the system स$_3$ is a highly sensitive one because of the presence of parameter identification problem for three states: $\begin{bmatrix}\boldsymbol{p}^T & \boldsymbol{\rho}_t^T & \bar{\boldsymbol{\eta}}^T\end{bmatrix}^T$. An uncertainty in the statistical details of these states can cause failure of convergence or divergence. Admittedly, at the onset of the estimation process, the statistical details are unknown.

In [**Fitzgerald1971**], Fitzgerald has described the terms: True divergence and Apparent divergence.

Divergence: The phenomenon during the process of stochastic estimation, which is observed if the higher-order moments (like variance) of the estimator and the real system are inconsistent. The estimated mean does not track the true state due to this.

It is tacitly understood that such a problem can occur in EKF with high likelihood since the second-moments are based on an assumption of linearized system. Especially when the filter is converging, the effect of nonlinearities is extremely high. In [**Jazwinski2007**, p. 358], Jazwinski has mentioned that it is essential to account for nonlinearities during the convergence phase. It has been suggested that the second moments should be compensated for, either by using a second-order truncation EKF or by using an iteration for the update. In either case, the EKF used in [**Aghili2009**] is likely to fail in the situation that the initial state is unknown in value or variance.

Apparent Divergence: This leads to a situation in which the higher-order moments are inconsistent but the inconsistency remains constant over time. This means that the state errors remain bounded and the estimator converges to another state-space with the corresponding stochastics.

It is important to note here that, for a system with low observability, the estimated states may be unique deterministically, but the stochastics or rather the assumption of it, may lead to multiple solutions for the same output as shown in 4.1, 4.2, 4.3, 4.4, 4.5.

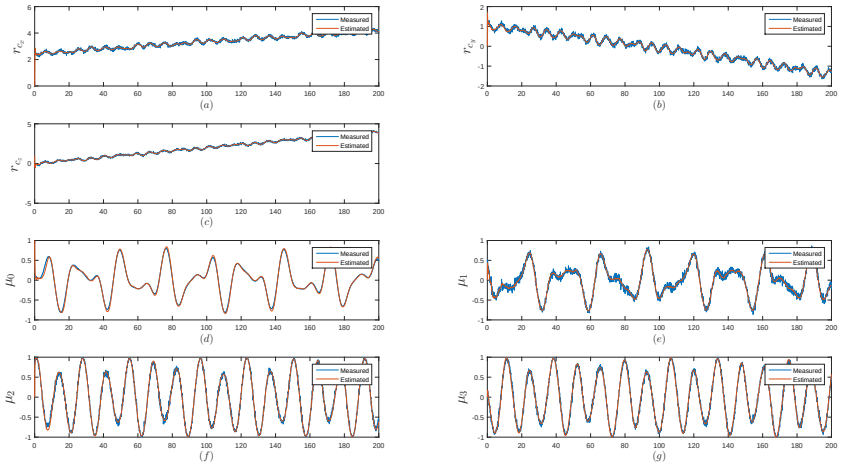

Figure 4.1.: $\mathfrak{sr}_3$: Convergence of output

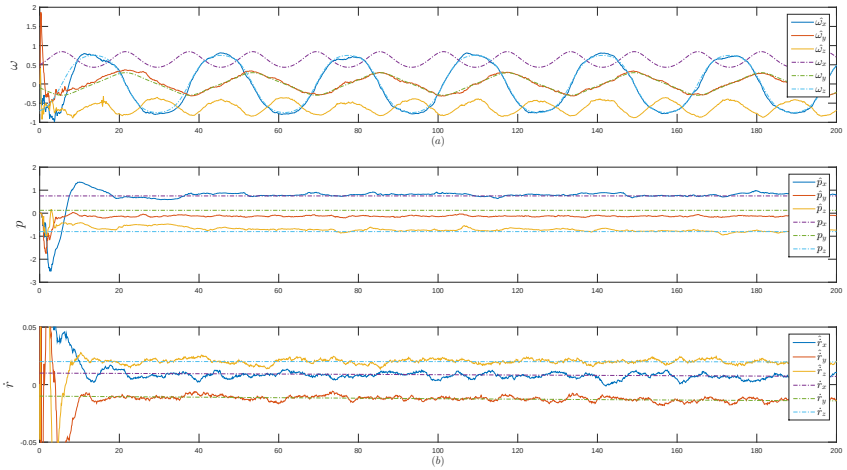

Figure 4.2.: $\mathfrak{sr}_3$: Divergence in angular velocity

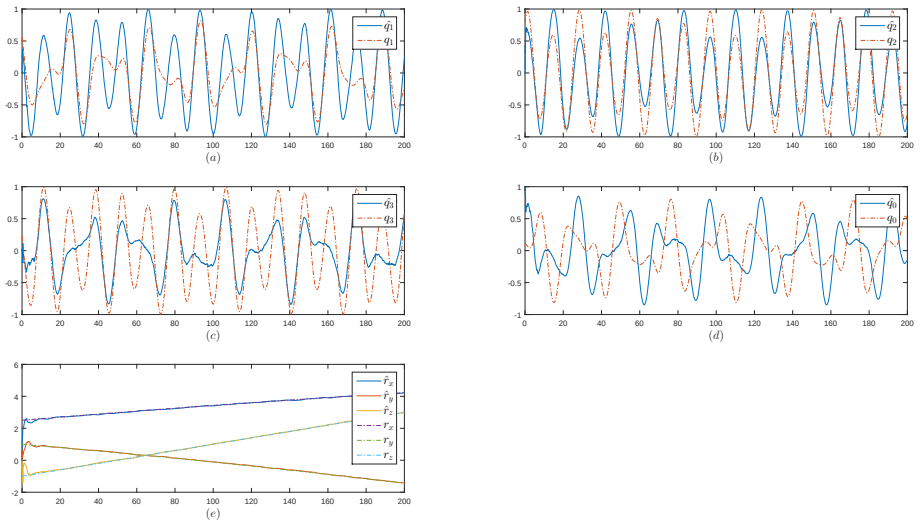

Figure 4.3.: $\mathfrak{sr}_3$: Divergence in pose relative to mass centers

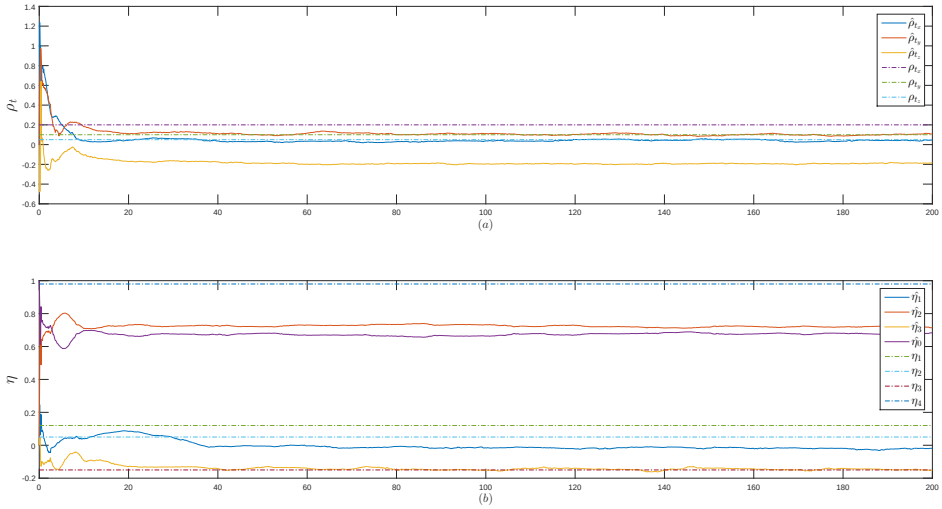

Figure 4.4.: $\mathfrak{sr}_3$: Divergence in grasping point a)position b)orientation

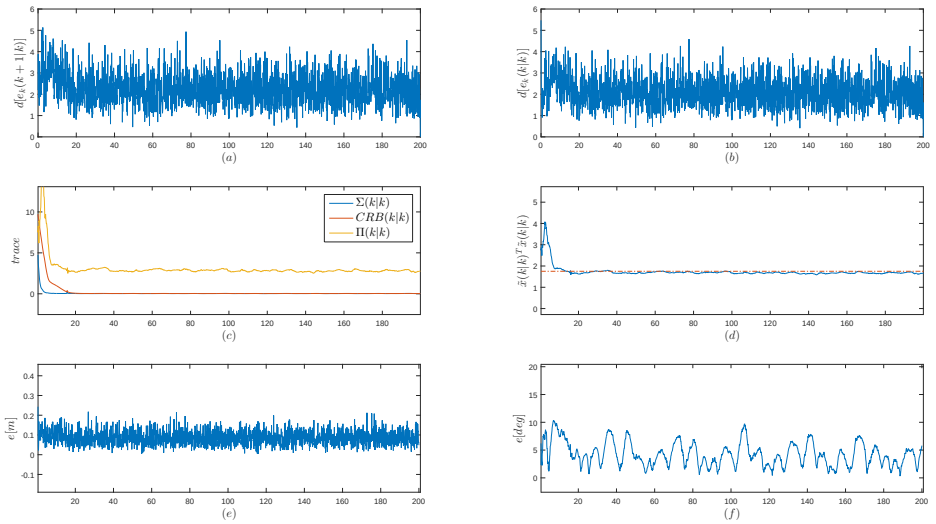

Figure 4.5.: स_3: Errors in Estimation a)Prediction Mahalanobis distance b)Filtering Mahalanobis distance c)Traces of State covariance, Cramer Rao Bound and the Squared Error matrix d)Squared Error e)Position Error and f)Orientation error

- In figure 4.1, it is clear that the observation function is being successfully tracked. In fact, in the figure 4.5 e) and f), the position and orientation errors are the same as in the case of convergence. Hence, the residual $\boldsymbol{y}_k - \boldsymbol{h}(\boldsymbol{x}(k+1|k)$ cannot be directly used as a gauge to determine divergence.

- From several passes of the EKF, it was observed that the exact states that diverged was not fixed. In this instance, $\boldsymbol{\omega}$ in 4.2, $\bar{\boldsymbol{q}}$ in 4.3 and, $\boldsymbol{\rho}_t$ and $\bar{\boldsymbol{\eta}}$ in 4.4 have diverged.

- From 4.5, it is seen that the measurement Mahalanobis distances a) and b) are low. But, there is divergence observed c) and d). $trace[\boldsymbol{\Pi}(k|k)]$ is comparatively higher but remains constant and so does the Eucledian error, $\tilde{\boldsymbol{x}}(k|k)^T\tilde{\boldsymbol{x}}(k|k)$.

Convergence of a EKF is a function of the eigenvalues of the system during convergence. It is natural that after convergence, the Kalman gain drops to nearly steady values and the eigenvalues are very close to the origin. In effect, the more negative these eigenvalues are during convergence, the faster the estimator converges. In 4.1, the minimum eigenvalue for $\boldsymbol{F}_k - \boldsymbol{K}_k\boldsymbol{H}_k$ for the linearized system has been shown for systems स_1 and स_3. For स_1, the minimum eigenvalue starts of with much higher negative value as compared to the system स_1. This indicates high sensitivity to not just noise but also the direction of propagation of the estimator in the state-space. In [**Boutayeb1997**],

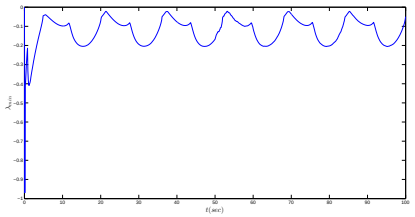

(a) सत्र$_1$: λ_{min}

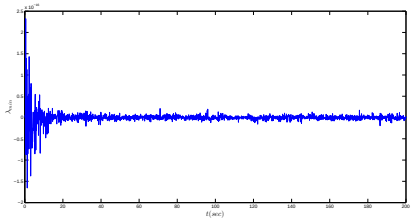

(b) सत्र$_3$: λ_{min}

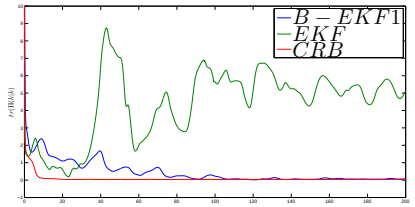

(c) trace of error square matrix for EKF and B-EKF

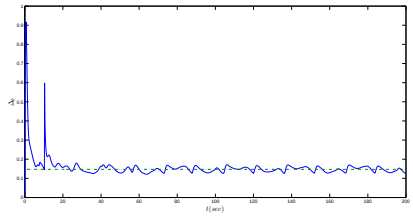

(d) Δ_k

Boutayeb, Rafaralahy, and Darouach have derived minimum conditions for convergence of an EKF. $\boldsymbol{\alpha}_k$ and $\boldsymbol{\beta}_k$ are orthogonal matrices that are introduced as premultipliers for the linearized process and measurement models. In the concluding remarks, they have observed that these matrices are unknown and it is the selection of $\boldsymbol{R}_k$ which ensures the following.

$$\boldsymbol{\alpha}_{k+1} \in [1-\sqrt{1-\Delta_{k+1}},\quad 1+\sqrt{1-\Delta_{k+1}}]$$
$$\boldsymbol{\beta}_{k+1} \in [-1,1]$$

where $\boldsymbol{\Delta}_{k+1} = \lambda_{max}(\boldsymbol{R}_{k+1})\lambda_{max}\left(\boldsymbol{R}_{k+1}^{-}\boldsymbol{H}_k\boldsymbol{R}(k+1|k)\boldsymbol{\Sigma}\boldsymbol{H}_{k+1}^{T}(\boldsymbol{H}_k\boldsymbol{\Sigma}(k+1|k)\boldsymbol{\Sigma}\boldsymbol{H}_{k+1}^{T}+\boldsymbol{R}_{k+1})^{-}\right)$

The generic form for measurement noise is given as,

$$\boldsymbol{R}_{k+1} = \mu_R\boldsymbol{H}_k\boldsymbol{\Sigma}(k+1|k)\boldsymbol{\Sigma}\boldsymbol{H}_{k+1}^{T}+\zeta\mathbb{I} \tag{4.1}$$

where μ_R and ζ are multipliers. A very similar formulation is provided in [**Perea2007**] as B-EKF 1. Perea et al. have described the problem of divergence and corroborated Jazwinski's postulation in [**Jazwinski2007**] that the EKF overestimates it's own ability in reducing the state variance. Jazwinski has suggested using multiple iterations during convergence. In this thesis, the B-EKF 1 has been employed to ensure convergence of the estimator which shows the least error according to the study in [**Perea2007**]. The formula has been modified as 4.1 since a rigorous mathematical proof is given in [**Boutayeb1997**].

$\mu_R = 5$ and $\zeta = 0.01$ was used for these simulations. In [**Boutayeb1997**], no closed formulation is found to relate Δ_{k+1} with $\boldsymbol{R}_{k+1}$. In [**Perea2007**], it has been mentioned that any approach to find the multiplier depends on the initial state error but no such method is known. By the parameters selected here, it was only ensured that $\Delta_k \leq 1$ [**Boutayeb1997**] as shown in 4.1(d). In 4.1, the error square matrix traces have been plotted with and without the convergence compensation. It is clear that $B - EKF1$, although slower than the ideal estimator with CRB converges successfully while the one used in [**Aghili2009**] diverges for the same initial conditions when intitial conditions are uncertain.

4.2. Adaptive EKF

The system definition for an EKF cannot be providred *a priori* for most systems. Within certain limits, it is possible to induce non-optimal behavior during operation to improve quality of the system specification [**Gelb1974**, p. 317]. In [**Mehra1970**], Mehra for the first time presented a classification of such adpative methods.

In the chapter 3.2, the residual, $\boldsymbol{\epsilon}_k = \boldsymbol{y}_k - \boldsymbol{h}(\boldsymbol{x}_k)$ is defined as a zero-mean gaussian process. Gelb in [**Gelb1974**] has explained how a sequence of residuals $\{\boldsymbol{\epsilon}\}^{1:k}$ can be used to determine either the process or the measurement noise covariances.

In the system defined by (1.13), a vision sensor is utilized which produces a pose estimate based on an internal optimization. As a result, the *a prior* measurement noise covariance matrix $\boldsymbol{R}_k$ is irrelevant. In [**Aghili2009**] and [**Aghili2007**], the author has maintained that the noise covariance matrix has to be estimated because of variable lighting conditions and occlusion. The methodology employed is covariance matching [**Mehra1970**]. In such a design, the selection of the window size (m) is a critical design criterion for responsiveness and has not been discussed in [**Aghili2009**]. Additionally, it was not clear how the system would behave when the noise characteristics changes. In contrast to [**Aghili2009**], a *Bayesian approach* [**Mehra1970**] is employed in this thesis and evaluated for changing noise covariances. Furthermore, it was also mentioned in the system definition that the measurement errors for orientation is state-dependent.

4.2.1. Variational Bayesian

VB inferencing is an approximate method that is used to express the posterior distribution in a tractable manner. For the purpose of Kalman filtering [**Kalman1960**], it is known that the posterior of the state has to be gaussian for the assumptions to hold true. As early as in 1970, in [**Mehra1970**], the approach to estimate $\boldsymbol{R}_k$ using an $Inv - Gamma$ disribution was already mentioned. In [**Piché2012**], a *Student-t* distribution is assumed on the measurement function. Although this is a very effective representation of a vision

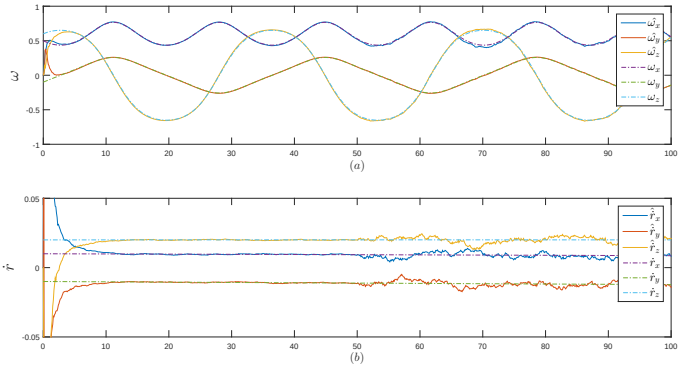

Figure 4.7.: स$_1$: angular and linear velocities affected by change in measurement noise characteristics

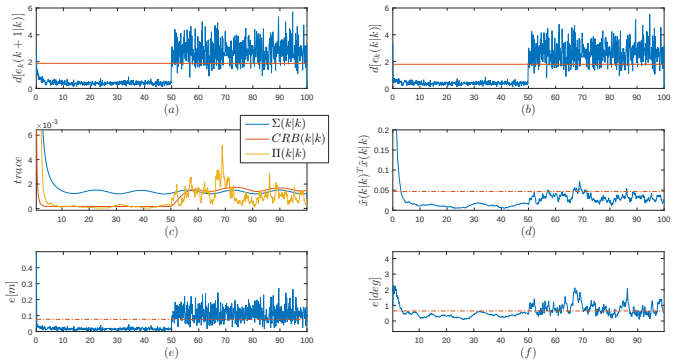

Figure 4.8.: स$_1$: Errors in Estimation a)Prediction Mahalanobis distance b)Filtering Mahalanobis distance c)Traces of State covariance, Cramer Rao Bound and the Squared Error matrix d)Squared Error e)Position Error and f)Orientation error; change in measurement noise

system, there are many parameters that need to be tuned *a priori*. In [**Roth2013**], the problem of determining $Student - t$ distribution parameters and other approximations have been discussed. This method is very elegant to specify the initial state as uncertain in both mean and variance. Despite being amenable to the problem of nonlinear estimation, this method was not pursued due to the dependency on multiple initial statistical parameters. In [**Särkkä2009**], an $Inv - Gamma$ distribution is assumed on the diagonal elements of the measurement noise covariance matrix. This methodlogy is employed here for adapting the measurement noise covariance.

In section 3.3 of the chatper 3, the Bayesian Filtering sequence was mentioned. The only difference in the adaptive case is that the both the prior (CK) and the posterior distributions will comprise of the measurement noise covariance distribution parameters.

- Prediction: CK equation

$$p(\boldsymbol{x}_k, \boldsymbol{R}_k) = \int p(\boldsymbol{x}_k|\boldsymbol{x}_{k-1}) p(\boldsymbol{R}_k|\boldsymbol{R}_{k-1}) p(\boldsymbol{x}_{k-1}, \boldsymbol{R}_{k-1}|\{\boldsymbol{y}\}^{1:k-1}) d\boldsymbol{x}_{k-1}\boldsymbol{R}_{k-1} \tag{4.2}$$

- Update: Bayesian equation

$$p(\boldsymbol{x}_k, \boldsymbol{R}_k|\{\boldsymbol{y}\}^{1:k}) \propto p(\boldsymbol{y}_k|\boldsymbol{x}_k, \boldsymbol{R}_k) p(\boldsymbol{x}_k, \boldsymbol{R}_k|\{\boldsymbol{y}\}^{1:k-1}) \tag{4.3}$$

VB methods rely on reasonable approximations to solve the Bayesian filtering problem. In a formulation like [**Särkkä2009**], we assume that the previous state and measurement noise is known with a distribution which the product of the Normal state distribution and $Inv-Gamma$ measurement covariance distribution.

$$p(\boldsymbol{x}_{k-1}, \boldsymbol{R}_{k-1}|\{\boldsymbol{y}\}^{1:k-1}) = \mathcal{N}\Big(\boldsymbol{x}_{k-1}|\hat{\boldsymbol{x}}(k-1|k-1), \hat{\boldsymbol{R}}(k-1|k-1)\Big) \times \prod_{i=1}^{d} \Gamma^{-}(r_{k-1}^2|\alpha, \beta) \tag{4.4}$$

where $\mathcal{N}(.)$ and $\Gamma^{-}(.)$ indicate the Normal and the $Inv-Gamma$ distributions.

- $Inv-Gamma$ is one of the conjugate prior distributions for a Gaussian distribution and it is common to model variances with it.
- The linear dynamics of the state and measurement noise variances are independent and hence the propagation equations are decoupled.
- In [**Särkkä2009**], an assumption on $p_k(r_k|r_{k-1})$ is made that the propagation maintains the same distribution. From the perspective of the vision system, the optimization cost or the reprojection errors can be used to compute this quantity. This is a subject for another study and has not been explored heretofore.
- The joint distribution of the prediction step is given by,

$$\begin{aligned} p(\boldsymbol{x}_k, \boldsymbol{R}_k|\{\boldsymbol{y}\}^{1:k-1}) = p(\boldsymbol{x}_k|\{\boldsymbol{y}\}^{1:k-1}) p(\boldsymbol{R}_k|\{\boldsymbol{y}\}^{1:k-1}) \\ \mathcal{N}\Big(\boldsymbol{x}_k|\hat{\boldsymbol{x}}(k|k-1)\Big) \prod_{i=1}^{d} \Gamma^{-}(r_{i,k}|\alpha_{i,k}, \beta_{i,k}) \end{aligned} \tag{4.5}$$

- The coupling of the probability distributions happens due to the likelihood function $p(\boldsymbol{y}_k|\boldsymbol{x}_k, \boldsymbol{R}_k)$ and an approximation has to be made on the posterior. For this purpose the Kullback-Leibler divergence is minimized.

- The purpose of VB is to find a joint distribution $\mathcal{Q}(x;\theta)$ over hidden variables of current state and noise covariance. The mean-field form assumes independence between the various variables. This means, $\mathcal{Q}(x;\theta) = \prod_i \mathcal{Q}_i(x_i;\theta_i)$.

- If $\mathcal{P}(x)$ is the true joint distribution, the KL operator gives us the amount of dissimilarity between $\mathcal{P}(x)$ and $\mathcal{Q}(x;\theta)$. The reader is referred to [**Fox2012**] which gives the required equations for minimizing KL-divergence. This technique is common for other distributions like *Student-t*, *Inverse-Wishart* et al.

$$KL[\mathcal{Q}(x)||\mathcal{P}(x|D)] = \int dx.\mathcal{Q}(x)ln\frac{\mathcal{Q}(x)}{\mathcal{P}(x|D)}] \tag{4.6}$$

  where $\mathcal{Q}(x)$ is the product of constituents as mentioned above.

Remark 19. $\mathcal{Q}$ approximates a joint distribution but $\mathcal{Q}_i$ is a poor approximation to true marginals $\mathcal{P}_i$.

The equations have been derived in [**Särkkä2009**] for a linear system. For a nonlinear system, the algorithm is given below in 1

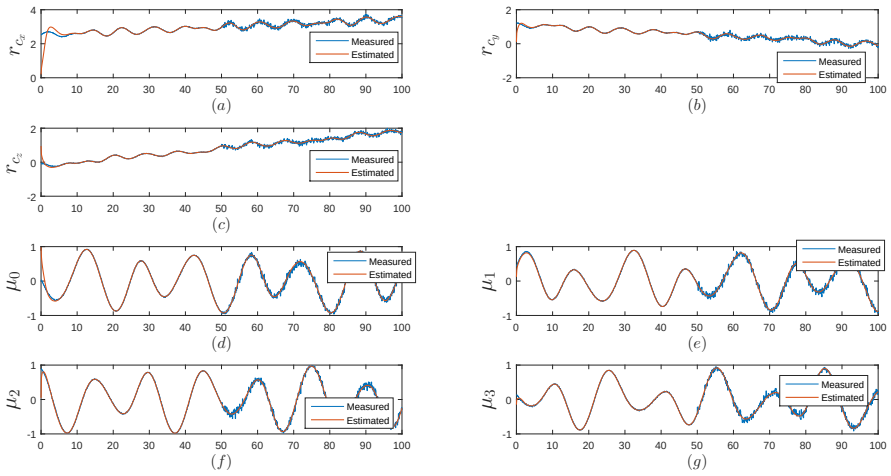

Figure 4.9.: सा$_1$: Estimated pose measurements after VB-EKF

- In figure 4.9, the scenario protracted is that the noise for all channels in the model start as $\boldsymbol{y}_k \equiv \mathcal{N}[\mathbf{0}, 1e^{-4}\mathbb{I}_{6,6}]$ which at time, $t = 50$ changes to $\boldsymbol{y}_k \equiv \mathcal{N}[\mathbf{0}, 5e^{-3}\mathbb{I}_{6,6}]$. This is show in 4.9 where the measurements become more noisy after 50 seconds.

Algorithm 1 VB-EKF

procedure PREDICT
  $\hat{\boldsymbol{x}}(k+1|k) \leftarrow \hat{\boldsymbol{x}}(k|k) + \int_{t_0}^{t_1} \boldsymbol{f}(\hat{\boldsymbol{x}}(k|k))$
  $\boldsymbol{\Sigma}(k+1|k) \leftarrow \boldsymbol{F}_k \boldsymbol{\Sigma}(k|k) \boldsymbol{F}_k^T + \boldsymbol{Q}_k$
  $\hat{\alpha}_{k+1,i} \leftarrow \rho_i \alpha_{k,i} \quad \forall\, i \in \begin{bmatrix} 1 & d \end{bmatrix}$
  $\hat{\beta}_{k+1,i} \leftarrow \rho_i \beta_{k,i} \quad \forall\, i \in \begin{bmatrix} 1 & d \end{bmatrix}$
procedure UPDATE(Set $\hat{\boldsymbol{x}}_0(k+1|k+1) \leftarrow \hat{\boldsymbol{x}}(k+1|k)$, $\boldsymbol{\Sigma}_0(k+1|k+1) \leftarrow \boldsymbol{\Sigma}(k+1|k)$, $\alpha^0_{k+1,i} \leftarrow \frac{1}{2} + \hat{\alpha}_{k+1,i}$, $\beta^0_{k+1,i} \leftarrow \hat{\beta}_{k+1,i}$)
  for n $\leftarrow$ 1 to N **do**
    $\hat{\boldsymbol{R}}^n_{k+1} \leftarrow diag[\frac{\beta^n_{k,1}}{\alpha^n_{k,1}} ... \frac{\beta^n_{k,d}}{\alpha^n_{k,d}}]$
    $\boldsymbol{K}^n_{k+1} \leftarrow \boldsymbol{\Sigma}_n(k+1|k) \boldsymbol{H}^T_{k+1} \left(\boldsymbol{H}_{k+1} \boldsymbol{\Sigma}(k+1|k) \boldsymbol{H}^T_{k+1} + \hat{\boldsymbol{R}}^n_{k+1} \right)^{-}$
    $\hat{\boldsymbol{x}}_n(k+1|k+1) \leftarrow \hat{\boldsymbol{x}}(k+1|k) + \boldsymbol{K}_{k+1}(\boldsymbol{y}_{k+1} - \boldsymbol{h}(\hat{\boldsymbol{x}}_n(k+1|k+1)))$
    $\boldsymbol{\Sigma}_n(k+1|k+1) \leftarrow (\mathbb{I} - \boldsymbol{K}^n_{k+1} \boldsymbol{H}_{k+1}) \boldsymbol{\Sigma}_n(k+1|k)$
    $\beta^n_{k+1,i} \leftarrow \hat{\beta}_{k+1,i} + \frac{1}{2}(\boldsymbol{y}_k - \boldsymbol{h}(\hat{\boldsymbol{x}}_n(k+1|k+1))^2_i +$
      $\frac{1}{2}(\boldsymbol{H}_{k+1} \boldsymbol{\Sigma}(k+1|k+1) H^T_{k+1})_{ii} \quad \forall\, i \in \begin{bmatrix} 1 & d \end{bmatrix}$
    $\boldsymbol{H}_{k+1} \leftarrow \nabla_x \boldsymbol{h}(\boldsymbol{x}_{k+1}) \Big|_{x=\hat{x}_n(k+1|k+1)}$
  Set $\hat{\beta}_{k+1,i} \leftarrow \beta^N_{k+1,i}$, $\hat{\boldsymbol{x}}(k+1|k+1) \leftarrow \hat{\boldsymbol{x}}_N(k+1|k+1)$, $\boldsymbol{\Sigma}(k+1|k+1)$
    $\leftarrow \boldsymbol{\Sigma}_n(k+1|k+1)$

- The tuning values used for the simulation studies were

$$\begin{aligned} \boldsymbol{\alpha}_0 &= 0.1[\mathbf{1}]_{6,1} \\ \boldsymbol{\beta}_0 &= 0.06[\mathbf{1}]_{6,1} \\ \rho &= 0.75 \\ N &= 2 \end{aligned}$$

  According to [**Särkkä2009**], a high value for ρ makes the noise adapting responsive. Based on the values above, the initial covariance elements are $\frac{\beta}{\alpha} = 1.67$ which is considerably high.

- It is worth noting here that initializing the EKF with an unknown noise covariance acts as converging manipulation. Since, $\boldsymbol{R}_k$ is very high in the beginning, it has the same effect as the B-EKF in terms of convergence. Despite this, in figure 4.10, it can be seen that the velocity estimates remain immune to change in noise characteristics. In figure 4.11 *e*), it is seen that the although the trace of error

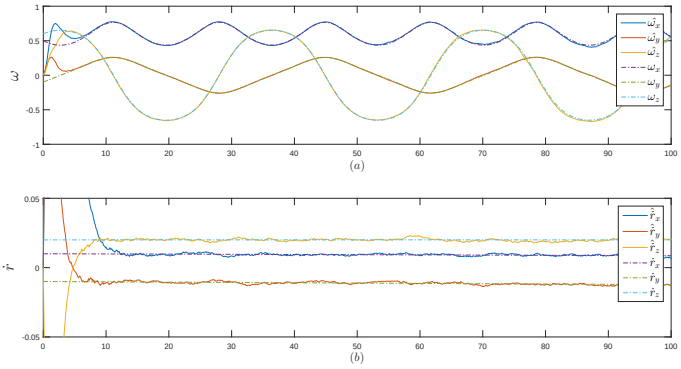

Figure 4.10.: सि$_1$:angular and linear velocities with VB-EKF

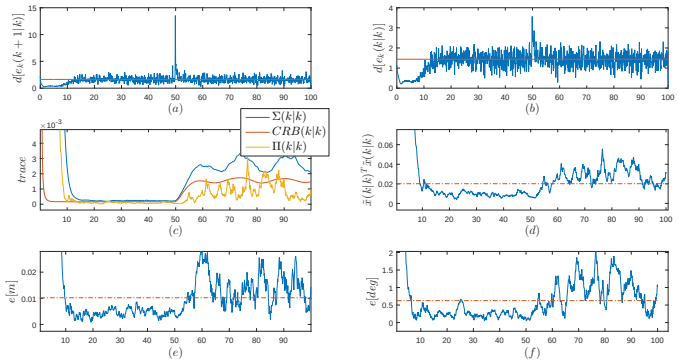

Figure 4.11.: Errors in Estimation a)Prediction Mahalanobis distance b)Filtering Mahalanobis distance c)Traces of State covariance, Cramer Rao Bound and the Squared Error matrix d)Squared Error e)Position Error and f)Orientation error

square matrix $\mathbf{\Pi}(k|k)$ increases, it is within the estimated $\mathbf{\Sigma}(k|k)$ and the theretical CRB. Moreover, except the peak, the Mahalanobis distances for the residual $\boldsymbol{\epsilon}_k$ $a)$ $b)$ before and after filtering remain consistent. This implies that the increase in residuals due changing noise characteristics is compensated by a change in $\boldsymbol{R}_k$

- In figure 4.12, the diagonal elements have been plotted for the scenario. The filter was able to track the variance changes but there are still some errors in the variance estimates. This is expected since the approximation and nonlinear errors have not been modeled into the Process noise covariance and are likely to be estimated into $\hat{\boldsymbol{R}}_k$.

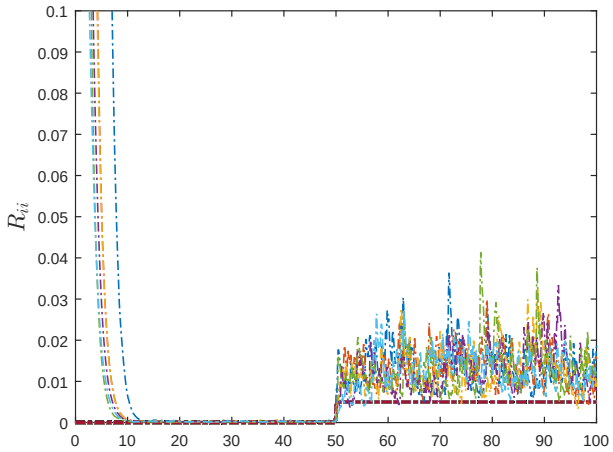

Figure 4.12.: स$_1$:Measurement Noise Covariance, $\boldsymbol{R}_k$

4.3. Outlier rejection

In the current system for the Servicer, the vision system is based on feature-matching and results in outliers in specific conditions. In this case, for the estimation scheme, it is essential to have an outlier detection/rejection scheme. This is attributed to the fact that the distributions are assumed to be gaussian and a higher density of outliers belies this. This problem becomes even more pertinent in vision systems as mentioned before. In [**Alcantarilla2016**], the non-gaussian nature of odometry algorithms has been discussed in detail.

The reprojection error or an optimization cost, $J(\theta)$, can be used to detect outliers in advance. In this thesis, this was not considered and an outlier system was built into the measurement update equation.

In the previous sections, the residual has been discussed extensively.

$$\begin{aligned} \boldsymbol{\epsilon} &= \boldsymbol{y}_k - \boldsymbol{h}(\hat{\boldsymbol{x}}(k+1|k)) \\ \mathcal{E}[\boldsymbol{\epsilon}] &= \mathbf{0} \\ \mathcal{E}[\boldsymbol{\epsilon}\boldsymbol{\epsilon}^T] &= \boldsymbol{H}_{k+1}\boldsymbol{\Sigma}(k+1|k)\boldsymbol{H}_{k+1}^T + \boldsymbol{R}_{k+1} \end{aligned}$$

It is known that the squared Mahalanobis distance ($d^2(\boldsymbol{\epsilon})$) has a χ^2-distribution. In figure 4.13, the residual $\boldsymbol{\epsilon}$ for the स$_1$ estimator was fit to a χ^2 distribution. The fit was found to be nearly χ^2 with a scale parameter $\beta = 2.87$. Under the Kalman fitler's gaussian zero-mean assumption for the residual, the Mahalanobis distance is computed

as,

$$d^2(\boldsymbol{\epsilon}) = \boldsymbol{\epsilon}^T(\boldsymbol{H}_k\boldsymbol{\Sigma}(k+1|k)\boldsymbol{H}_k^T + \boldsymbol{R}_k)^{-}\boldsymbol{\epsilon} \tag{4.7}$$

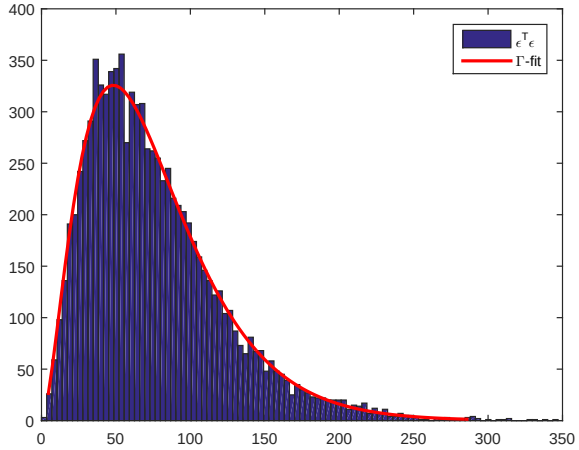

Figure 4.13.: स$_1$:$\chi^2 - fit$ for the residual ϵ

If $d^2(\boldsymbol{\epsilon}) \leq \chi^2(\alpha)$, Measurement $\boldsymbol{y}_k$ is acceptable. Otherwise, $\boldsymbol{y}_k$ is rejected and $K \leftarrow \mathbf{0}$

A similar Filtering method was explained in Chang in [**Chang2014**]. In his work, scaling factors are employed for manipulating $\boldsymbol{R}_k$. In order to avoid tampering with $\boldsymbol{R}_k$ which is also derived through Bayesian Inferencing, a simpler approach of rejecting the measurement altogether is used. The simulations results are shown below.

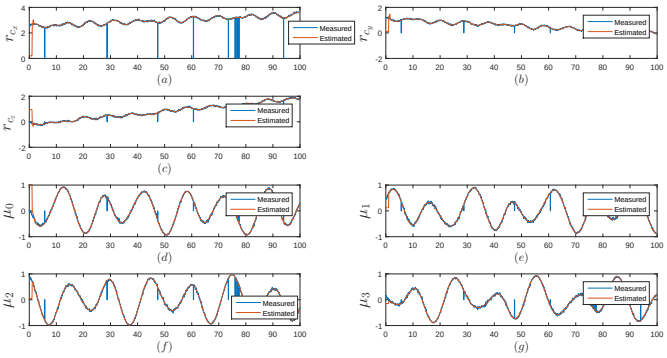

Figure 4.14.: स$_1$:Estimated and Measurements of Pose affected by outliers

- In 4.14, the pose measurements that are affected with outliers are shown. In this

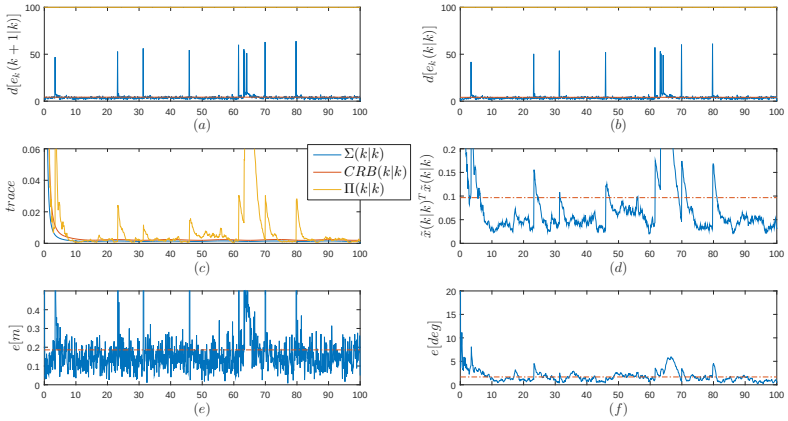

Figure 4.15.: π_1:Errors in Estimation a)Prediction Mahalanobis distance b)Filtering Mahalanobis distance c)Traces of State covariance, Cramer Rao Bound and the Squared Error matrix d)Squared Error e)Position Error and f)Orientation error; for EKF due to outliers in measurement

example, the outliers have been generated by setting randomly selected samples to 0 across all channels of measurement. This replicates a typical situation like a packet-loss or failure of Pose-detection system.

- In effect, an EKF converges to a steady-state wherein even highly variable residual $\boldsymbol{\epsilon}$ has substantially minimal effect. But as shown in figure 4.15, the estimate error measures are too high for servoing purposes.
- In 4.16, the outlier-robust EKF was able to reject all the outliers with $p - value = 0.6$. The χ^2 distribution was assumed to have a *degree-of-freedom* as 6, which is the same as the number of measurement channels.

Remark 20. It is important to point out that the threshold selection in this study was arbitrary and a rigorous Receiver Operating Characteristic (ROC) analysis has to be performed. It was observed that the threshold changes with varying measurement noise characteristics. So, the VB-EKF and the Outlier-Robust EKF have to be operated together, which is an open area for future work.

References

[**Fitzgerald1971**] R. Fitzgerald. "Divergence of the Kalman filter." In: *IEEE Transactions on Automatic Control* 16.6 (Dec. 1971), pp. 736–747. ISSN: 0018-9286. DOI: 10.1109/TAC.1971.1099836.

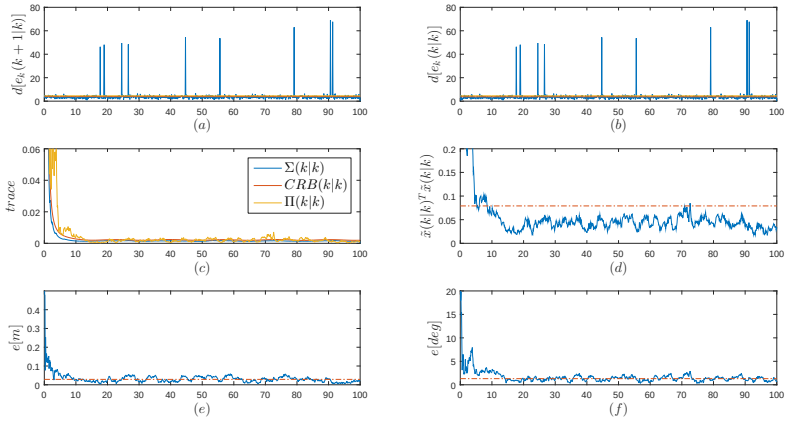

Figure 4.16.: π_1:Errors in Estimation a)Prediction Mahalanobis distance b)Filtering Mahalanobis distance c)Traces of State covariance, Cramer Rao Bound and the Squared Error matrix d)Squared Error e)Position Error and f)Orientation error for Outlier-Robust EKF

[**Jazwinski2007**] A.H. Jazwinski. *Stochastic Processes and Filtering Theory*. Dover Books on Electrical Engineering Series. Dover Publications, 2007. ISBN: 9780486462745. URL: https://books.google.co.in/books?id=4AqL3vE2J-sC.

[**Aghili2009**] Farhad Aghili and Kourosh Parsa. "Motion and Parameter Estimation of Space Objects Using Laser-Vision Data." In: *JOURNAL OF GUIDANCE, CONTROL, AND DYNAMICS* 32.2 (Mar. 2009), pp. 538–550. ISSN: 10.2514/1.37129. DOI: 10.1109/70.258046.

[**Boutayeb1997**] M. Boutayeb, H. Rafaralahy, and M. Darouach. "Convergence analysis of the extended Kalman filter used as an observer for nonlinear deterministic discrete-time systems." In: *IEEE Transactions on Automatic Control* 42.4 (Apr. 1997), pp. 581–586. ISSN: 0018-9286. DOI: 10.1109/9.566674.

[**Perea2007**] Laura Perea et al. "Nonlinearity in Sensor Fusion: Divergence Issues in EKF, Modified Truncated GSF, and UKF." In: Guidance, Navigation, and Control and Co-located Conferences. doi:10.2514/6.2007-6514. American Institute of Aeronautics and Astronautics, Aug. 2007. DOI: http://dx.doi.org/10.2514/6.2007-6514.

[**Gelb1974**] A. Gelb. *Applied Optimal Estimation*. MIT Press, 1974. ISBN: 9780262570480. URL: https://books.google.co.in/books?id=KlFrn8lpPP0C.

[**Mehra1970**] R. K. Mehra. "Approaches to adaptive filtering." In: *Adaptive Processes (9th) Decision and Control, 1970. 1970 IEEE Symposium on.* Dec. 1970, pp. 141–141. DOI: 10.1109/SAP.1970.269992.

[**Aghili2007**] Farhad Aghili and Kourosh Parsa. "Adaptive motion estimation of a tumbling satellite using laser-vision data with unknown noise characteristics." In: *2007 IEEE/RSJ International Conference on Intelligent Robots and Systems.* Oct. 2007, pp. 839–846. DOI: 10.1109/IROS.2007.4399143.

[**Kalman1960**] Rudolph Kalman. "A New Approach to Linear Filtering and Prediction Problems." In: *Transactions of the ASME–Journal of Basic Engineering* 82.Series D (1960), pp. 35–45.

[**Piché2012**] R. Piché, S. Särkkä, and J. Hartikainen. "Recursive outlier-robust filtering and smoothing for nonlinear systems using the multivariate student-t distribution." In: *2012 IEEE International Workshop on Machine Learning for Signal Processing.* Sept. 2012, pp. 1–6. DOI: 10.1109/MLSP.2012.6349794.

[**Roth2013**] M. Roth, E. Özkan, and F. Gustafsson. "A Student's t filter for heavy tailed process and measurement noise." In: *2013 IEEE International Conference on Acoustics, Speech and Signal Processing.* May 2013, pp. 5770–5774. DOI: 10.1109/ICASSP.2013.6638770.

[**Särkkä2009**] S. Särkkä and A. Nummenmaa. "Recursive Noise Adaptive Kalman Filtering by Variational Bayesian Approximations." In: *IEEE Transactions on Automatic Control* 54.3 (Mar. 2009), pp. 596–600. ISSN: 0018-9286. DOI: 10.1109/TAC.2008.2008348.

[**Fox2012**] Charles W. Fox and Stephen J. Roberts. "A tutorial on variational Bayesian inference." In: *Artificial Intelligence Review* 38.2 (2012), pp. 85–95. ISSN: 1573-7462. DOI: 10.1007/s10462-011-9236-8. URL: http://dx.doi.org/10.1007/s10462-011-9236-8.

[**Alcantarilla2016**] Pablo Alcantarilla and Oliver Woodford. "Noise Models in Feature-based Stereo Visual Odometry." In: *Physics Letters A* (July 2016). arXiv: 1607.00273v1 [Computer Vision and Pattern Recognition (cs.CV)].

[**Chang2014**] Guobin Chang. "Robust Kalman filtering based on Mahalanobis distance as outlier judging criterion." In: *Journal of Geodesy* 88.4 (2014), pp. 391–401. ISSN: 1432-1394. DOI: 10.1007/s00190-013-0690-8. URL: http://dx.doi.org/10.1007/s00190-013-0690-8.

Chapter 5: Implementation

5.1. Multi-rate & Event-driven Implementation

The equations pertaining to the multi-rate implementation were derived in the chapter 3.2 in 3. The main integrator/predictor/controller was run at a sampling time, $\Delta t_i = 0.01$ seconds. Camera-based systems are typically slower and the reference system at DLR was operating at 0.1 seconds. Evidently, for accurate and responsive servo control, the estimator is required to produce accurate state-estimates from slow-sampled measurements. This point has been adequately emphasized by Palmerini, Sabatini, and Gasbarri in [**Palmerini2016**] concerning grasping assistance. Furthermore, vision systems are not uniformly sampled and hence the $time - of - arrival$ is not deterministic. Hence, in this thesis, a trigger-based Kalman filter was designed. Figure 5.1 demonstrates this where the number of samples generated are incrementing randomly in a range, $\delta t \in \begin{bmatrix} 0.6, & 0.9 \end{bmatrix}$. The benefits of this approach to vision systems was first discussed in [**Sridhar1993**].

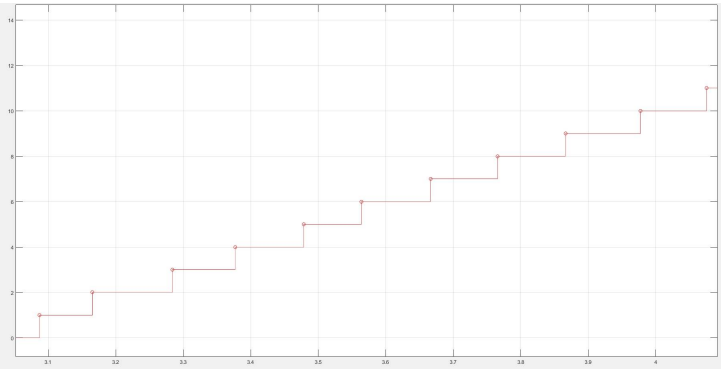

Figure 5.1.: Number of samples generated in vision systems, non-uniform

Another significant point that strikes out in vision systems is that, at the *time-of-arrival*, the measurement is a function of a past state. That is, $\boldsymbol{y}_k = \boldsymbol{h}(\boldsymbol{x}_{\boldsymbol{k}-\boldsymbol{\tau}})$, where τ is the the number of samples back in history where the state was recorded. This scenario has been delineated in figure 5.2.

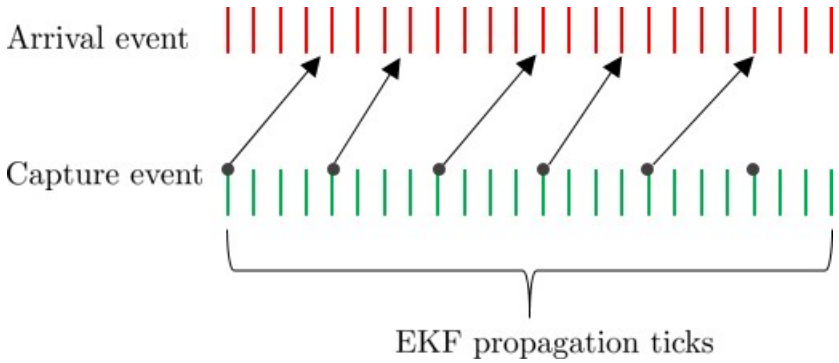

Figure 5.2.: Out of Sequence Vision Measurements

Hence, after the update is made, a corresponding state propagation has to be performed, so that the controller operates with the most recent state estimate. Particularly, in systems with high dynamics, this can cause large estimation errors. As an alternative, one can take a look at [**Julier2005**] and [**Alexander1991**] where the fusion of time-delayed measurements has been derived. For a state-propagation, one must set $K \leftarrow \mathbf{0}$ in the equations derived in the above works.

$$\hat{\boldsymbol{x}}(k_d|k_d) = \hat{\boldsymbol{x}}(k_d|k_d-1) + \boldsymbol{K}\Big(\boldsymbol{y}_{k_d} - \boldsymbol{h}(\hat{\boldsymbol{x}}(k_d|k_d-1)\Big) \tag{5.1}$$

$$\hat{\boldsymbol{x}}(k|k_d) = \hat{\boldsymbol{x}}(k_d|k_d) + \int_{k_d}^{k} \boldsymbol{f}(\hat{\boldsymbol{x}}(k_d|k_d)) \tag{5.2}$$

where $k_d = k - \tau$.

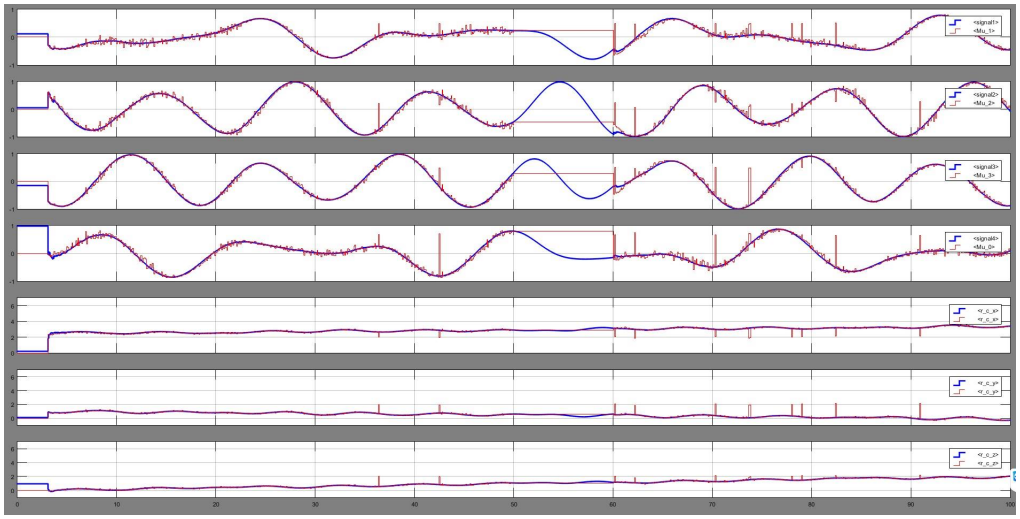

Figure 5.3.: estimates: a), b), c) and d) → orientation quaternion $\bar{\mu}$ and e), f) and g) → position $\boldsymbol{r}_c$ of the Target grasping center with respect to Seriver end-effector

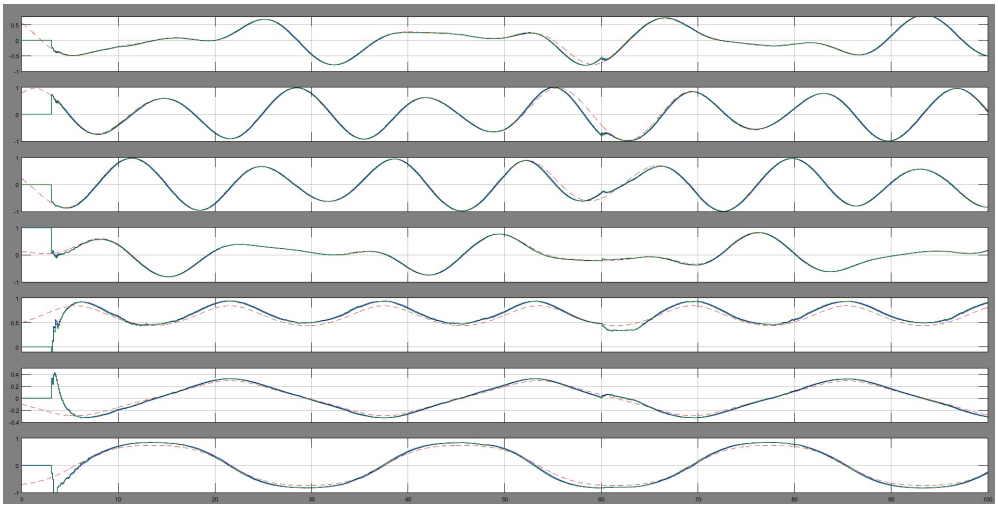

Figure 5.4.: estimates: a), b), c) and d) → orientation quaternion $\bar{\mathbf{q}}$ and e), f) and g) → angular velocity ω

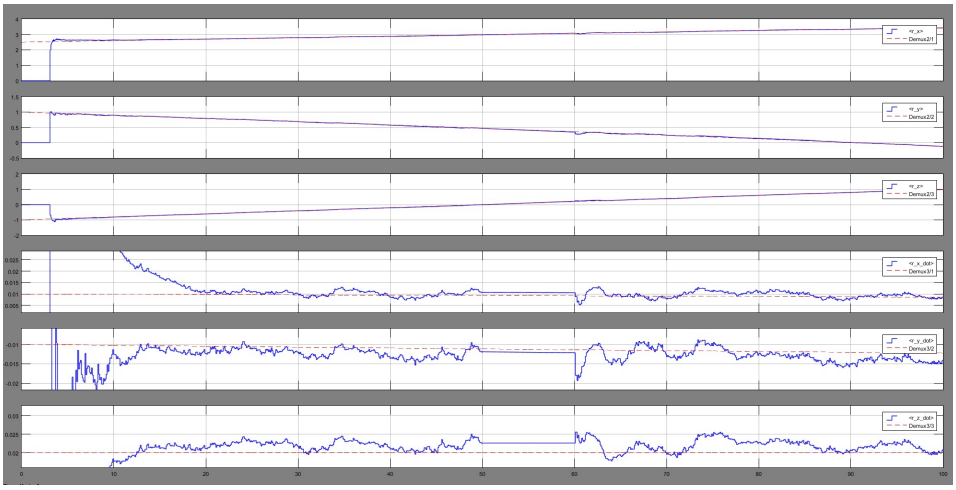

Figure 5.5.: estimates: a), b), c) → position vector **r** while d), e) and f) → linear velocity $\dot{\boldsymbol{r}}$ of the Target mass center with respect to Servicer mass center

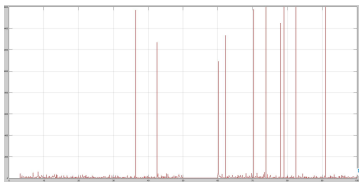

(a) Mahalanobis distance, $d(\boldsymbol{\epsilon})$

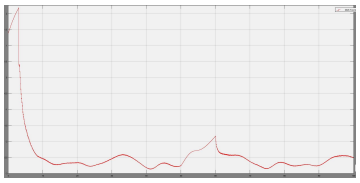

(b) $log[trace(\boldsymbol{\Sigma}(k|k))]$

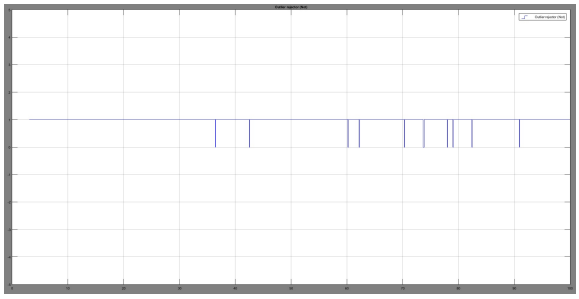

Figure 5.7.: EKF switching in presence pf outliers

- The sequence of figures from 5.3 to 5.7 show the results from a single pass of the Multi-rate Event driven EKF for the nonlinear system स_1. The theory from previous sections about outlier rejection, multi-rate fusion et al have been employed in this section.
- In the scenario, the first measurement arrives at $t = 3$ seconds. In $t \in \begin{bmatrix}50, & 60\end{bmatrix}$, a possible occlusion is simulated. The measurement is infested with quite a few outliers too.
- In the time $t \in \begin{bmatrix}50, & 60\end{bmatrix}$, the state estimates start deviating mainly due to integrator sampling time and integrator type. A higher sampling rate provides a longer feasible time-interval in which the measurements may be absent before the EKF starts becoming erroneous.
- The velocity $\dot{\boldsymbol{r}}$ estimates are poor since this quantity is not directly sensed.
- Based on the theory in the previous chapter, it is easy to see the effectiveness of Mahalanobis distance as a discriminator function for multivariate systems. All the outliers have been rejected in the time period.

5.2. Multiple-sensor fusion

In the previous section, it was made clear that vision systems inherently come with a delayed state measurement and the results were obtained for a single-sensor system. For the purpose of grasping uncooperative targets, multiple sensors may be employed for relative navigation, as mentioned in [**Palmerini2016**]. Hence, the requirement is to perform multiple-fusion using the EKF. One of the seminal works in multi-sensor fusion is found in [**Willner1976**]. Willner, Chang, and Dunn have discussed several strategies that can employed. The strategy employed in this thesis is the Parallel filter in which the measurement updates occur independently. No particular performance difference was found in context of EKF whether Parallel or Sequential strategy was chosen.

For *Parallel* update

$$\begin{aligned}
\hat{\boldsymbol{x}}(k+1|k+1) &= \hat{\boldsymbol{x}}(k+1|k) + \sum_{i=1}^{n} \boldsymbol{K}_i(\boldsymbol{z}_{k+1} - \boldsymbol{h}_i(\hat{\boldsymbol{x}}(k+1|k)) \\
\boldsymbol{K}_i &= \boldsymbol{\Sigma}(k+1|k)\boldsymbol{H}_{k+1,i}^T \boldsymbol{S}_{k+1,i}^- \\
\boldsymbol{\Sigma}(k+1|k+1)^- &= \boldsymbol{\Sigma}(k+1|k)^- + \sum_{i=1}^{n} \boldsymbol{H}_{k+1,i}^T \boldsymbol{S}_{k+1,i} \boldsymbol{H}_{k+1,i}^T
\end{aligned} \tag{5.3}$$

The following sampling data was used to simulate the multiple-sensor fusion scenario.

$$\begin{aligned}
\text{Integration Time }, \Delta t_i &= 0.01 \text{seconds} \\
\text{Sampling Time for sensor } \mathcal{A}, \Delta t_1 &= 0.05 \text{seconds} \\
\text{Sampling Time for sensor } \mathcal{B}, \Delta t_2 &= 0.1 \text{seconds} \\
\text{Transmission delay for sensor } \mathcal{B}, \delta t_d &= 0.09
\end{aligned}$$

For the purpose of this thesis, the two sets of measurements were taken as both differently sampled time-series of the same sensor.

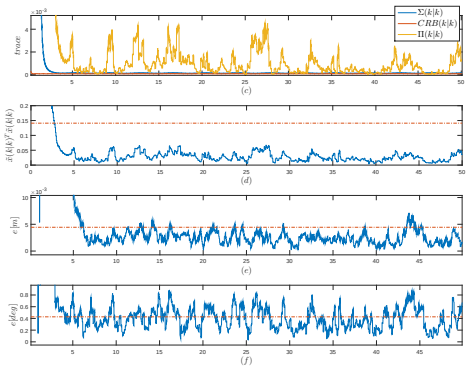

Figure 5.8.: ब_1:Errors in Estimation a)Traces of State covariance, Cramer Rao Bound and the Squared Error matrix b)Squared Error c)Position Error and d)Orientation error; for EKF in multi-rate Parallel update operation and no delay

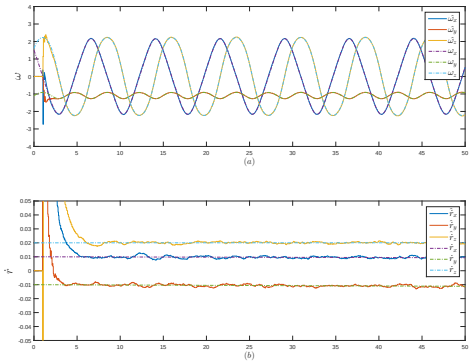

Figure 5.9.: Angular velocity $\boldsymbol{\omega}$ and Linear velocity $\dot{\boldsymbol{r}}$ in multi-rate Parallel update operation and no delay

It was previously mentioned that measurements reported by the vision systems are representative of a past state. In single sensor systems, as in, section 5.1, this was not

a problem as a state propagation produced the optimal state. In a system with sensors having different transmission delays, τ, the update mechanism becomes a little more convoluted. It would be prudent to point out that in system with rapid dynamics, this can cause large estimation errors.

The mathematical foundation of such measurement updates have been found by Julier and Uhlmann, Alexander and Zhang, Li, and Zhu. Zhang, Li, and Zhu termed this situation with transmission delays as an *OOSM*. From the ones in [**Zhang2005**], the *Algorithm-1* Global update equations were employed in this thesis. This was based on the assumption that timestamps of measurement capture and reporting are well known. This is akin to vision systems in which the camera's image capture and the vision systems' pose estimate timestamps are likely to be known. Failure to account for the *Out of Sequence Measurements* can lead to large errors as shown in 5.10 as compared to 5.8.

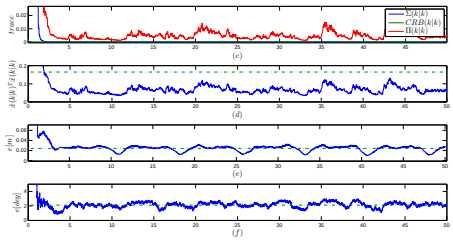

Figure 5.10.: स$_1$:Errors in Estimation a)Traces of State covariance, Cramer Rao Bound and the Squared Error matrix b)Squared Error c)Position Error and d)Orientation error; for EKF operated without considering OOSM

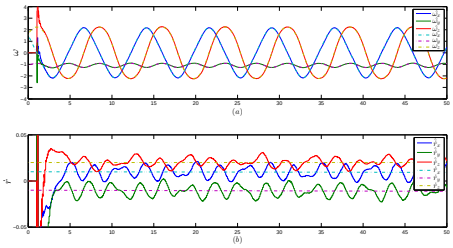

Figure 5.11.: स$_1$:Errors in Estimation a)Traces of State covariance, Cramer Rao Bound and the Squared Error matrix b)Squared Error c)Position Error and d)Orientation error; for EKF operated without considering OOSM

It is interesting to note the oscillating behavior in the velocity in figure 5.11 in contrast to the expected response in 5.9. This provides us with sufficient reason to develop an EKF which is enabled for OOSM to avoid these errors when performing multiple sensor

update in the EKF.

5.2.1. Optimal Update for Mulitple sensors

In 3.15 and 5.8, we had already built the mathematical foundation of using time-delayed measurement to update the current state estimate. Following Zhang, Li, and Zhu's work, the formulae on *Algorithm-1* are employed in this thesis.

$$\begin{aligned}\hat{\boldsymbol{x}}(d|k-l) &= \hat{\boldsymbol{x}}(k-l|k-l) + \int_{k-l}^{d} \boldsymbol{f}(\hat{\boldsymbol{x}}(k-l|k-l) \\ \boldsymbol{\Sigma}(d|k-l) &= \boldsymbol{\Phi}(k-l,d)\boldsymbol{\Sigma}\boldsymbol{\Phi}(k-l,d)^T + \boldsymbol{Q}_{k-l,d}\end{aligned} \tag{5.4}$$

Equation (5.4) nominally propagates the system as soon as it receives the event for camera's captured image. Subsequently, an initialization of the recursion is made as given in [**Zhang2005**].

$$\begin{aligned}\hat{\boldsymbol{x}}(d|k-l+1) &= \hat{\boldsymbol{x}}(d|k-l)+ \\ &\quad \boldsymbol{\Sigma}\boldsymbol{\Phi}(d,k-l+1)^T\boldsymbol{H}_{k-l+1}\boldsymbol{S}_{k-l+1}^{-}(\boldsymbol{y}_{k-l+1} - \boldsymbol{h}(\hat{\boldsymbol{x}}(k-l+1|k-l) \\ \boldsymbol{\Sigma}(d|k-l+1) &= \boldsymbol{\Sigma}(d|k-l)- \\ &\quad \boldsymbol{\Sigma}(d|k-l)\boldsymbol{\Phi}(d,k-l+1)^T\boldsymbol{H}_{k-l+1}\boldsymbol{S}_{k-l+1}^{-}\boldsymbol{H}_{k-l+1}\boldsymbol{\Phi}(d,k-l+1)\boldsymbol{\Sigma}(d|k-l) \\ &\quad \boldsymbol{U}_{k-l+1,d} = (\mathbb{I} - \boldsymbol{K}_{k-l+1}\boldsymbol{H}_{k-l+1})\boldsymbol{\Phi}(d,k-l+1)\boldsymbol{\Sigma}(d|k-l)\end{aligned} \tag{5.5}$$

Thereafter, the following recursion continues until the measurement arrives.

$$\begin{aligned}\hat{\boldsymbol{x}}(d|n+1) &= \hat{\boldsymbol{x}}(d|n)+ \\ &\quad \boldsymbol{U}_{n,d}\boldsymbol{\Phi}(n,n+1)^T\boldsymbol{H}_{n+1}\boldsymbol{S}_{n+1}^{-}(\boldsymbol{y}_{n+1} - \boldsymbol{h}(\hat{\boldsymbol{x}}(n+1|n)) \\ \boldsymbol{\Sigma}(d|n+1) &= \boldsymbol{\Sigma}(d|n)- \\ &\quad \boldsymbol{\Sigma}(d|n)\boldsymbol{\Phi}(n,n+1)^T\boldsymbol{H}_{n+1}\boldsymbol{S}_{n+1}^{-}\boldsymbol{H}_{n+1}\boldsymbol{\Phi}(n,n+1)\boldsymbol{\Sigma}(d|n) \\ &\quad \boldsymbol{U}_{n+1,d} = (\mathbb{I} - \boldsymbol{K}_{n+1}\boldsymbol{H}_{n+1})\boldsymbol{\Phi}(d,n+1)\boldsymbol{\Sigma}(d|n)\end{aligned} \tag{5.6}$$

As soon as the measurement arrives, the optimal state is obtained as a linear combination of the current state and the measurement residual as given in (3.15),

$$\begin{aligned}\hat{\boldsymbol{x}}(k|k,k_d) =& \hat{\boldsymbol{x}}(k|k) + \boldsymbol{U}_{k_d,k}\boldsymbol{H}_{k_d}^T \\ & (\boldsymbol{H}_{k_d}\boldsymbol{\Sigma}(k_d|k)\boldsymbol{H}_{k_d}^T + \boldsymbol{R}_{k_d})^{-}(\boldsymbol{y}_{k_d} - \boldsymbol{H}_{k_d}\hat{\boldsymbol{x}}(k_d|k))\end{aligned} \tag{5.7}$$

The state error covariance is,

$$\boldsymbol{\Sigma}(k|k,k_d) = \boldsymbol{\Sigma}(k|k) - \boldsymbol{K}_{k_d}\boldsymbol{S}_{k_d}\boldsymbol{K}_{k_d}^T \tag{5.8}$$

where instead of d, the delay is shown as k_d. The total OOS time for the measurements in the following simulation is 0.09 seconds, which still manages to affect the velocity estimates as we witnessed before. On applying the above set of equations as an OOSM component which remains live in the period, $k-l+1 < n < k$, the following results are obtained.

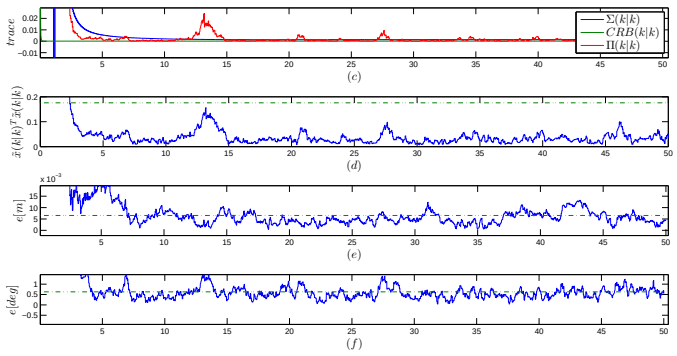

Figure 5.12.: स$_1$:Errors in Estimation a)Traces of State covariance, Cramer Rao Bound and the Squared Error matrix b)Squared Error c)Position Error and d)Orientation error; Errors reduced due to OOSM update

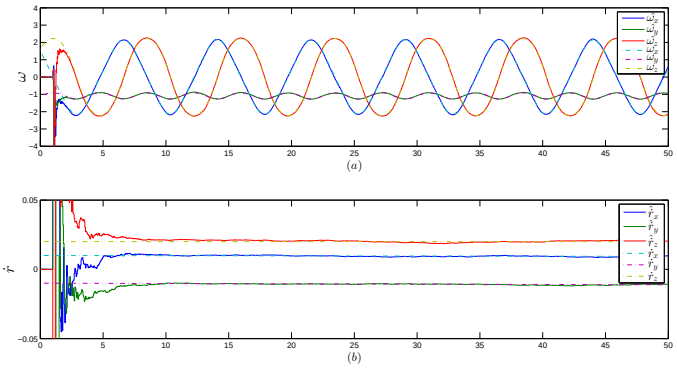

Figure 5.13.: ω and $\dot{r}$: Improved estimates due to OOSM

- From 5.13, it is clear that the introduction of OOSM to the algorithm makes the state current and hence is more accurate.

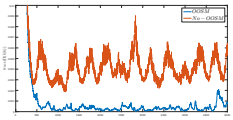

(a) $log[trace(\mathbf{\Pi}(k|k))]$

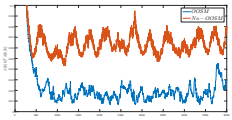

(b) $\tilde{x}(k|k)^T\tilde{x}(k|k)]$

- The difference is glaring in the figure 5.2.1. $trace[\Pi(k|k)]$ is simply the covariance between the residuals. The squared-error is also higher when OOSM is not being employed.

Remark 21. Of course the impact of the OOSM depends on the noise characteristics of the constituent sensors of the system. If the overall noise floor is high, the effect of not using OOSM is small. However, for precise relative navigation, it is important to consider time-aspects like this to increase the overall accuracy of the estimator.

References

[**Palmerini2016**] G. B. Palmerini, M. Sabatini, and P. Gasbarri. "Guidelines for active removal of non-functional targets designed to assist rendezvous and capture." In: *2016 IEEE Aerospace Conference*. Mar. 2016, pp. 1–13. DOI: 10.1109/AERO.2016.7500709.

[**Sridhar1993**] B. Sridhar et al. "Multirate and event-driven Kalman filters for helicopter flight." In: *IEEE Control Systems* 13.4 (Dec. 1993), pp. 26–33. ISSN: 1066-033X. DOI: 10.1109/37.229556.

[**Julier2005**] S. J. Julier and J. K. Uhlmann. "Fusion of time delayed measurements with uncertain time delays." In: *Proceedings of the 2005, American Control Conference, 2005.* June 2005, 4028–4033 vol. 6. DOI: 10.1109/ACC.2005.1470607.

[**Alexander1991**] Harold L. Alexander. *State estimation for distributed systems with sensing delay*. 1991. DOI: 10.1117/12.44843. URL: http://dx.doi.org/10.1117/12.44843.

[**Willner1976**] D. Willner, C. B. Chang, and K. P. Dunn. "Kalman filter algorithms for a multi-sensor system." In: *Decision and Control including the 15th Symposium on Adaptive Processes, 1976 IEEE Conference on*. Dec. 1976, pp. 570–574. DOI: 10.1109/CDC.1976.267794.

[**Zhang2005**] Keshu Zhang, X. R. Li, and Yunmin Zhu. "Optimal update with out-of-sequence measurements." In: *IEEE Transactions on Signal Processing* 53.6 (June 2005), pp. 1992–2004. ISSN: 1053-587X. DOI: 10.1109/TSP.2005.847830.

Chapter 6: Future work and discussion

In this thesis, an estimator was designed with robust features for pose estimation. However, there are some natural extensions to this volume of work that need to be pursued.

- In chapter 2, the observability analysis can be extended to studying sensor placement strategy so that the manipulator's end-effector positioning can aid the process of estimation. In [**Hinson2014**], Hinson has made a similar study in his PhD dissertation based on ideas shared in this thesis.
- Also, once the states and parameters have been estimated in $स_3$, a balanced truncation technique can be used to reduce the state-space to $स_2$ and $स_1$ sequentially. In [**Sandberg2002**], Sandberg has provided detailed results for truncation of state-space in time-varying systems. For a nonlinear observer like the EKF, these results are directly usable.
- As observers for nonlinear systems, the Unscented Kalman Filter and the Particle Filter have not been used for comparison. These comparisons will yield intuition into the usability of the EKF for realtime systems.
- In chapter 1, the measurement model was defined with manipulator motion. The equations of motion of the robot base due to actuation of the robot are given by the generalized Jacobian as explained in [**Umetani1989**]. The model used in this thesis should be improved with manipulator motion, so that the estimates are produced even when the end-effector and base change their poses relative to the inertial frame. The observation equation can be modified as given in (1.8).
- Such an extension also yields a multiple sensor fusion problem as discussed in chapter 5. The measurement vector from the joint angles or Global Navigation Satellite System (GNSS) can be used to improve the estimates. The results derived in that chapter were intended for such utility. This is a direct extension of the current volume of work.

- There was no theoretical study made on the integrator choice for the state propagator of the EKF. The standard Euler integration technique was used across the breadth of this thesis. Numerical stability of the EKF is important for convergence [**Fitzgerald1971**].

- At present, the SIL implementation is incomplete. The work has to be expanded to incorporate the free-floating dynamics. This will greatly reduce the amount of time taken to test control/estimation algorithms. Also, at DLR, such a system would yield a testbench for basic tests before the the code is uploaded on to the OOS-simulator.

- Although the VB-adpative system implemented in this thesis in chapter 4 is fully functional, it is advisable to directly use the cost function or reprojection errors from the vision-system as functional parameters for the measurement covariance matrix. This will yield faster dynamic response for the estimation of the covariance matrix.

- In this thesis, the pose measurements from the vision system are directly used for the estimation problem. It is also an extension to combine the pose-estimation scheme directly with the EKF derived here. In such a case, the measurement vector would be a feature-set and the vision system can aid directly from the EKF state estimates.

- Since the state error covariance matrix is a measure of accuracy of the estimation scheme, this can be used directly for creating shared autonomy arbitration for the purpose of grasping.

In the end, based on error timeseries presented for the different models, it can be concluded that the visual servoing module of the OOS will benefit from an estimating scheme for the purpose of grasping. The code developed during the thesis was installed in the OOS-simulator at DLR. The results will be published later. Based on theoretical and simulation studies pursued in this thesis, the servoing tasks should demonstrate stability during times of occlusion, outliers in vision-system or other contingencies which can cause the feedback mechanism of the controller to fail. In the pre-grasping phase, the convergence mechanisms will ensure that the parameter identification problem does not cause an estimation failure. Hence, the problems of On-orbit servicing and ADR can be addressed as a common one. The OOSM update has created a framework for multiple sensor fusion for future extension work by adding more sensor units. Additionally, it was shown that this ensures that the state remains current with minimum squared error as compared to without it. Additionally, the model developed in the first chapter acts

as foundation for performing estimation during manipulation, which will be pursued as the next step forward.

References

[**Hinson2014**] Brian Hinson. "Observability-Based Guidance and Sensor Placement." PhD thesis. University of Washington, 2014.

[**Sandberg2002**] Henrik Sandberg. "Linear Time-Varying Systems: Modeling and Reduction." PhD thesis. Lund Institute of Technology, 2002.

[**Umetani1989**] Yoji Umetani and Kayuya Yoshida. "Resolved Motion Rate Control Of Space Manipulators with Generalized Jacobian Matrix." In: *IEEE Transactions on Robotics and Automation* 5.3 (1989), pp. 303–313.

[**Fitzgerald1971**] R. Fitzgerald. "Divergence of the Kalman filter." In: *IEEE Transactions on Automatic Control* 16.6 (Dec. 1971), pp. 736–747. ISSN: 0018-9286. DOI: 10.1109/TAC.1971.1099836.

Appendix A: SIL

A.1. SIL for the Robotic manipulator

A SIL can be viewed as a simulation-based evaluation of software algorithms. As a part of the thesis work, a SIL solution for the problem of uncooperative Target grasping was developed. The simulations were developed using `MATLAB` as a proof of concept but for a hardware target implementation, the program for सत्र$_1$ was developed on `Simulink`. This program is implemented in *On Obrit Servicer* simulator for the purpose of accurate pose estimations at DLR, Oberpfaffenhofen.

(a) EKF for सत्र$_1$

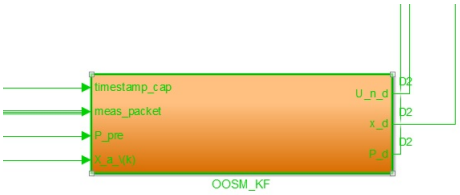

(b) OOSM for camera delays

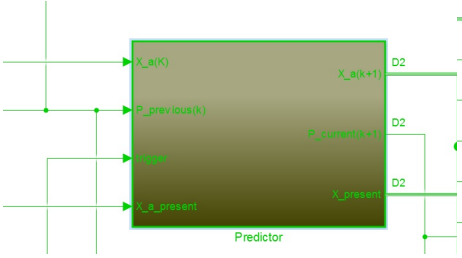

(a) EKF predictor for सत्र$_1$ at $100Hz$

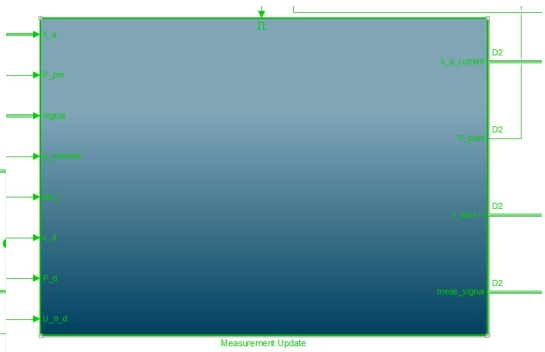

(b) EKF asyncrhonous measurement update at [0.18, 0.22] seconds

In this thesis, the estimation and control algorithms were written in `MATLAB/Simulink`. In figure A.1, the EKF and the OOSM blocks, and in A.1, the Predictor/Update blocks have been shown. The predictor works at the controller rate, which is $100Hz$ for simulations and $1KHz$ for hardware. The camera captures uniformly every 0.1 second but the vision system has a transmission delay because of computing time.

A.1.1. Camera simulation using `simEvents`

The vision system as a measurement device is asynchronous in its data reporting.

The camera's functining was simulated in `simEvents` which is a `Simulink` toolbox that provides Discrete-event simulation engine for analyzing event-driven models, like the EKF.

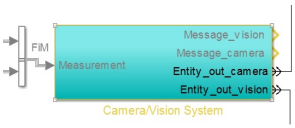

(a) Camera/Vision system

- The camera itself was simulated by a constant pulse running at $10Hz$, which generated the discrete-event *entities* in `simEvents`. The reader is referred to [**Gray2007**] for more details about the software.
- As soon as an *attribute* (computed pose), is set to the *entity*, a function call named `cam_start_time` is generated which triggers the OOSM to start running its recursion.
- The vision system's indeterminate delay is modeled using the *server* block. By attaching an *Event based Random number* to its input, the camera pose data is delayed in the range of 0.08 to 0.12. This is similar to typical observations of the vision system on the Servicer simulator at DLR. This is shown in figure A.4.
- Once the *server* has dispatched the *entity*, another function call named `meas_trigger` is generated which is when the measurement is available, as shown in figure A.5. At this point OOSM must terminate and perform the update as explained in the previous chapter.

A.1.2. Dynamic Simulation

The environment dynamics were simulated using `V-REP` which is a standard testbed for such simulations as in [**Rohmer2013**]. In [**Ivaldi2014**], the authors have made a

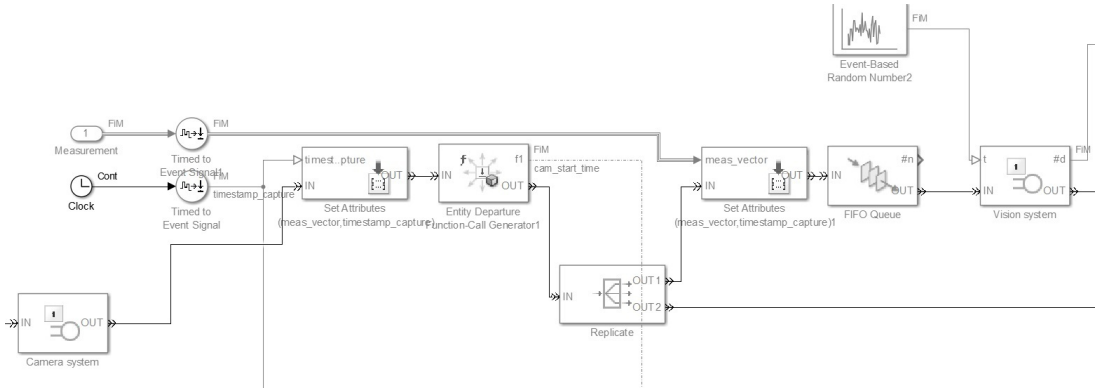

Figure A.4.: Trigger generation for image capture

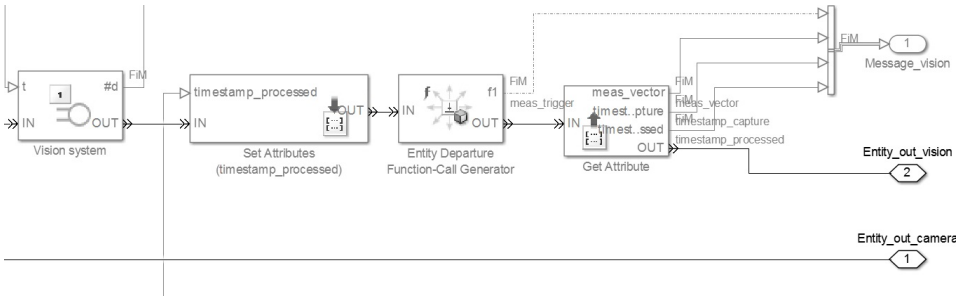

Figure A.5.: Trigger generation for available measurement

comprehensive study on simulation software for dynamics. `V-REP` was chosen because of its flexibility, off the shelf CAD models and active user support community.

- A UR5 (universal robot) was configured with *DH-parameters* in `V-REP` for forward kinematics.
- A simple resolved-rate motion-controller was designed for the UR5.
- A vision-sensor was mounted on the end-effector of the robot as shown in figure A.6 a). The software does not provide the internal calibration matrix of the vision sensor. As a result, a Checkerboard calibration was performed with a 10×7-board as shown in c) and d) in figure A.6. The intrinsic camera matrix was found to be,

$$\boldsymbol{K}_i = \begin{bmatrix} 442.3313 & 0 & 0 \\ 0 & 442.0068 & 0 \\ 344.017 & 284.6112 & 1 \end{bmatrix} \tag{A.1}$$

  with mean reprojection error of 0.1956.

- The CAD model of the OOS-Target was imported and the *scene* was created, as demonstrated in figure A.6 *a*) which could be manipulated remotely using `MATLAB/Simulink`.
- At the time, there was no dedicated client-server software to connect to `V-REP` directly from `Simulink` but there is support for `MATLAB`. A *System Object* was developed which could allow a `V-REP-SIMULINK client-server` connection for SIL simulations.

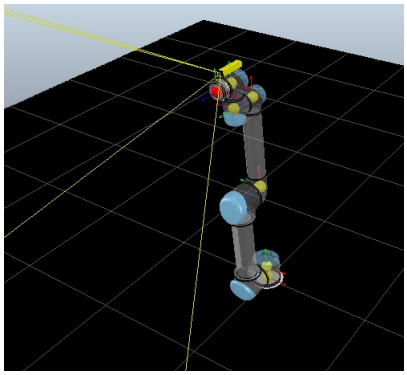

(a) UR5 mounted with vision sensor, `V-REP`

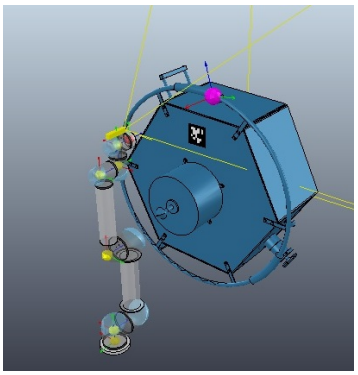

(b) UR5 servicer with OOS-SIM-Target

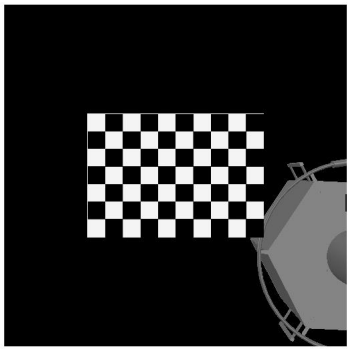

(c) Calibration instance: 1

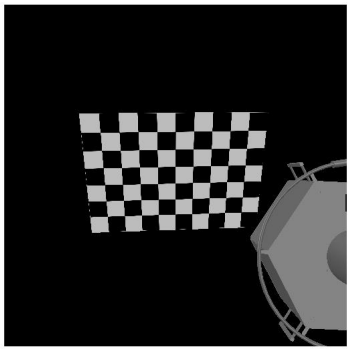

(d) Calibration instance: 7

Figure A.6.: V-REP environment

In [**Hosseini2016**], a similar prototyping was performed for an Octorotor using `MATLAB` and `ADAMS`.

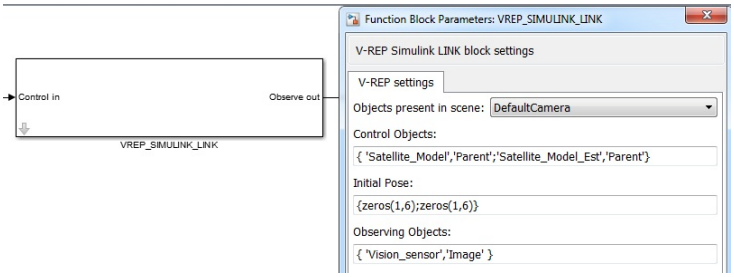

Figure A.7.: `V-REP-SIMULINK client-server`

A.1.3. Pose estimation

Although the thesis is titled around pose estimation, the aspects of machine vision are off the scope of this work. At DLR, the vision system is a monocular odometry system. For the purpose of SIL, *AprilTags* were attached to the Target model which could be identify the pose of the body using a `C++` library. A `mex`-function was written to perform this simple task.

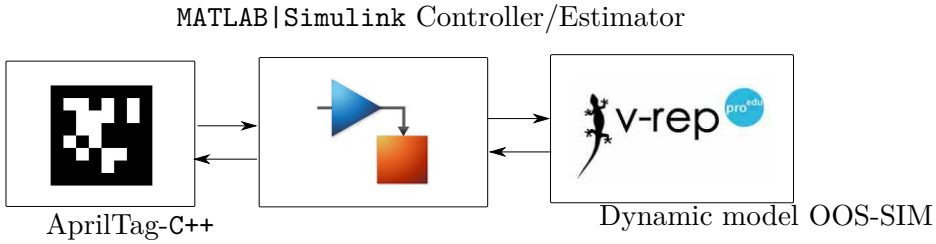

Figure A.8.: SIL block-diagram

Finally, a SIL framework was setup which will enable evaluation of estimation and control algorithms, especially those pertaining to grasping bodies that move under torque-free motion in space. An example of AprilTag is shown on the Target satellite in figure A.6 *b*).

References

[**Gray2007**] M. A. Gray. "Discrete Event Simulation: A Review of SimEvents." In: *Computing in Science Engineering* 9.6 (Nov. 2007), pp. 62–66. ISSN: 1521-9615. DOI: 10.1109/MCSE.2007.112.

[**Rohmer2013**] E. Rohmer, S. P. N. Singh, and M. Freese. "V-REP: A versatile and scalable robot simulation framework." In: *2013 IEEE/RSJ International Conference on Intelligent Robots and Systems*. Nov. 2013, pp. 1321–1326. DOI: 10.1109/IROS.2013.6696520.

[**Ivaldi2014**] Serena Ivaldi, Vincent Padois, and Francesco Nori. "Tools for dynamics simulation of robots: a survey based on user feedback." In: *CoRR* abs/1402.7050 (2014). URL: http://arxiv.org/abs/1402.7050.

[**Hosseini2016**] A. Hosseini et al. "Modeling and control of an octorotor flying robot using the software in a loop." In: *2016 4th International Conference on Control, Instrumentation, and Automation (ICCIA)*. Jan. 2016, pp. 52–57. DOI: 10.1109/ICCIAutom.2016.7483135.